

Data In brief: Hearing loss impacts gray and white matter across the lifespan: systematic review, meta-analysis and meta-regression

Francis A. M. Manno^{1†}, Raul Rodríguez-Cruces^{2*}, Rachit Kumar^{3,4*}, J. Tilak Ratnanather⁵, Condon Lau^{1†}

1. Department of Physics, City University of Hong Kong, Kowloon, Hong Kong SAR, China

2. Montreal Neurological Institute, McGill University, Montreal, Canada

3. Perelman School of Medicine, University of Pennsylvania, Philadelphia, USA

4. Medical Scientist Training Program at the University of Pennsylvania, Philadelphia, USA

5. Center for Imaging Science and Institute for Computational Medicine, Department of Biomedical Engineering, Johns Hopkins University, Baltimore, MD, USA

Corresponding Author:

†Francis A.M. Manno

Department of Physics

City University of Hong Kong

HKSAR, China Email: francis.Manno@gmail.com

†Condon Lau

Department of Physics

City University of Hong Kong

HKSAR, China

Email: condon.lau@cityu.edu.hk

Data availability statement: The entire dataset, analyses and code used in this work can be downloaded by contacting the corresponding author and from the Open Science Framework: Manno, et al., 2018. “Profound Hearing Loss.” OSF. <https://osf.io/7y59j/>.

Declaration of Interests: The authors declare no competing financial interests and no non-financial competing interests.

Author Contributions: Conceptualization, FAMM JTR, CL; Methodology, FAMM, RRC; Formal Analysis, FAMM, RRC, RK; Visualization FAMM, RRC, RK; Investigation, FAMM, JTR; Writing, Editing, FAMM, RRC, RK, JTR, CL; Funding CL

*Equal contributions

Keywords: Sensorineural hearing loss, Structural MRI, DTI, Bilateral hearing loss, Unilateral hearing loss.

Abstract

Importance. Hearing loss is a heterogeneous disorder thought to affect brain reorganization across the lifespan. The exact structural endophenotype of hearing loss is not known, although it is assumed to affect the auditory regions of the temporal lobe such as Heschl's gyrus.

Objective. Here we assessed the structural alterations of hearing loss by using a meta-analysis of effect size measures based on MNI coordinate mapping of MRI studies. Unique effect size metrics based on Cohen's d and Hedges' g were created to map coordinates of gray matter (GM) and white matter (WM) alterations from bilateral congenital and acquired hearing loss populations. Three coordinate mapping techniques were used and compared: coordinate-based anatomic likelihood estimation (ALE), multi-level kernel density analysis (mKDA), and seed-based d Mapping (SDM). Using a meta-regression, GM and WM trajectories were mapped to visualize the progression of congenital and acquired hearing loss throughout the lifespan. Heterogeneity in effect size metrics was determined using the forest, Baujat, Funnel, Galbraith and bubble plots to discern dispersion and spread of datapoints. Lastly, we displayed an endophenotype map of hearing loss alterations in GM and WM obtained from a multivariable meta-regression of the effect size.

Data Sources. PubMed, Google Scholar and Scopus primary and secondary literature was searched from inception to May 2020, augmented by expert recommendations, grey searchers, and primary literature citation inclusions.

Study Selection. Any peer-reviewed publication irrespective of language that involved the structural neuroimaging of the human brain in participants with hearing loss at any age.

Data Extraction and Synthesis. Data was collected on 1) October 10th, 2012 through November 1st, 2012, 2) June 6th through July 20th 2018, 3) directly prior to publication following the Preferred Reporting Items for Systematic Review and Meta-Analyses. Results were summarized across studies in a random-effects model.

Main Outcomes and Measures. Effect sizes for GM and WM metrics associated with hearing loss in structural MNI coordinates were used for the outcome measure.

Results. The systematic review and meta-analysis revealed $n = 72$ studies with structural alterations measured by MRI (bilateral=64, unilateral=8). The bilateral studies contained more than 66,545 variable datapoint metrics broadly categorizing hearing loss into congenital and acquired cases from mild to profound impact ($n = 7445$) and control cases ($n = 2924$) with ages of 34.92 ± 23.08 and 30.61 ± 19.45 years, respectively. We found hearing loss affects GM and underlying WM in nearly every region of the brain. In congenital hearing loss, GM decreased most in the frontal lobe. Acquired hearing loss similarly had a decrease in frontal lobe GM, albeit the insula was most decreased. Congenital white matter underlying the frontal lobe GM was most decreased. The temporal lobe had different GM alterations in congenital and acquired, decreasing in the former and increasing in the latter, possibly due to age-dependent compensation. The WM alterations most frequently underlined GM alterations in congenital hearing loss, while acquired hearing loss studies did not assess the WM metric frequently.

Limitations. There were several limitations of neuroimaging studies in the hearing loss field with manuscripts many for example not reporting mean and SD for GM or WM metrics, lack of MNI coordinates, and some not reporting sufficient control populations. These factors could have contributed to heterogeneity as underlying explanatory variables.

Conclusions and Relevance. Although temporal lobe auditory regions are most commonly thought to be affected in hearing loss, the present analysis found the frontal lobe gray matter and underlying white matter most decreased in both congenital and acquired hearing loss. The present study demonstrates hearing loss across the lifespan and the compensatory adaptations which occur to the brain due to lack of auditory input. This meta-analysis review presents a novel 'hit-enter' repeatability format for assessing hearing loss, providing all data, scripts and analysis from data curation to visualization available for reproducibility. Future studies should use the endophenotype of hearing loss as a prognostic template for discerning impact and clinical outcomes.

Truncated Abstract

Hearing loss is a heterogeneous disorder thought to affect brain reorganization across the lifespan. The exact structural endophenotype of hearing loss is not known, although it is assumed to affect the auditory regions of the temporal lobe such as Heschl's gyrus. Here we assessed the structural alterations of hearing loss by using a meta-analysis of effect size measures based on MNI coordinate mapping of MRI studies. Unique effect size metrics based on Cohen's d and Hedges' g were created to map coordinates of gray matter (GM) and white matter (WM) alterations from bilateral congenital and acquired hearing loss populations. Three mapping techniques were used and compared: coordinate-based anatomic likelihood estimation (ALE), multi-level kernel density analysis (mKDA), and seed-based d Mapping (SDM). Using a meta-regression, GM and WM trajectories were mapped to visualize the progression of hearing loss throughout the lifespan. Heterogeneity in effect size metrics was determined using the forest, Baujat, Funnel, Galbraith and bubble plots to discern dispersion and spread of datapoints. Lastly, we displayed an endophenotype map of hearing loss alterations in GM and WM obtained from a multivariable meta-regression of the effect size. The systematic review and meta-analysis revealed $n = 72$ studies with structural alterations measured with MRI (bilateral=64, unilateral=8). The bilateral studies contained more than 28000 variable datapoint metrics broadly categorizing hearing loss into congenital and acquired cases ($n = 7445$) and control cases ($n = 2924$) with ages of 34.92 ± 23.08 and 30.61 ± 19.45 years, respectively. We found hearing loss affects GM and underlying WM in nearly every region of the brain. In congenital hearing loss, GM decreased most in the frontal lobe. Acquired hearing loss similarly had a decrease in frontal lobe GM, albeit the insula was most decreased. Congenital white matter underlying the frontal lobe GM was most decreased. The temporal lobe had different GM alterations in congenital and acquired, decreasing in the former and increasing in the latter. The WM alterations most frequently underlined GM alterations in congenital hearing loss, while acquired hearing loss studies did not assess the WM metric frequently. There were several limitations of studies in the hearing loss field with manuscripts for example not reporting mean and SD for GM or WM metrics, lack of MNI coordinates, and some not reporting sufficient control populations. These factors could have contributed to heterogeneity as underlying explanatory variables. The present article presents a novel 'hit-enter' repeatability format for assessing hearing loss, providing all data, scripts and analysis from data curation to visualization available for reproducibility. Future studies should use the endophenotype of hearing loss as a prognostic template for discerning impact and clinical outcomes.

Contents

Abstract	2
Truncated Abstract	3
1. Supplemental information	6
2. Methods	6
2.1. Eligibility criteria and study search	6
2.2. Data acquisition, metrics and outcome measures	7
2.3. Creating the standardized metric Cohen's d and Hedges'g	7
2.4. Regions of interest in hearing loss	8
2.4.1. Coordinate-based anatomic likelihood estimation	8
2.4.2. Multi-Level Kernel Density Analysis	8
2.4.3. Seed-based d Mapping (SDM)	9
2.5. Meta-regression longitudinal progression of GM and WM trajectories in hearing loss	9
2.6. Heterogeneity of gray matter and white matter	10
2.7. Surface visualization of ROI mapping to create hearing loss endophenotype	11
2.8. Research statistical strategy: Analysis overview, hypothesis, assumptions, and interpretation .	11
3. References	11
Literature research	16
Figure SI.1 Flow diagram	17
Eligibility Criteria for the meta-regression	17
Tables of included studies	19
Unusual MRI measurements	21
Formulas	22
Estimation of heterogeneity per model	22
References (64 bilateral studies)	23
Unilateral hearing loss (total n=8)	26
Signed differential mapping (SDM)	26
Anatomic Likelihood Estimation	30
Multi-Level Kernel Density Analysis (mKDA): Wager Methods	30
Definitions for mKDA	30
Cluster comparisons list	31

Studies characteristics	46
Relation between hearing loss (dB) and age (Figure 2.D)	46
Studies characteristics (Figure 2.E, 2.F)	47
Brain structure (GM, WM) and MRI measures	48
Frequency table: Brain structure (GM, WM) and MRI measures	49
Brain structure (GM, WM) and side	50
Studies characteristics (Figure 2.A, 2.B): Brain structure (GM, WM) by MRI measure (volume and FA)	51
MRI measures by ROI (Figure 2.C)	51
Relations of all MRI measurements of GM and WM with age	52
Gray matter relation with Age by volume (Figures 3.A and 3.B)	53
White matter relation with Age by volume and FA (Figures 3.C, 3.D and 3.F)	54
Gray and White matter relation with Age by asymmetry	54
Table of estimates and meta-regression: WM and GM relation with age by MRI measures (volume and FA)	55
Meta-regression	56
Included variables by Etiology, Brain matter and MRI measure	56
Meta-regressions of Gray Matter in the Heschl Gyrus	58
Meta-regressions of Gray Matter in Congenital by severity and side (volume and VBM)	59
Congenital - Meta-regressions of Gray Matter Volume	60
Acquired - Meta-regressions of Gray Matter by Volume	63
Congenital - White Matter by VOLUME	66
Acquired - White Matter by VOLUME (ONLY BILATERAL)	69
Congenital - White Matter by FA fractional anisotropy	70
Acquired - White Matter by FA fractional anisotropy (ONLY RIGHT)	73
Supplementary material: heterogeneity per model	75
Heterogeneity: GM volume Right	75
Heterogeneity: GM volume Left	76
Heterogeneity: WM FA Right	77
Heterogeneity: WM FA Left	78
Heterogeneity: WM volume Right	79
Heterogeneity: WM volume Left	80
Meta-regressions of Gray Matter Volume & Brain Areas: Random effects model no intercept covariated by Side	81
Meta-regressions of White Matter FA & Brain Areas: Random effects model no intercept covariated by Side	92

Meta-regressions of White Matter Volume & Brain Areas: Random effects model no intercept covariated by Side	100
Supplementary material: Forest-plots of other Measures	106
Hesch gyrus FA white matter	106
STG Volume White matter	107
Measures of White matter Integrity	108
White matter: RD	108
White matter: MD	109
White matter: Mean Kurtosis	110
White matter: AD	111
Other Measures of White Matter	112
White matter: Thickness	112
White matter: VBM	113

List of Tables

1	Total unique studies	64	19
2	Acquired studies	19	19
3	Congenital studies	42	19
4	Mixed studies	3	19
5	Studies without Hedges'G (n=7). These studies do not have control population (NA)	20	20
6	Studies with Hedges'G (n=57, mixed etiology=3)	20	20
7	Studies Measuring White Matter Thickness (n=4)	21	21
8	Studies Measuring Gray Matter FA (n=2)	21	21
9	SDM: congenital	27	27
10	SDM: congenital... continuation	28	28
11	SDM: acquired	28	28
12	SDM: pediatric	28	28
13	SDM: adult	29	29
14	SDM: AgedAdult	29	29
15	SDM: GM	29	29
16	SDM: WM	30	30
17	ALE report of first 10 clusters	30	30
18	mKDA report	31	31
19	Matter vs measure (continued below)	49	49
20	Table continues below	49	49
22	Matter vs Side	49	49
24	Gray Matter in Heschl Gyrus	58	58
25	Congenital Gray Matter by severity	59	59
26	REM by big area- Congenital - Gray Matter Volume	60	60
27	Congenital - Gray Matter Volume	60	60
28	REM by big area - Acquired - Gray Matter Volume	63	63
29	Acquired - Gray Matter Volume	63	63
30	REM by big area - Congenital - White Matter Volume	66	66
31	Congenital White Matter Volume	66	66
32	REM by big area - Acquired White Matter Volume	69	69
33	acquired White Matter Volume	69	69
34	REM by big area - Congenital White Matter FA	70	70
35	Congenital White Matter FA	70	70
36	REM by big area - Acquired White Matter FA	73	73
37	acquired White Matter FA	73	73

1. Supplemental information

An extensive amount of data associated with the MNI coordinate mapping is presented in the supplemental information to support our conclusions for ALE, mKDA, SDM. Tables and figures outline ROI of interest and significance. Additionally sub-analyses associated with the heterogeneity plots (Forest plot, Baujat plot, Funnel plot, Galbraith plot and bubble plot) in the meta-analysis are presented for all assessments. All supplemental information is additive in nature and bolsters our results.

2. Methods

We followed the Preferred Reporting Items for Systematic Reviews and Meta-Analyses of Individual Participant Data (PRISMA Guidelines).^{22–25} The study was registered in 2018 and supplementary information, code, csv files, and extended analyses can be found at OSF (<https://osf.io/7y59j/>). Detailed, annotated, expanded, and updated code can be found at GitHub (<https://github.com/FrancisManno/MetaHearingLoss> or www.fmanno.com). The literature review had been initiated by two authors nearly 6 years prior to registration (FAMM, JTR). The review followed the checklist enumerations as outlined by the Organization for Human Brain Mapping (OHBM) *Committee on Best Practices* in Data Analysis and Sharing (COBIDAS; <http://www.humanbrainmapping.org/cobidas>).¹¹ All analyses for the present study used custom Matlab scripts (2017a: The Mathworks, Natick, USA) and R version 3.6.3²⁶, specifically the packages meta^{27,28} and metafor.^{29,30} The manuscript is completely reproducible, replicable, and amendable for future iterations, with a ‘hit-enter’ repeatability, considered the gold-standard.¹¹

2.1. Eligibility criteria and study search

Criteria for study eligibility were peer-reviewed publications in any language of an original investigation involving human participants who underwent structural MRI neuroimaging of the brain due to hearing loss. The search was performed in English, Chinese, Spanish and French and had no language restriction. Bilateral hearing loss (BHL) and unilateral hearing loss (UHL) of any degree (mild, moderate, severe and profound) were included in the literature search. For the quantitative portions of the analysis UHL was excluded, due to the small number of studies ($n \approx 10$; See Supplementary Information) and not to bias the results due to side of hearing. Therefore, the final inclusion criteria were any MRI studies of BHL (**Figure 1a** and **Supplementary Figure SI.1 Flow Diagram**). We identified potentially eligible studies using PubMed, Google Scholar and Scopus. The literature search was performed at 3 timepoints: 1) Wednesday October 10th, 2012 through November 1st, 2012, 2) June 6th through July 20th 2018 and 3) directly prior to publication to ensure capture of all relevant articles. On all three instances, the search was first performed in PubMed to identify primary literature with follow-up searching using Google Scholar. Once primary literature was identified, a Scopus search of citing literature was performed (secondary and grey). These secondary literature sources were screened similarly as primary literature sources. Primary and secondary sources were then-cross-checked for citing sources and additional references. In the Supplementary Information, the Scopus citations are listed as of July 2019. The Medical Subject Headings (MeSH) search terms were: (deafness OR “hearing loss” OR “bilateral hearing loss” OR “unilateral hearing loss” OR “conductive hearing loss” OR “sensorineural hearing Loss”) AND (“magnetic resonance imaging” OR MRI OR “diffusion tensor imaging” OR DTI) NOT (Review[Filter] OR Editorial[Filter] OR Comment[Filter]). Additionally, the search was augmented by correspondence with a distributed network of scientists with hearing loss who are familiar with the field (JTR).³¹ To our knowledge this is the first systematic, meta-analytic, or quantitative review of effect sizes of structural neuroimaging in hearing loss.¹² Two authors (FAMM and JTR) screened the titles and abstracts of all records retrieved. Of those articles retrieved, studies that provisionally met eligibility criteria were assessed for eligibility by examining the full text and following the data acquisition protocol (Details appear in the Methods and Table 1 in the Supplementary Information) All information was tabulated into ISA-tab formatted CSV data descriptors by manual data entry (meta_sideDeaf.csv; Checked by two authors FAMM and JTR). The ISA format <http://isa-tools.org/>) is built around the Investigation

(I: the project context), Study (S: a unit of research) and Assay (A: analytical measurement) data model serializations (tabular). The unit of analysis for the present manuscript was the study in addition to region of interest and GM and WM metric information tabulated from the study as described in the Data Acquisition section.

2.2. Data acquisition, metrics and outcome measures

All eligible studies were included to contribute basic structural neuroimaging data (GM, WM, volume, etc), audiometric data (hearing loss degree in dB), demographic data (age, sex, etc), and MRI scanning characteristics (FOV, voxel size in mm^3 , slices, etc) which were used as the sub-unit of analysis (see **Figure 1b; meta_sideDeaf.csv**). The variables extracted from the studies can be found in **meta_sideDeaf.csv**, as columns: 1) study, 2) etiology (i.e. congenital acquired), 3) side deaf (i.e. bilateral in the present review), 4) severity (i.e., mild, moderate, severe, profound), 5) number hearing loss (i.e. experiment group size), 6) HL and control male and female number (i.e. hearing loss males and females), 7) HL and control age (i.e. hearing loss cohort age with SD), 8) HL and control age range low and high categories, 9) average dB HL and SD, 10) left and right ear average dB HL and SD, 11) sign language (i.e. French, American), 12) MRI strength (1T, 1.5T, 3T), 13) acquisition matrix size in mm^2 , 14) slices in scan sequence, 15) slice thickness (mm), 15) field of view (FOV in cm), 16) scan sequence (i.e. T1), 17) technique (i.e., DTI, VBM), 18) system of analysis (i.e. SPM, FMRIB, Freesurfer, etc), 19) for the region of interest, MNI coordinates in MNI-x, MNI-y, MNI-z, 20) Brodmann location, 21) lobar region of interest (general ROI, i.e. temporal lobe, frontal lobe), 22) specific ROI (i.e. Heschl's gyrus), 23) hemispheric side (i.e. left or right or bilateral), 24) measure (i.e. cortical thickness, volume, asymmetry, fractional anisotropy, etc), 25) matter (i.e. gray matter or white matter), 26) effect (i.e. increase, decrease, same), 27) Cohen's d, and 28) effect correlation r. Cohen's d and effect correlation r were derived measures.^{32–37} Cohen's d was used to derive Hedges' g as described. Several studies did not contribute this information (see Limitations in Discussion) because they lacked quantitative metrics to derive Cohen's d and Hedges' g (see **Supplementary Figure PRISMA Flow Diagram**).

2.3. Creating the standardized metric Cohen's d and Hedges'g

Effect size Cohen's d was used to compare values between studies.³² Cohen's d uses the means and standard deviations of two groups (HL and control), where $M = mean$, $SD = standard deviation$, $n = sample size$, $df = degrees of freedom$:

$$Cohen's\,sd = (M1 - M2)/SD_{pooled} \text{ where } SD_{pooled} = \sqrt{(SD1^2 + SD2^2)/2}$$

Hedges' g uses the means and standard deviations of two groups (HL and control), and the sample size weighted pooled standard deviation for correction. $Hedges'g = (M1 - M2)/SD_{pooled}$, where $SD_{pooled} = \sqrt{(n1 - 1)SD1^2 + (n2 - 1)SD2^2}/(n1 + n2 - 2)$. Cohen's d and Hedges' g of 0.2 is considered small, 0.5 is medium and above 0.8 is a large effect size.³⁴ Hedges' g was used for most analyses to avoid scaling issues.³³ Cohen's d and Hedges' g were used for assessing the ROI meta-regression (**Figure 1a** and **1d**). When available, experimental group (i.e. HL) and control group sample size, degrees of freedom, raw values for the measure (i.e. volume mm^3 and sd), Z score, F test, t-value, or P-value were used for creating the effect size metrics³⁵, as not all studies reported identical variables of input for effect size measure calculations. Converting between values given by a study was done with standard formula.^{36–37} As an example, a study might report sample size, t value and a p-value for a measure of Heschl's gyrus volume between hearing loss and control, but not the actual group volume in mm^3 . Cohen's d, outcome measures and variables of the studies are reported in the **meta_sideDeaf.csv**, as columns as described above. A variability score was estimated for those studies that did not provide standard deviation or error of the mean distribution (see SI variance estimation formula).

2.4. Regions of interest in hearing loss

A central interest in neuroscience is determining how different brain regions are modified due to changes in sensory experience over developmental periods.²⁰ More specifically, sensory deprivation due to hearing loss is known to elicit cross-modal plasticity, where the primary auditory cortex is more than likely to be recruited by visual inputs.²¹ The longitudinal processes associated with structural cortical reorganization in the brain due to hearing loss in humans is currently unknown. Here we map specific ROI from MNI coordinates in hearing loss throughout the human lifespan to ascertain the longitudinal progression of changes in GM and WM. Because hearing loss affects the brain in a widespread nature^{12,20,21}, we are interested in the general and specific areas and thus performed unthresholded and thresholded analyses. The MNI coordinate mapping is divided into general coordinate-based anatomic likelihood estimation (ALE), multi-level kernel density analysis (mKDA), and Seed-based Differential Mapping (SDM). ALE investigates where location probabilities reflect spatial uncertainty associated with the foci of each experiment overlap and mKDA tests how many foci are reported close to any individual voxel. These theoretical differences, that ALE evaluates probabilities of activity localization, where mKDA uses experimental foci counts, allow two different and precise interpretations of the resultant MNI coordinate maps. The SDM analysis is a combination of the methodology and assumptions of ALE and mKDA, using effect sizes and a representation of both positive and negative differences in the same structural brain map.^{39,40} Two levels of structure were assessed: 1) ROIs grouped under a cortical region (i.e. Lobar region: temporal (Heschl's gyrus and superior temporal gyrus) and 2) areas spatially distant Heschl's gyrus and occipital pole.

2.4.1. Coordinate-based anatomic likelihood estimation

The specific question for this procedure is: where is foci convergence across experiments higher than would be expected by chance if their results were independently distributed? GingerALE version 2.3.6. from BrainMap was used which performs coordinate-based anatomic likelihood estimation (ALE) meta-analytic random effects analyses on MNI coordinates (performed in C+).^{41–44} For the present study, MNI coordinates were used and all figures are presented in MNI space. Structural data from the studies was registered with and entered into Scribe (<http://www.brainmap.org/scribe/>) for ease of future replication (meta_sideDeaf.csv; <https://osf.io/7y59j/>).⁴¹ The ALE plots estimate the clustering between foci in hearing loss (Figure 1c).^{42–44} The convergence of foci reported from different experiments is modelled as probability distributions (blobs in **Figure 1c**) whose width is based on empirical estimates of the spatial uncertainty due to the between-subject and between template variability of neuroimaging data.⁴⁴ The ALE was assessed against a null-distribution of random special association between experiments using a false discovery rate (FDR) for correcting the family-wise error rate (FWER) and cluster-level inference.⁴⁴ Input variables were sample size = N and MNI in x/y/z. The settings were cluster-level FWER = 0.01, FDR corrected threshold of $P < 0.05$ for cluster-level inference, threshold permutations = 10,000, and cluster forming threshold level of $P < 0.001$, chosen minimum cluster size = 50mm^3 for analysis and reported only cluster size $> 200\text{mm}^3$. The output was the ALE modelled activation map (MA map) in MNI space, a significant peaks list which detailed up to 10 ROI, based on cluster statistics including volume (mm^3), bounds, weighted center (x/y/z), and the locations and values at peaks within the region.^{42–44} The final ALE output (after union of voxel-wise Gaussians of all foci from ALE MA maps) is a ALE image map at a given α value.^{42–44} The ALE image map is a construction of reported MNI foci spatial probability distributions at the coordinates associated with hearing loss. The conclusion and interpretation of the ALE image map based on the body of literature in hearing loss is the generalization of ROI peaks in the brain most affected by hearing loss. The mKDA precedes in a similar manner, assessing MNI coordinate localization significance, and creating clustering of MNI coordinates (**Figure 1c**).

2.4.2. Multi-Level Kernel Density Analysis

The specific question for this procedure is: how many foci are reported close to any individual voxel among experiments? The mKDA procedure evaluates consistency and specificity of regional structural alterations

based on previous studies reported MNI coordinates (performed in Matlab 2017a). The mKDA represents activation focus as a sphere given arbitrary weights based on sample size = N.^{45,46} Peaks from each comparison study map are separately convolved with the kernel to generate comparison indicator maps (CIMs). Subsequently, the summary density map resulting in the proportion of activated comparisons is subjected to statistical thresholding by a Monte Carlo iteration procedure where locations of the centers of each blob are selected at random and uniformly distributed.^{45,46} Here, the null hypothesis is rejected in voxels where the number of nearby peaks is greater than expected by chance.^{45,46} Lastly, the final mKDA montage map is created by FWER control utilizing extent thresholding.^{45,46} Input variables were sample size = N and MNI in x/y/z, sphere size 10 mm (**Figure 1c** – MNI input).^{45,46} The output was a series CIMs (blobs on **Figure 1c**). The CIMs were used for determining significance by: 1) height-based thresholding used the center of a 10 mm sphere (yellow in figures, representing $P < 0.05$) for identifying the number of contiguous voxels needed to say that a cluster was significant and 2) extent-based thresholding was used to estimate which individual voxels show greater activation at different α levels, $P < 0.001$ clusters (orange – stringent), $P < 0.01$ clusters (red – medium), and $P < 0.05$ clusters (purple – lenient).^{45,46} The aforementioned coloring scheme is applicable to all mKDA maps. The final output was a mKDA montage union map based on height and extent thresholding.^{45,46} Further output was significant region location (x/y/z), voxels, cluster sizes range, volume (mm^3), and maxstat (maximum of the z field) for extent-based thresholding at stringent, medium and lenient α levels.^{45,46} The conclusion and interpretation of the mKDA montage map based on the body of literature in hearing loss is the generalizability of particular regions being structurally altered at a specific α level.^{45,46}

2.4.3. Seed-based d Mapping (SDM)

The specific question for this procedure is: how do increases and decreases in GM and WM relate among groups (congenital and acquired versus control) of experimental subjects. The SDM analysis examines regions of increased and decreased grey matter volume accounting for ‘peaks’ effect-size in experimental dataset and signing a positive and negative difference.^{48,49} SDM calculates effect sizes from given p-values or t-values to determine lower and upper bounds of possible effect sizes for each voxel using an anisotropic unnormalized kernel, with the resultant effect size and error estimated using MetaNSUE.⁴⁹ A meta-analysis of the effect size metrics from the imputed datasets is then computed using Rubin’s rules to combine effect sizes in these datasets into a singular set of parameters that can be used for the final analysis (i.e. image derivation). Lastly, a permutation test is used to determine the distribution of possible maxima activations/deactivations found and this distribution is used to correct for multiple comparisons. Parameters were kept consistent with the above, with the exception of “modality,” which was changed to “other” to account for the heterogeneity of modalities employed in the studies selected. For example, in each group (GM, WM, adult, aged adult, and pediatric), SDM reported a specific set of MNI coordinates found to be statistically significant compared to the null hypothesis that there was no significant difference at that coordinate at various thresholds (including $p < 0.05$) and the direction of the difference (positive or negative).^{48,49} Output was provided in the form of coordinates that contributed to a peak coordinate exhibiting significance, the size of the region found to be significant (in voxels), and a general description of the region based on a standard atlas (i.e., right superior temporal gyrus, BA 42).^{48,49} The conclusion and interpretation of the SDM map are increases or decreases in GM or WM represented by p-values on brain coordinates.

2.5. Meta-regression longitudinal progression of GM and WM trajectories in hearing loss

To determine the longitudinal GM and WM trajectories associated with hearing loss, a random effects meta-regression was performed using Cohen’s d or Hedges’ g and the variability estimated with the standard deviation.²⁵ The specific question for this procedure is: how does GM and WM alterations change in hearing loss over the lifespan? The multivariate meta-regression covaried age, sample size = n with GM or WM metrics by ROI.

2.6. Heterogeneity of gray matter and white matter

To determine heterogeneity among measures (GM and WM metrics) between experiments,^{22–25} heterogeneity plots (forest plot, Baujat plot, Funnel plot, Galbraith plot and bubble plot), were constructed using R²⁶ packages meta^{27,28} and metafor.^{29,30} Heterogeneity allows determining the dispersion of a particular measure due to variability or uncertainty. The question for these procedures is: how does heterogeneity in a particular GM or WM metric effect generalizability to the ROI in hearing loss. The forest plot used Hedges' g to demonstrate effect size by measure (GM or WM) and included a summary estimate (centre of diamond) with 95% confidence intervals.⁵⁰ The reported metrics were Test for Heterogeneity χ^2 , Cochran's Q (computed by summing the squared deviations of each study's estimate from the overall meta-analytic estimate, weighting the contribution of each study by its inverse variance),⁵¹ and the value I^2 (the consistency of the results of studies in meta-analyses: $I^2 = 100$, where Q is Cochran's heterogeneity statistic).^{52,53} Cochran's Q is distributed as a chi-square statistic χ^2 with a P value.⁵² I^2 is scaled from 0% to 100% and interpreted as a value of 0% indicating no heterogeneity, and larger values show increasing heterogeneity.^{52,53} Effects were summarized across studies using the generic inverse-variance weighting method (DerSimonian and Laird random effects weighted by $1/SE^2 - standarderror$). Heterogeneity in results was estimated using the τ^2 statistic (standard deviation of effect sizes between studies).^{24,25} The Baujat plot was used to identify studies contributing to heterogeneity.⁵⁴ The X-axis represents the contribution of the measure (GM and WM) to the overall Cochran Q-test for heterogeneity. The Y-axis represents the influence of the measure (GM and WM), defined as the standardized squared difference between the treatment effects (acquired/congenital) estimated with and without the ith study.⁵⁴ The Baujat plot is interpreted as heterogeneous when influential measures (GM or WM) appear in the upper right quadrant of the graph.⁵⁴ The Funnel plot was used to illustrate 'bias', based on effect size estimates of GM and WM against sample size (plots have 95% CI in light grey and bias exists on $P < 0.1$).^{55–57} The Y-axis represents standard error (of the GM or WM metric, normalized across values [0 since we have not added mean and SD]) and the X-axis the residual value of the effect size. The degree of funnel plot asymmetry was measured by the intercept from regression of the standard normal deviates (odds ratio divided by its standard error) against the estimates precision.^{55–57} The funnel plot precision in estimating the underlying effect of the measure will increase as sample size increases and in the absence of bias the plotted effect size estimates will be scattered in the white region, resembling a symmetrical inverted funnel.^{55–57} To interpret the Funnel plot, bias is represented as asymmetry where GM or WM measures skew the results and therefore, are found outside of funnel CI area. The Galbraith plot (radial plot) was used to estimate metric (GM or WM) error.^{58–60} The Y-axis represents a transformed scale of standardized effect size estimates, centered at the reference value and having the unit standard error.^{58–60} The Y-axis for effect size has ± 2 standard error (shaded in grey) for any point estimate.^{58–60} The X-axis indicates precision (defined as reciprocal of standard error), where points with large error fall near the origin and points with small error are further away near the arc.^{58–60} On the right-hand side of the plot, an arc is drawn corresponding to the individual observed effect sizes (Hedges' g)^{58–60} A line projected from the origin (0,0) through a particular point within the plot onto this arc indicates the value of the individual observed effect size for that point.^{58–60} The interpretation of the Galbraith plot is made based on effect size scattering for GM and WM. If a set of effect size estimates agree with one another, in addition to having precision correctly assessed, they will scatter homoscedastically (with unit standard deviations on the y-scale) about a line through the origin.^{58–60} If the effect size estimates disagree with one another, they will vary heteroscedastically, resulting in statistical dispersion.^{58–60} Said another way, consistent effect size estimates are grouped closely together, while those that are uncertain are found as outliers. The bubble plot was used to display the results of the meta-regression of GM or WM with the bubble extent representing effect size and the regression dependent on the corresponding variable (ROI). The quantile-quantile (QQ) plot is used for testing normality of the data.⁶¹ Interpretation of the QQ plot is made by datapoints circumscribing the diagonal line within the confidence boundaries whereas data not normally distributed lies outside the 95% CI.⁶¹ The graphical display of study heterogeneity (GOSH) plots⁶² is a method to visualize the effect of study-level heterogeneity using a fixed-effects model between subset variable characteristics. The X-axis is the log ratio of the GM or WM metric and the Y-Axis is Cochran Q-statistic. The interpretation of GOSH plots is based on the model estimates forming a symmetric, contiguous, and unimodal distribution whereas a multimodal distribution suggests heterogeneity in GM or WM metrics.⁶² The bubble plot is interpreted by size of bubble having larger effect on the regression line for the metric (GM or WM). The heterogeneity

plot analyses will allow the determination of metric (GM or WM) variability or uncertainty.

2.7. Surface visualization of ROI mapping to create hearing loss endophenotype

Acquired and congenital multivariate meta-regression models by brain area were calculated. Random effects models covariated by main brain area were fitted to obtain the weights of left and right ROIs with GM or WM metrics. The resultant effect size estimates were backprojected to the respective brain area to create a meta-analytic endophenotype of hearing loss of GM and WM.⁶³ Here the effect size is visualized on the cortical surface with the meta-regression estimate per ROI derived from the meta-analysis.⁶³ Interpretation of the surface visualization is done with a cold-hot color bar which represents negative to positive effect sizes, respectively. Brain surface visualization and surface projection was done using Freesurfer and SurfStat⁶⁴ merging lobe mapping with an annotation file. A mixed effects model was used to account for the variation in GM or WM effect size metrics for a particular ROI within the congenital or acquired hearing loss groups. The meta-analytic test of moderators in the model determines whether we can reject the null hypothesis of no effect of GM or WM by ROI for congenital or acquired hearing loss in the constructed endophenotype.

2.8. Research statistical strategy: Analysis overview, hypothesis, assumptions, and interpretation

Our main research question was what are the structural manifestations of hearing loss? The research strategy followed a four-pronged approach. First, we assessed general and specific GM and WM alterations associated with where alterations occur in hearing loss. Second, we assessed general and specific ROI GM and WM longitudinal trends in hearing loss. Third, we wanted to understand the heterogeneity attributed to GM or WM by general and specific ROI. Lastly, we created a novel effect size meta-regression backplotting of the alterations in hearing loss to a cortical surface, in order to visualize the endophenotype of hearing loss. Studies were not excluded for any analysis, but discussed if considered biased (the Methods and SI Table 1 in the Supplemental Information). The overall null hypothesis for the analyses was no effect due to hearing loss for GM or WM. The effect size measure was used as the outcome variable. The alternative hypothesis was accepted if hearing loss effected GM or WM was $P < 0.05$, indicating the ROI was significantly altered. The assumptions underlying the statistics were normal distribution and datapoint effect size errors were independent and identically distributed. Nevertheless, a few studies contributed pseudoreplicated data by assessing the same patient population, albeit different GM and WM metrics. We did not note these metrics altering the results for any analysis. The unit of analysis was GM or WM metrics or effect size metrics such as Hedges' g.

3. References

1. Morton CC, Nance WE. Newborn hearing screening - A silent revolution. *N Engl J Med.* 2006 May 18;354(20):2151-64.
2. GBD 2017 Disease and Injury Incidence and Prevalence Collaborators. Global, regional, and national incidence, prevalence, and years lived with disability for 354 diseases and injuries for 195 countries and territories, 1990-2017: a systematic analysis for the Global Burden of Disease Study 2017. *Lancet.* 2018 Nov 10;392(10159):1789-1858.
3. Cunningham LL, Tucci DL. Hearing loss in adults. *N Engl J Med.* 2017 Dec 21;377(25):2465-2473.
4. Thompson DC, McPhillips H, Davis RL, Lieu TL, Homer CJ, Helfand M. Universal newborn hearing screening: summary of evidence. *JAMA.* 2001 Oct 24-31;286(16):2000-10.
5. Kral A, O'Donoghue GM. Profound deafness in childhood. *N Engl J Med.* 2010 Oct 7;363(15):1438-50.
6. Kral A, Kronenberger WG, Pisoni DB, O'Donoghue GM. Neurocognitive factors in sensory restoration of early deafness: a connectome model. *Lancet Neurol.* 2016 May;15(6):610-21.
7. Reed NS, Altan A, Deal JA, Yeh C, Kravetz AD, Wallhagen M, Lin FR. Trends in health care costs and utilization associated with untreated hearing loss over 10 Years. *JAMA Otolaryngol Head Neck Surg.* 2019;145(1):27-34.

8. Lin et al., Hearing loss and cognitive decline in older adults JAMA Intern Med. 2013 Feb 25;173(4):293-9.
9. Huddle et al., The economic impact of adult hearing loss: A systematic review. JAMA Otolaryngol Head Neck Surg. 2017 Oct 1;143(10):1040-1048.
10. Ferguson MA, Kitterick PT, Chong LY, Edmondson-Jones M, Barker F, Hoare DJ. Hearing aids for mild to moderate hearing loss in adults. Cochrane Database Syst Rev. 2017 Sep 25;9:CD012023.
11. Nichols TE, et al. Best practices in data analysis and sharing in neuroimaging using MRI. Nat Neurosci. 2017 Feb 23;20(3):299-303.
12. Tarabichi O, Kozin ED, Kanumuri VV, Barber S, Ghosh S, Sitek KR, Reinshagen K, Herrmann B, Remenschneider AK, Lee DJ. Diffusion tensor imaging of central auditory pathways in patients with sensorineural hearing loss: A systematic review. Otolaryngol Head Neck Surg. 2018;158(3):432-442.
13. Simon M, Campbell E, Genest F, MacLean MW, Champoux F and Lepore F (2020) The Impact of Early Deafness on Brain Plasticity: A Systematic Review of the White and Gray Matter Changes. *Front. Neurosci.* 14:206. doi: 10.3389/fnins.2020.00206
14. Ratnanather JT. Structural neuroimaging of the altered brain stemming from pediatric and adolescent hearing loss—Scientific and clinical challenges. Wiley Interdiscip Rev Syst Biol Med. 2020 Mar;12(2):e1469.
15. Feng G, Ingvalson EM, Grieco-Calub TM, Roberts MY, Ryan ME, Birmingham P, Burrowes D, Young NM, Wong PCM. Neural preservation underlies speech improvement from auditory deprivation in young cochlear implant recipients. Proc Natl Acad Sci U S A. 2018 Jan 30;115(5):E1022-E1031. <https://doi.org/10.1073/pnas.1717603115>
16. Ropers FG, Pham ENB, Kant SG, Rotteveel LJC, Rings EHJM, Verbist BM, Dekkers OM. Assessment of the clinical benefit of imaging in children with unilateral sensorineural hearing loss: A systematic review and meta-analysis. JAMA Otolaryngol Head Neck Surg 2019 [doi:10.1001/jamaoto.2019.0121]
17. Moore JK, Niparko JK, Miller MR, Linthicum FH. Effect of profound hearing loss on a central auditory nucleus. Am J Otol. 1994 Sep;15(5):588-95.
18. Moore JK, Niparko JK, Perazzo LM, Miller MR, Linthicum FH. Effect of adult-onset deafness on the human central auditory system. Ann Otol Rhinol Laryngol. 1997 May;106(5):385-90.
19. Kral A, Sharma A. Developmental neuroplasticity after cochlear implantation. Trends Neurosci. 2012 Feb;35(2):111-22.
20. Sanes DH, Woolley SMN. A behavioral framework to guide research on central auditory development and plasticity. Neuron. 2011 Dec 22;72(6):912-29.
21. Bavelier D, Neville HJ. Cross-modal plasticity: where and how? Nat Rev Neurosci. 2002 Jun;3(6):443-52.
22. Liberati A, et al. The PRISMA statement for reporting systematic reviews and meta-analyses of studies that evaluate healthcare interventions: explanation and elaboration. BMJ 2009;339:b2700 <https://doi.org/10.1136/bmj.b2700>; <http://prisma-statement.org/>
23. Moher D, Liberati A, Tetzlaff J, Altman DG, PRISMA Group. Preferred reporting items for systematic reviews and meta-analyses: the PRISMA statement. BMJ 2009;339:b2535 <https://doi.org/10.1136/bmj.b2535>
24. Higgins JPT, Green S, eds. Cochrane handbook for systematic reviews of interventions. John Wiley, 2008.
25. Borenstein M, Hedges LV, Higgins JPT, Rothstein H. Introduction to Meta-Analysis. Wiley, 2009.
26. R Core Team (2014). R: A language and environment for statistical computing. R Foundation for Statistical Computing, Vienna, Austria. URL <http://www.R-project.org/>.
27. Schwarzer G, Carpenter J, and Rücker G. (2015). Meta-Analysis with R. Springer.
28. Schwarzer G. (2015). meta: An R package for meta-analysis. R package version 4.9-2. <https://cran.r-project.org/web/packages/meta/>; <https://github.com/guido-s/meta>; <http://meta-analysis-with-r.org>;
29. Viechtbauer W. (2010). Conducting meta-analyses in R with the metafor package. J Stat Softw. 36(3):1-48. <https://wviechtb.github.io/metafor/>
30. Viechtbauer W. (2010). metafor: Meta-Analysis Package for R. R package version 2.0-0. <https://cran.r-project.org/web/packages/metafor/>
31. Adler et al., Community network for deaf scientists. Science. 2017 Apr 28;356(6336):386-387.
32. Cohen J. A power primer. Psychol Bull. 1992 Jul;112(1):155-9.
33. Hedges LV. (1983) A random effects model for effect sizes. Psychol Bull. 93:388-395.
34. Cohen J. (1988). Statistical power analysis for the behavioral sciences (2nd ed.). Hillsdale, NJ: Lawrence Erlbaum Associates.
35. Rosnow RL, Rosenthal R. (1996). Computing contrasts, effect sizes, and counternulls on other people's published data: General procedures for research consumers. Psychol Methods. 1(4), 331-340.
36. Rosnow RL, Rosenthal R. (2003). Effect sizes for experimenting psychologists. Can J Exp Psychol. 57(3), 221-237.
37. Zar JH. (1999) Biostatistical analysis. Fourth Edition. Prentice Hall, New Jersey.
38. Jansen A, et al. Menke R, Sommer J, Förster AF, Bruchmann S, Hempleman J, Weber B, Knecht S. (2006). The assessment of hemispheric lateralization in functional MRI—robustness and reproducibility. Neuroimage.

- 33(1):204-17.
39. Radua J, Mataix-Cols D. Voxel-wise meta-analysis of grey matter changes in obsessive-compulsive disorder. *Br J Psychiatry*. 2009; 195:393–402.
 40. Radua J, van den Heuvel OA, Surguladze S, Mataix-Cols D. Meta-analytical comparison of voxel based morphometry studies in obsessive-compulsive disorder vs other anxiety disorders. *Arch Gen Psychiatry*. 2010; 67:701–711.
 41. Fox PT, Lancaster JL. Mapping context and content: the BrainMap model. *Nat Rev Neurosci*. 2002 Apr;3(4):319-21. [<http://www.brainmap.org/ale/>] [Archived copy <https://osf.io/7y59j/>].
 42. Eickhoff SB, Laird AR, Grefkes C, Wang LE, Zilles K, Fox PT. Coordinate-based activation likelihood estimation meta-analysis of neuroimaging data: A random-effects approach based on empirical estimates of spatial uncertainty. *Hum Brain Mapp*. 2009 Sep;30(9):2907-26.
 43. Turkeltaub PE, Eickhoff SB, Laird AR, Fox M, Wiener M, Fox P. Minimizing within-experiment and within-group effects in Activation Likelihood Estimation meta-analyses. *Hum Brain Mapp*. 2012 Jan;33(1):1-13.
 44. Eickhoff SB, Bzdok D, Laird AR, Kurth F, Fox PT. Activation likelihood estimation meta-analysis revisited. *Neuroimage*. 2012 Feb 1;59(3):2349-61.
 45. Wager TD, Lindquist M, Kaplan L. Meta-analysis of functional neuroimaging data: Current and future directions. *Soc Cogn Affect Neurosci*. 2007 Jun;2(2):150-8.
 46. Wager TD, Lindquist MA, Nichols TE, Kober H, Van Snellenberg JX. Evaluating the consistency and specificity of neuroimaging data using meta-analysis. *Neuroimage*. 2009 Mar;45(1 Suppl):S210-21.
 47. Radua J, Mataix-Cols D, Phillips ML, El-Hage W, Kronhaus DM, Cardoner N and Surguladze S. A new meta-analytic method for neuroimaging studies that combines reported peak coordinates and statistical parametric maps. *Eur Psychiatry* 2012; 27:605–611.
 48. Radua J, van den Heuvel OA, Surguladze S, Mataix-Cols D. Meta-analytical comparison of voxel based morphometry studies in obsessive-compulsive disorder vs other anxiety disorders. *Arch Gen Psychiatry*. 2010; 67:701–711.
 49. Albajes-Eizagirre A, Solanes A, Radua J. Meta-analysis of Non-statistically Significant Unreported Effects (MetaNSUE). *Stat Methods Med Res*. 2019 Dec;28(12):3741-3754.
 50. Riley RD, Higgins JP, Deeks JJ. Interpretation of random effects meta-analyses. *BMJ*. 2011 Feb 10;342:d549.
 51. Cochran WG. The combination of estimates from different experiments. *Biometrics* 1954;10:101-29.
 52. Higgins JP, Thompson SG. Quantifying heterogeneity in a meta-analysis. *Stat Med*. 2002 Jun 15;21(11):1539-58.
 53. Higgins JP, Thompson SG, Deeks JJ, Altman DG. Measuring inconsistency in meta-analyses. *BMJ*. 2003 Sep 6;327(7414):557-60.
 54. Baujat B, Mahé C, Pignon JP, Hill C. (2002). A graphical method for exploring heterogeneity in meta-analyses: Application to a meta-analysis of 65 trials. *Stat Med* 21(18):2641–2652.
 55. Egger M, Davey Smith G, Schneider M, Minder C. Bias in meta-analysis detected by a simple, graphical test. *BMJ*. 1997 Sep 13;315(7109):629-34.
 56. Sterne JA, Egger M. Funnel plots for detecting bias in meta-analysis: guidelines on choice of axis. *J Clin Epidemiol*. 2001 Oct;54(10):1046-55.
 57. Lau J, Ioannidis JP, Terrin N, Schmid CH, Olkin I. The case of the misleading funnel plot. *BMJ*. 2006 Sep 16;333(7568):597-600.
 58. Galbraith R (1988a). Graphical display of estimates having differing standard errors. *Technometrics*. 30 (3): 271–281.
 59. Galbraith RF. (1988b). A note on graphical presentation of estimated odds ratios from several clinical trials. *Stat Med*. 7(8): 889–894.
 60. Galbraith RF. (1994). Some applications of radial plots. *J Am Stat Assoc*. 89(428):1232–1242.
 61. Wang MC, Bushman BJ. (1998). Using the normal quantile plot to explore meta-analytic data sets. *Psychol Methods*. 3(1):46–54.
 62. Olkin I, Dahabreh IJ, Trikalinos TA. (2012). GOSH - a graphical display of study heterogeneity. *Res Synth Methods*. 3(3):214–223.
 63. Waskom M, Gramfort A, Burns S, Luessi M, Larson E. PySurfer: Python Neuroimaging Visualization. Python package version 0.9.0. <https://pysurfer.github.io/>; <https://github.com/nipy/PySurfer>
 64. Worsley KJ, Taylor JE, Carbonell F, Chung MK, Duerden E, Bernhardt B, Lyttelton O, Boucher M, Evans AC. SurfStat: A Matlab toolbox for the statistical analysis of univariate and multivariate surface and volumetric data using linear mixed effects models and random field theory. *NeuroImage*, 47 (Supplement 1) July 2009, S39-S41. [https://doi.org/10.1016/S1053-8119\(09\)70882-1](https://doi.org/10.1016/S1053-8119(09)70882-1)
 65. Smith KM, Mecoli MD, Altaye M, Komlos M, Maitra R, Eaton KP, Egelhoff JC, Holland SK. Morphometric differences in the Heschl's gyrus of hearing impaired and normal hearing infants. *Cereb Cortex*. 2011;21(5):991-8. <https://doi.org/10.1093/cercor/bhq164>

66. Zheng W, Wu C, Huang L, Wu R. Diffusion kurtosis imaging of microstructural alterations in the brains of paediatric patients with congenital sensorineural hearing loss. *Sci Rep* 2017;7:1543. <https://doi.org/10.1038/s41598-017-01263-9>
67. Feng G, Ingvalson EM, Grieco-Calub TM, Roberts MY, Ryan ME, Birmingham P, Burrowes D, Young NM, Wong PCM. Neural preservation underlies speech improvement from auditory deprivation in young cochlear implant recipients. *Proc Natl Acad Sci U S A.* 2018;115(5):E1022-E1031. <https://doi.org/10.1073/pnas.1717603115>
68. Li J, Li W, Xian J, Li Y, Liu Z, Liu S, Wang X, Wang Z, He H. Cortical thickness analysis and optimized voxel-based morphometry in children and adolescents with prelingually profound sensorineural hearing loss. *Brain Res.* 2012;1430:35-42. <https://doi.org/10.1016/j.brainres.2011.09.057>
69. Li W, Li J, Wang Z, Li Y, Liu Z, Yan F, Xian J, He H. Grey matter connectivity within and between auditory, language and visual systems in prelingually deaf adolescents. *Restor Neurol Neurosci.* 2015;33(3):279-90. <https://doi.org/10.3233/rnn-140437>
70. Li W, Li J, Xian J, Lv B, Li M, Wang C, Li Y, Liu Z, Liu S, Wang Z, He H, Sabel BA. Alterations of grey matter asymmetries in adolescents with prelingual deafness: A combined VBM and cortical thickness analysis. *Restor Neurol Neurosci.* 2013;31(1):1-17. <https://doi.org/10.3233/RNN-2012-120269>
71. Liu Z.-H, Li M, Xian J.-F, He H.-G, Z.-C, Li Y, Li J.-H, Wang X.-C, Liu S. Investigation of the white matter with tract-based spatial statistics in congenitally deaf patients. *Chinese Journal of Medical Imaging Technology.* 2010; 26(7):1226-1229.
72. Miao W, Li J, Tang M, Xian J, Li W, Liu Z, Liu S, Sabel BA, Wang Z, He H. Altered white matter integrity in adolescents with prelingual deafness: A high-resolution tract-based spatial statistics imaging study. *AJNR Am J Neuroradiol.* 2013;34(6):1264-70. <https://doi.org/10.3174/ajnr.a3370>
73. Wenjing Li, Yong Li, Junxi X, Zhaoxue L, Xiaocui W, Sha L, Zhenchang W, Huiguang H. A voxel-based morphometric analysis of brain in congenitally deaf patients. *J Clin Rad.* 2010; 29(2):166-169. <https://doi.org/10.13437/j.cnki.jcr.2010.02.031>
74. Xia S, Qi J, Li Q. High-resolution MR study of auditory cortex in prelingual sensorineural hearing loss. *Chinese Journal of Medical Imaging Technology.* 2008; 24(11):1705-1707.
75. Xia S, Qi J. The study of diffusion weighted imaging and MR spectroscopy in auditory cortex and related area of prelingual hearing-loss patients. *Chinese Journal of Radiology.* 2008; 42(7):702-705.
76. Li J, Li W, Xian J, Li Y, Liu Z, Liu S, Wang X, Wang Z, He H. Cortical thickness analysis and optimized voxel-based morphometry in children and adolescents with prelingually profound sensorineural hearing loss. *Brain Res.* 2012;1430:35-42. <https://doi.org/10.1016/j.brainres.2011.09.057>
77. Li W, Li J, Wang Z, Li Y, Liu Z, Yan F, Xian J, He H. Grey matter connectivity within and between auditory, language and visual systems in prelingually deaf adolescents. *Restor Neurol Neurosci.* 2015;33(3):279-90. <https://doi.org/10.3233/rnn-140437>
78. Li W, Li J, Xian J, Lv B, Li M, Wang C, Li Y, Liu Z, Liu S, Wang Z, He H, Sabel BA. Alterations of grey matter asymmetries in adolescents with prelingual deafness: A combined VBM and cortical thickness analysis. *Restor Neurol Neurosci.* 2013;31(1):1-17. <https://doi.org/10.3233/RNN-2012-120269>
79. Liu Z.-H, Li M, Xian J.-F, He H.-G, Z.-C, Li Y, Li J.-H, Wang X.-C, Liu S. Investigation of the white matter with tract-based spatial statistics in congenitally deaf patients. *Chinese Journal of Medical Imaging Technology.* 2010; 26(7):1226-1229.
80. Miao W, Li J, Tang M, Xian J, Li W, Liu Z, Liu S, Sabel BA, Wang Z, He H. Altered white matter integrity in adolescents with prelingual deafness: A high-resolution tract-based spatial statistics imaging study. *AJNR Am J Neuroradiol.* 2013;34(6):1264-70. <https://doi.org/10.3174/ajnr.a3370>
81. Tae, W.-S. 2015. Reduced gray matter volume of auditory cortical and subcortical areas in congenitally deaf adolescents: A voxel-based morphometric study. *Investig Magn Reson Imaging* 19, 1-9. <https://doi.org/10.13104/imri.2015.19.1.1>
82. Chang Y, Lee SH, Lee YJ, Hwang MJ, Bae SJ, Kim MN, Lee J, Woo S, Lee H, Kang DS. Auditory neural pathway evaluation on sensorineural hearing loss using diffusion tensor imaging. *Neuroreport.* 2004;15(11):1699-703. <https://doi.org/10.1097/01.wnr.0000134584.10207.1a>
83. Huang L, Zheng W, Wu C, Wei X, Wu X, Wang Y, Zheng H. Diffusion tensor imaging of the auditory neural pathway for clinical outcome of cochlear implantation in pediatric congenital sensorineural hearing loss patients. *PLoS One.* 2015;10(10):e0140643. <https://doi.org/10.1371/journal.pone.0140643>
84. Shi B, Yang LZ, Liu Y, Zhao SL, Wang Y, Gu F, Yang Z, Zhou Y, Zhang P, Zhang X. Early-onset hearing loss reorganizes the visual and auditory network in children without cochlear implantation. *Neuroreport.* 2016;27(3):197-202. <https://doi.org/10.1097/wnr.0000000000000524>
85. Chinnadurai V, Sreedhar CM, Khushu S. Assessment of cochlear nerve deficiency and its effect on normal maturation of auditory tract by diffusion kurtosis imaging and diffusion tensor imaging: A correlational approach. *Magn Reson Imaging.* 2016;34(9):1305-1313. <https://doi.org/10.1016/j.mri.2016.07.010>

86. Wu C, Huang L, Tan H, Wang Y, Zheng H, Kong L, Zheng W. Diffusion tensor imaging and MR spectroscopy of microstructural alterations and metabolite concentration changes in the auditory neural pathway of pediatric congenital sensorineural hearing loss patients. *Brain Res.* 2016;1639:228-34. <https://doi.org/10.1016/j.brainres.2014.12.025>
87. Emmorey K, Allen JS, Bruss J, Schenker N, Damasio H. A morphometric analysis of auditory brain regions in congenitally deaf adults. *Proc Natl Acad Sci U S A.* 2003;100(17):10049-54. <https://doi.org/10.1073/pnas.1730169100>
88. Penhune VB, Cismaru R, Dorsaint-Pierre R, Petitto LA, Zatorre RJ. The morphometry of auditory cortex in the congenitally deaf measured using MRI. *Neuroimage.* 2003;20(2):1215-25. [https://doi.org/10.1016/s1053-8119\(03\)00373-2](https://doi.org/10.1016/s1053-8119(03)00373-2)
89. Shibata DK. Differences in brain structure in deaf persons on MR imaging studied with voxel-based morphometry. *AJNR Am J Neuroradiol.* 2007;28(2):243-9.
90. Meyer M, Toepel U, Keller J, Nussbaumer D, Zysset S, Friederici AD. Neuroplasticity of sign language: implications from structural and functional brain imaging. *Restor Neurol Neurosci.* 2007;25(3-4):335-51.
91. Meyer M, Toepel U, Keller J, Nussbaumer D, Zysset S, Friederici AD. Neuroplasticity of sign language: implications from structural and functional brain imaging. *Restor Neurol Neurosci.* 2007;25(3-4):335-51.
92. Leporé N, Vachon P, Lepore F, Chou YY, Voss P, Brun CC, Lee AD, Toga AW, Thompson PM. 3D mapping of brain differences in native signing congenitally and prelingually deaf subjects. *Hum Brain Mapp.* 2010;31(7):970-8. <https://doi.org/10.1002/hbm.20910>
93. Allen JS, Emmorey K, Bruss J, Damasio H. Morphology of the insula in relation to hearing status and sign language experience. *J Neurosci.* 2008;28(46):11900-5. <https://doi.org/10.1523/jneurosci.3141-08.2008>
94. Allen JS, Emmorey K, Bruss J, Damasio H. Neuroanatomical differences in visual, motor, and language cortices between congenitally deaf signers, hearing signers, and hearing non-signers. *Front Neuroanat.* 2013;7:26. <https://doi.org/10.3389/fnana.2013.00026>
95. Olulade OA, Koo DS, LaSasso CJ, Eden GF. Neuroanatomical profiles of deafness in the context of native language experience. *J Neurosci.* 2014;34(16):5613-20. <https://doi.org/10.1523/jneurosci.3700-13.2014>
96. Kim et al. J, Choi JY, Eo J, Park HJ. Comparative evaluation of the white matter fiber integrity in patients with prelingual and postlingual deafness. *Neuroreport.* 2017;28(16):1103-1107. <https://doi.org/10.1097/wnr.0000000000000894>
97. Geschwind N, Levitsky W. Human brain: left-right asymmetries in temporal speech region. *Science.* 1968;161(3837):186-7. <https://doi.org/10.1126/science.161.3837.186>
98. Geschwind N. The organization of language and the brain. *Science.* 1970;170(3961):940-4. <https://doi.org/10.1126/science.170.3961.940>
99. Geschwind N, Galaburda AM. Cerebral lateralization. Biological mechanisms, associations, and pathology: I. A hypothesis and a program for research. *Arch Neurol.* 1985a May;42(5):428-59. <https://doi.org/10.1001/archneur.1985.04060050026008>
100. Geschwind N, Galaburda AM. Cerebral lateralization. Biological mechanisms, associations, and pathology: II. A hypothesis and a program for research. *Arch Neurol.* 1985b Jun;42(6):521-52. <https://doi.org/10.1001/archneur.1985.04060060019009>
101. Geschwind N, Galaburda AM. Cerebral lateralization. Biological mechanisms, associations, and pathology: III. A hypothesis and a program for research. *Arch Neurol.* 1985c Jul;42(7):634-54. <https://doi.org/10.1001/archneur.1985.04060070024012>
102. Kral A, Hartmann R, Tillein J, Heid S, Klinke R. (2000). Congenital auditory deprivation reduces synaptic activity within the auditory cortex in a layer-specific manner. *Cereb Cortex.* 2000 Jul;10(7):714-26.
103. Crow TJ. The 'big bang' theory of the origin of psychosis and the faculty of language. *Schizophr Res.* 2008;102(1-3):31-52. <https://doi.org/10.1016/j.schres.2008.03.010>
104. Crow TJ. The XY gene hypothesis of psychosis: origins and current status. *Am J Med Genet B Neuropsychiatr Genet.* 2013;162B(8):800-24. <https://doi.org/10.1002/ajmg.b.32202>
105. Van Essen DC. A tension-based theory of morphogenesis and compact wiring in the central nervous system. *Nature.* 1997;385(6614):313-8. <https://doi.org/10.1038/385313a0>
106. Amaral L, Gelho-Ávila A, Osório A, Soares MJ, He D, Chen Q, Mahon BZ, Gonçalves OF, Sampaio A, Fang F, Bi Y, Almeida J. Hemispheric asymmetries in subcortical visual and auditory relay structures in congenital deafness. *Eur J Neurosci.* 2016;44(6):2334-9. <https://doi.org/10.1111/ejn.13340>
107. Karns CM, Stevens C, Dow MW, Schorr EM, Neville HJ. Atypical white-matter microstructure in congenitally deaf adults: A region of interest and tractography study using diffusion-tensor imaging. *Hear Res.* 2017;343:72-82. <https://doi.org/10.1016/j.heares.2016.07.008>
108. Shiell MM, Zatorre RJ. White matter structure in the right planum temporale region correlates with visual motion detection thresholds in deaf people. *Hear Res.* 2017;343:64-71. <https://doi.org/10.1016/j.heares.2016.06.011>
109. Shiell MM, Champoux F, Zatorre RJ. The right hemisphere planum temporale supports enhanced visual motion detection ability in deaf people the right hemisphere planum temporale supports enhanced visual motion detection ability in deaf people. *Neural Plasticity* 2016; 7217630. <https://doi.org/10.1155/2016/7217630>

110. Boyen K, Langers DR, de Kleine E, van Dijk P. Gray matter in the brain: Differences associated with tinnitus and hearing loss. *Hear Res.* 2013 Jan;295:67-78. <https://doi.org/10.1016/j.heares.2012.02.010>
111. Luan Y, Wang C, Jiao Y, Tang T, Zhang J, Teng GJ. Prefrontal-temporal pathway mediates the cross-modal and cognitive reorganization in sensorineural hearing loss with or without tinnitus: A multimodal MRI study. *Front Neurosci.* 2019 Mar 12;13:222. <https://doi.org/10.3389/fnins.2019.00222>
112. Husain FT, Medina RE, Davis CW, Szymko-Bennett Y, Simonyan K, Pajor NM, Horwitz B. Neuroanatomical changes due to hearing loss and chronic tinnitus: a combined VBM and DTI study. *Brain Res.* 2011 Jan 19;1369:74-88. <https://doi.org/10.1016/j.brainres.2010.10.095>
113. Peelle JE, Troiani V, Grossman M, Wingfield A. Hearing loss in older adults affects neural systems supporting speech comprehension. *J Neurosci.* 2011 Aug 31;31(35):12638-43. <https://doi.org/10.1523/jneurosci.2559-11.2011>
114. Lin FR, Ferrucci L, An Y, Goh JO, Doshi J, Metter EJ, Davatzikos C, Kraut MA, Resnick SM. Association of hearing impairment with brain volume changes in older adults. *Neuroimage.* 2014 Apr 15;90:84-92. <https://doi.org/10.1016/j.neuroimage.2013.12.059>
115. Rigters SC, Bos D, Metselaar M, Roshchupkin GV, Baatenburg de Jong RJ, Ikram MA, Vernooij MW, Goedegebure A. Hearing impairment is associated with smaller brain volume in aging. *Front Aging Neurosci.* 2017 Jan 20;9:2 <https://doi.org/10.3389/fnagi.2017.00002>
116. Rigters SC, Creemers LGM, Ikram MA, van der Schroeff MP, de Groot M, Roshchupkin GV, Niessen WJN, Baatenburg de Jong RJ, Goedegebure A, Vernooij MW. White-matter microstructure and hearing acuity in older adults: a population-based cross-sectional DTI study. *Neurobiol Aging.* 2018 Jan;61:124-131
117. Pereira-Jorge MR, Andrade KC, Palhano-Fontes FX, Diniz PRB, Sturzbecher M, Santos AC, Araujo DB. Anatomical and functional MRI changes after one year of auditory rehabilitation with hearing aids. *Neural Plast.* 2018 Sep 10;2018:9303674. <https://doi.org/10.1155/2018/9303674>

Literature research

- Literature Search Methodology (eFigure PRISMA)
 1. PubMed searches were performed to acquire the requisite background information for this review. The searches had the purpose of identifying all sources concerning structural MRI assessments of unilateral or bilateral hearing loss. All studies must have utilized MRI as a structural assessment for hearing loss.
 2. Search Terminology: "*Unilateral hearing loss OR single-sided deafness, "Bilateral hearing loss OR deafness", "AND MRI OR magnetic resonance imaging*"
- First Search Oct/Nov 2012
 1. A literature search in PubMed using MeSH and truncated (wildcard) terms was performed for studies pertaining to “unilateral hearing loss” or “bilateral hearing loss on Wed October 10, 2012 through Thurs November 1, 2012. The literature search returned precisely 3,057 results. All abstracts returned were read for descriptions of congenital unilateral/bilateral hearing loss using MRI. Approximately, 905 studies meet the following inclusion criteria. These studies were surveyed to ascertain whether they were relevant for inclusion based on the ‘Review inclusion criteria.’
 2. The primary inclusion and exclusion criteria were predetermined by following recommendations on meta-analysis (Sutton, et al., 2000)
- Inclusion criteria
 1. Structural MRI study of bilateral or unilateral hearing loss
 2. Study had at least one cohort of participants whom had congenital unilateral/bilateral hearing loss
 3. The study, with a cohort of hearing impaired participants, had an adequate hearing control
 4. The normal hearing controls were sufficiently matched to the hearing impaired cohort (i.e age, gender, education, etc.)
 5. An experiment comparing the two cohorts was performed consisting of, but not limited to, MRI structural assessment
- Exclusion criteria

1. All studies were first included in the review and then given an asterisk if deemed inappropriate for inclusion.
 2. Case studies (i.e., reports with only one patient)
 3. Manuscripts with insufficient power of replication (i.e., manuscript with 2 patients)
 4. Manuscripts with an inadequate or absent normal hearing control cohort (i.e., no control cohort was reported) – indicated in table.
 5. Normal hearing control cohort lacked matching demographic characteristics (i.e. the study had a group of hearing loss pediatric children and the normal hearing control group was adults)
 6. Manuscripts without an experiment comparing the hearing loss and normal cohort (i.e., bilateral hearing loss was not compared to hearing controls).
- Second Search June/July 2018
 1. Searches from first search and second search were combined along with personal correspondences of articles from JTR.
 2. Pubmed; (deafness OR "hearing loss" OR "bilateral hearing loss" OR "unilateral hearing loss" OR "conductive hearing loss" OR "sensorineural hearing Loss") AND ("magnetic resonance imaging" OR MRI OR DTI OR "diffusion tensor imaging") NOT (Review[Filter] OR Editorial[Filter] OR Comment[Filter])
 3. Returned 4,179 articles. Articles were checked again throughout June/July 2018. Final article list was checked through Scopus.
 4. All references we checked at date indicated in table.
 5. Approximately 911 studies meet inclusion criteria
 6. Approximately 178 studies were screened from both periods and invited
 7. Approximately 118 were excluded based on exclusion criteria or not pertaining to inclusion criteria
 8. A total of 51 studies were analyzed
 - Controls
 - Our requirements for duplicated studies were studies which used the identical participants but had different methodology, participants age was identical, or it was stated participants were used by authors in two studies
 - Only included original statistics here from the studies. All derived effect sizes were from study information. Asymmetry statistics were created if a study included a left and a right side for an identical ROI. Statistics from our analysis could be derived from, example asymmetry as indicated above.
 - Asymmetry if included was converted to: only for asymmetry (check asymmetry) $(L - R) /[(L+R)/2]$, where positive result = LEFT, negative result = RIGHT
 - If studies included acquired and congenital we only used congenital metrics.

Figure SI.1 Flow diagram

Eligibility Criteria for the meta-regression

We included peer-review publications in English, involving patients with bilateral congenital and mixed hearing loss and controls with structural Magnetic Resonance Imaging. We included cross-sectional studies with control groups, that investigated the structural relation between MRI changes and the hearing loss. The most common MRI measures were **volume**, **FA**, **VBM** and **thickness**. Each measure was assigned to a specific ROI and to a big brain area. (eg. HG and superior temporal lobe belong to **temporal lobe**). A total of 59 studies were included, 6 of them contained incomplete information. A total of 2778 patients and 4214 controls.

Notes for inclusion:

1. Xia et al. Chin J Rad, 2008 was excluded because it appears to be the same data as Xia et al. Chin J Med Img Tech, 2008.

Figure S1-1 | Flow Diagram

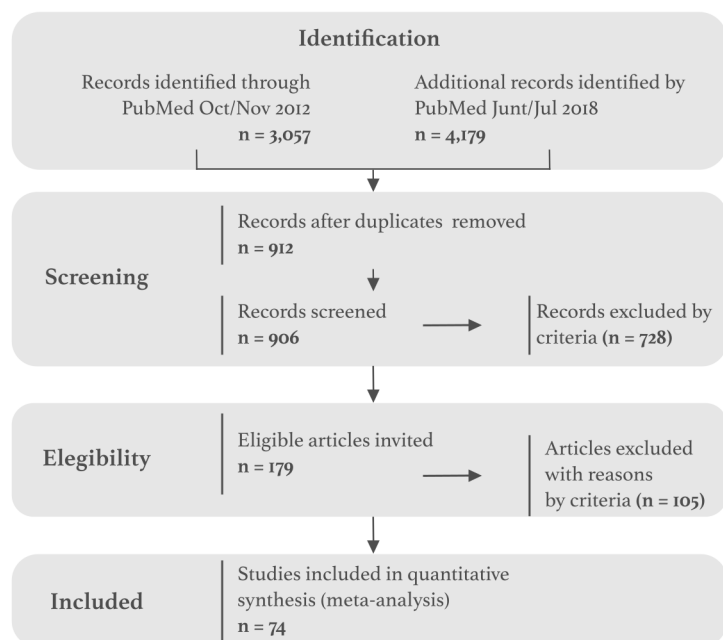


Figure 1: Flowchart of data-acquisition* All available bilateral/unilateral studies were analyzed.

2. Kim et al. Hear Res 2014 used two groups *prelingual deaf* and *post lingual deaf*, we used the average for the main table.
3. Xia et al. Chin J Med Img Tech, 2008 had 40 patients in total, in two groups 9-12 years and 19-22 years.
4. For some studies (eg. 2017, Ritgers et al. Front. Aging Neurosci) it was not possible to calculate the Hegdes'G variance and were not include in some specific meta-regressions.
5. Studies with *Mixed etiology* were excluded, due to a non representative low number (n=3).
6. Zheng et al. Sci Rep, 2017 this variables change; Con rangeLow Con rangeHigh.

Tables of included studies

A total of **64** unique bilateral studies were included (19 acquires, 42 congenital and 3 mixed etiologies).

Table 1: Total unique studies 64

	Hearing Loss	Healthy
Total number of patients	7445	2924
Number mean	116.3	51.3
Number sd	479.3	204.3
Age mean	34.92	30.61
Age SD	23.08	19.45
%Female mean	50.41	54.97
%Female sd	12.2	12.64

Table 2: Acquired studies 19

	Hearing Loss	Healthy
Total number of patients	6469	1899
Number mean	340.5	146.1
Number sd	853.3	426.1
Age mean	65.31	56.44
Age SD	8.254	11.97
%Female mean	47.51	53.65
%Female sd	14.86	11.86

Table 3: Congenital studies 42

	Hearing Loss	Healthy
Total number of patients	927	976
Number mean	22.07	23.8
Number sd	17.06	14.63
Age mean	21.55	21.97
Age SD	12.21	12.68
%Female mean	51.16	55.23
%Female sd	10.95	13.2

Table 4: Mixed studies 3

	Hearing Loss	Healthy
Total number of patients	49	49
Number mean	16.33	16.33
Number sd	0.5774	0.5774
Age mean	25.26	25.13
Age SD	18.53	17.97
%Female mean	56.86	56.86
%Female sd	11.89	11.89

Table 5: Studies without Hedges'G (n=7). These studies do not have control population (NA)

Source	Etiology	Number.Control
2011, Peelle et al. J Neurosci	acquired	NA
2012, Chang et al., Clin Exp Otorhinolaryngol	congenital	NA
2012, Eckert et al. J Assoc Res Otolaryngol	acquired	NA
2013, Eckert et al. J Assoc Res Otolaryngol	acquired	NA
2017, Qian et al. Neuroimage Clin	acquired	NA
2017, Ritgers et al. Front. Aging Neurosci	acquired	NA
2018, Ritgers et al. Neurobiol Aging	acquired	NA

Table 6: Studies with Hedges'G (n=57, mixed etiology=3)

Source	Etiology	all.techniques	all.measures
2010, Liu et al. Chin J Med Img Tech	congenital	CT	FA
2012, Li et al. Brain Res	congenital	CT	Thickness
2015, Li et al. Restor Neurol Neurosci	mixed	CT	volume
2016, Shiell et al. Neural Plasticity	congenital	CT	Thickness
2016, Smittenaar et al. Open Neuroimaging J	congenital	CT	CT
2018, Ren et al. Front Neurosci	acquired	CT, VBM	Thickness, volume
2004, Chang et al. Neuroreport	congenital	DTI	asymmetry, FA
2009, Wang et al. Chin J Med Img Tech	congenital	DTI	FA
2012, Li et al. Hum Brain Mapp	congenital	DTI	AD, FA, RD
2013, Miao et al. Am J Neuroradiol	congenital	DTI	FA, RD
2014, Lyness et al. Neuroimage	congenital	DTI	FA, MD, RD
2015, Huang et al. PLoS One	congenital	DTI	FA, MD
2016, Chinnadurai et al. Magn Reson Imaging	congenital	DTI	AD, Axial Kurtosis, FA, Mean Kurtosis, Radial Kurtosis, RD
2016, Ma et al. AJNR Am J Neuroradiol	acquired	DTI	AD, FA, MD, RD
2017, Karns et al. Hear Res	congenital	DTI	AD, FA, RD, volume
2017, Kim et al. Neuroreport	congenital	DTI	FA
2017, Shiell & Zatorre. Hear Res	congenital	DTI	AD, MD, RD, volume
2017, Zheng et al. Sci Rep	congenital	DTI	FA, Mean Kurtosis
2018, Benetti et al. Neuroimage	congenital	DTI	AD, FA, RD
2018, Park et al. Biomed Res Int	congenital	DTI	FA
2018, Zou et al. Otol Neurotol	congenital	DTI	AK, FA, MK, RK
2009, Kim et al. Neuroreport	congenital	DTI, VBM	FA, volume
2010, Husain et al. Brain Res	acquired	DTI, VBM	FA, volume
2014, Hribar et al. Hear Res	congenital	DTI, VBM	AD, FA, Thickness
2014, Profant et al. Neuroscience	acquired	DTI, VBM	AD, CT, FA, MD, RD, Surface, volume
2019, Luan et al. Front Neurosci	acquired	DTI, VBM	FA, MD, volume
2000, Bavelier et al. J Neurosci	congenital	VBM	volume
2003, Emmorey et al. PNAS	congenital	VBM	asymmetry, GM+WM, ratio
2003, Penhune et al. Neuroimage	congenital	VBM	GM/WM, volume
2006, Kara et al. J Neuroradiol	congenital	VBM	asymmetry, ratio GM/WM, volume
2007, Meyer et al. Restor Neurol Neurosci	congenital	VBM	length, Thickness, volume
2007, Shibata DK. Am J Neuroradiol	congenital	VBM	volume
2008, Allen et al. J Neurosci	congenital	VBM	asymmetry, ratio GM/WM, Vol proportion, volume
2008, Xia et al. Chin J Med Img Tech	congenital	VBM	volume
2010, Leporé et al. Hum Brain Mapp	congenital	VBM	VBM
2010, Li, et al. J Clin Rad	congenital	VBM	volume
2011, Smith et al. Cereb Cortex	congenital	VBM	asymmetry, ratio GM/WM, volume
2013, Allen et al. Front Neuroanat	congenital	VBM	asymmetry, volume
2013, Boyen et al. Hear Res	acquired	VBM	volume
2013, Li et al. Restor Neurol Neurosci	mixed	VBM	Thickness
2013, Pénicaud et al. Neuroimage	congenital	VBM	volume
2014, Kim et al. Hear Res	congenital	VBM	volume

Source	Etiology	all.techniques	all.measures
2014, Lin et al. Neuroimage	acquired	VBM	volume
2014, Olulade et al. J Neurosci	congenital	VBM	volume
2015, Tae Investig Magn Reson Imaging	congenital	VBM	VBM
2016, Amaral et al. Eur J Neurosci	congenital	VBM	asymmetry, Thickness
2016, Shi et al. Neuroreport	congenital	VBM	volume
2016, Wu et al. Brain Res	congenital	VBM	ADC, FA
2018, Alfandari et al. Trends Hear	mixed	VBM	volume
2018, Chen et al. Behav Neurosci	acquired	VBM	volume
2018, Feng et al. PNAS	congenital	VBM	VBM
2018, Kumar U, Mishra M. Brain Res Plast	congenital	VBM	Thickness, VBM
2018, Pereira-Jorge et al. Neural	acquired	VBM	volume
2018, Uchida et al. Front Aging Neurosci	acquired	VBM	volume
2019, Belkhiria et al. Front. Aging Neurosci	acquired	VBM	CT, volume
2019, Ponticorvo et al. Hum Brain Mapp	acquired	VBM	volume
2019, Xu et al. J Magn Reson Imaging	acquired	VBM	volume

Unusual MRI measurements

Table 7: Studies Measuring White Matter Thickness (n=4)

Source	MRI measure	Matter	Brain area	Side	ROI
2012, Li et al. Brain Res	Thickness	WM	frontal	left	middle frontal gyrus
2012, Li et al. Brain Res	Thickness	WM	occipital	right	inferior occipital gyrus
2014, Hribar et al. Hear Res	Thickness	WM	temporal	left	HG
2006, Kara et al. J Neuroradiol	Thickness	WM	corpus callosum	bilateral	corpus callosum (anterior thickness)
2006, Kara et al. J Neuroradiol	Thickness	WM	corpus callosum	bilateral	corpus callosum (middle thickness)
2006, Kara et al. J Neuroradiol	Thickness	WM	corpus callosum	bilateral	corpus callosum (posterior thickness)
2006, Kara et al. J Neuroradiol	Thickness	WM	corpus callosum	bilateral	corpus callosum genu
2006, Kara et al. J Neuroradiol	Thickness	WM	corpus callosum	bilateral	splenium of corpus callosum
2018, Kumar U, Mishra M. Brain Res	Thickness	WM	temporal	left	STG
2018, Kumar U, Mishra M. Brain Res	Thickness	WM	temporal	right	STG

Table 8: Studies Measuring Gray Matter FA (n=2)

Source	MRI measure	Matter	Brain area	Side	ROI
2019, Luan et al. Front Neurosci	FA	GM	frontal	left	dorsolateral prefrontal cortex
2019, Luan et al. Front Neurosci	FA	GM	frontal	right	dorsolateral prefrontal cortex
2019, Luan et al. Front Neurosci	FA	GM	occipital	bilateral	inferior fronto-occipital fasciculus
2019, Luan et al. Front Neurosci	FA	GM	temporal	bilateral	inferior longitudinal fasciculus
2019, Luan et al. Front Neurosci	FA	GM	parietal	bilateral	superior longitudinal fasciculus

Source	MRI measure	Matter	Brain area	Side	ROI
2019, Luan et al. Front Neurosci	FA	GM	temporal	right	STG
2018, Zou et al. Otol Neurotol	FA	GM	temporal	left	STG
2018, Zou et al. Otol Neurotol	FA	GM	temporal	right	STG

Formulas

Effect size direction was directly include in the Cohen's D value by mutipling by -1 if the effect was decrease and by 1 if it was none or increased. The value of $Cohen's D r_{Y1}$, was calculated using the means and standard deviations of two groups (M_1 =treatment and M_2 =control):

$$Cohen's D = \frac{M_1 - M_2}{S_{pooled}}$$

where

$$S_{pooled} = \sqrt{\frac{(n_1 - 1) \times s_1^2 + (n_2 - 1) \times s_2^2}{n_1 + n_2 - 2}}$$

and the effect-size correlation is:

$$r_{Y1} = \frac{d}{\sqrt{d^2 + 4}}$$

We calculate the value of Cohen's d and the effect size correlation, r_{Y1} , using the t test value for a between subjects $t - test$ and the degrees of freedom, the following formula was used:

$$Cohen's D = \frac{2t}{\sqrt{df}} \text{ and } r_{Y1} = \sqrt{\frac{t^2}{t^2 + df}}$$

Effects were summarized across studies using the generic inverse-variance weighting method with DerSimonian and Laird random effects. Studies were weighted by $1/SE^2$ (where SE is the standard error). For the effect size we used Hedges'G, which takes into account the sample size.

$$Hedges'G = \frac{X_1 - X_2}{\sqrt{\frac{(n_1 - 1)s_1^2 + (n_2 - 1)s_2^2}{n_1 + n_2 - 2}}}$$

Finally, the variance was estimated using the cohen's D and sample size of each study. Our estimated variance was used for all meta-regressions, therefore we could have had additional bias in-between studies variance and heterogeneity calculations. We should have calculated the effect size from the mean and standard deviation from each study. Variance was estimated using the following formula:

$$Variance = \frac{n_1 + n_2}{n_1 \times n_2} + \frac{Hedges'G^2}{2 \times (n_1 + n_2 - 2)}$$

Estimation of heterogeneity per model

We estimated heterogeneity in results using the τ statistic, which represents the standard deviation in the meta-regression models, we used the heterogeneity test x^2 and I^2 .

We performed a multi-level meta-analytic model, over our multiple effect size estimates nested within variables: Etiology, side and Big brain area. We expected that the underlying true effects are more similar for the same level of the grouping variables than true effects arising from different levels.

We can account for the correlation in the true effects by adding a random effect to the model at the level corresponding to the grouping variable.

The dataset contains the result from 54 studies, each comparing different measurements between patients and controls. The difference of between groups was quantified in terms of Hedges'G and Cohen's D.

References (64 bilateral studies)

- [1] "Emmorey K, Allen JS, Bruss J, Schenker N, Damasio H., A morphometric analysis of auditory brain regions in congenitally deaf adults., Proc Natl Acad Sci U S A. 2003 Aug 19;100(17):10049-54. , <https://doi.org/10.1073/pnas.1730169100>, emmorey@salk.edu"
- [2] "Allen JS, Emmorey K, Bruss J, Damasio H., Morphology of the insula in relation to hearing status and sign language experience., J Neurosci. 2008 Nov 12;28(46):11900-5., <https://doi.org/10.1523/JNEUROSCI.3141-08.2008>, kemmorey@mail.sdsu.edu"
- [3] "Allen JS, Emmorey K, Bruss J, Damasio H., Neuroanatomical differences in visual, motor, and language cortices between congenitally deaf signers, hearing signers, and hearing non-signers., Front Neuroanat. 2013 Aug 2;7:26., <https://doi.org/10.3389/fnana.2013.00026>, Hanna Damasio: hdamasio@college.usc.edu; Karen Emmorey: kemmorey@mail.sdsu.edu"
- [4] "Shibata DK., Differences in brain structure in deaf persons on MR imaging studied with voxel-based morphometry., AJNR Am J Neuroradiol. 2007 Feb;28(2):243-9. , <http://www.ajnr.org/content/28/2/243>, shibatad@u.washington.edu"
- [5] "Li J, Li W, Xian J, Li Y, Liu Z, Liu S, Wang X, Wang Z, He H., Cortical thickness analysis and optimized voxel-based morphometry in children and adolescents with prelingually profound sensorineural hearing loss., Brain Res. 2012 Jan 9;1430:35-42., <https://doi.org/10.1016/j.brainres.2011.09.057>, cjr.wzheh@vip.163.com (Z. Wang); huiguang.he@ia.ac.cn (H. He)"
- [6] "Miao W, Li J, Tang M, Xian J, Li W, Liu Z, Liu S, Sabel BA, Wang Z, He H., Altered white matter integrity in adolescents with prelingual deafness: A high-resolution tract-based spatial statistics imaging study., AJNR Am J Neuroradiol. 2013 Jun-Jul;34(6):1264-70., <https://doi.org/10.3174/ajnr.a3370>, huiguang.he@ia.ac.cn & cjr.xianjunfang@vip.163.com"
- [7] "Liu Z.-H, Li M, Xian J.-F, He H.-G, Z.-C, Li Y, Li J.-H, Wang X.-C, Liu S., Investigation of the white matter with tract-based spatial statistics in congenitally deaf patients., Chinese Journal of Medical Imaging Technology. 2010: 26(7):1226-1229., www.cjmit.com/cjmit/ch/reader/view_abstract.aspx?flag=1&file_no=20100708&journal_id=cjmit, cjr.xianjunfang@vip.163.com; lzhtrhos@sina.com"
- [8] "Li W, Li J, Wang Z, Li Y, Liu Z, Yan F, Xian J, He H., Grey matter connectivity within and between auditory, language and visual systems in prelingually deaf adolescents., Restor Neurol Neurosci. 2015;33(3):279-90., <https://doi.org/10.3233/RNN-140437>, huiguang.he@ia.ac.cn; cjr.xianjunfang@vip.163.com"
- [9] "Wenjing Li, Yong Li, Junxi X, Zhaoxue L, Xiaocui W, Sha L, Zhenchang W, Huiguang H., A voxel-based morphometric analysis of brain in congenitally deaf patients., J Clin Rad. 2010; 29(2):166-169., <https://doi.org/10.13437/j.cnki.jcr.2010.02.031>, wenjing.li@bjut.edu.cn"
- [10] "Li W, Li J, Xian J, Lv B, Li M, Wang C, Li Y, Liu Z, Liu S, Wang Z, He H, Sabel BA., Alterations of grey matter asymmetries in adolescents with prelingual deafness: A combined VBM and cortical thickness analysis., Restor Neurol Neurosci. 2013;31(1):1-17., <https://doi.org/10.3233/RNN-2012-120269>, huiguang.he@ia.ac.cn; cjr.xianjunfang@vip.163.com"
- [11] "Meyer M, Toepel U, Keller J, Nussbaumer D, Zysset S, Friederici AD., Neuroplasticity of sign language: implications from structural and functional brain imaging., Restor Neurol Neurosci. 2007;25(3-4):335-51., <https://content.iospress.com/articles/restorative-neurology-and-neuroscience/rnn253415>, mmeyer@access.uzh.ch"
- [12] "Park KH, Chung WH, Kwon H, Lee JM., Evaluation of cerebral white matter in prelingually deaf children using diffusion tensor imaging., Biomed Res Int. 2018 Feb 4;2018:6795397., <https://doi.org/10.1155/2018/6795397>, whchung@skku.edu"
- [13] "Penhune VB, Cismaru R, Dorsaint-Pierre R, Petitto LA, Zatorre RJ., The morphometry of auditory cortex in the congenitally deaf measured using MRI., Neuroimage. 2003 Oct;20(2):1215-25., [https://doi.org/10.1016/s1053-8119\(03\)00373-2](https://doi.org/10.1016/s1053-8119(03)00373-2), vpenhune@vax2.concordia.ca"
- [14] "Smith KM, Mecoli MD, Altaye M, Komlos M, Maitra R, Eaton KP, Egelhoff JC, Holland SK., Morphometric differences in the Heschl's gyrus of hearing impaired and normal hearing infants., Cereb Cortex. 2011 May;21(5):991-8., <https://doi.org/10.1093/cercor/bhq164>, scott.holland@cchmc.org"
- [15] "Chang Y, Lee SH, Lee YJ, Hwang MJ, Bae SJ, Kim MN, Lee J, Woo S, Lee H, Kang DS., Auditory neural pathway evaluation on sensorineural hearing loss using diffusion tensor imaging., Neuroreport. 2004 Aug 6;15(11):1699-703., <https://doi.org/10.1097/01.wnr.0000134584.10207.1a>, leeshu@knu.ac.kr"
- [16] "Chang Y, Lee HR, Paik JS, Lee KY, Lee SH., Voxel-wise analysis of diffusion tensor imaging for clinical outcome of cochlear implantation: retrospective study., Clin Exp Otorhinolaryngol. 2012 Apr;5 Suppl 1:S37-42., <https://doi.org/10.3342/ceo.2012.5.s1.s37>, leeshu@knu.ac.kr"
- [17] "Shiell MM, Zatorre RJ., White matter structure in the right planum temporale region correlates with visual motion detection thresholds in deaf people., Hear Res. 2017 Jan;343:64-71., <https://doi.org/10.1016/j.heares.2016.06.011>, martha.shiell@mail.mcgill.ca; Robert.Zatorre@mcgill.ca"
- [18] "Shiell MM, Champoux F, Zatorre RJ., The right hemisphere planum temporale supports enhanced visual motion detection ability in deaf people the right hemisphere planum temporale supports enhanced visual motion detection ability in deaf people., Neural Plasticity 2016: 7217630., <https://doi.org/10.1155/2016/7217630>, francois.champoux@umontreal.ca; martha.shiell@mail.mcgill.ca; Robert.Zatorre@mcgill.ca"
- [19] "Kim DJ, Park SY, Kim J, Lee DH, Park HJ., Alterations of white matter diffusion anisotropy in early deafness., Neuroreport. 2009 Jul 15;20(11):1032-6., <https://doi.org/10.1097/wnr.0b013e32832e0cdd>, parkhj@yuhs.ac; hjpark0@gmail.com"
- [20] "Kim J, Choi JY, Eo J, Park HJ., Comparative evaluation of the white matter fiber integrity in patients with prelingual and postlingual deafness., Neuroreport. 2017 Nov 8;28(16):1103-1107, <https://doi.org/10.1097/wnr.00000000000000894>, parkhj@yuhs.ac; hjpark0@gmail.com"

- [21] "Amaral L, Ganho-Ávila A, Osório A, Soares MJ, He D, Chen Q, Mahon BZ, Gonçalves OF, Sampaio A, Fang F, Bi Y, Almeida J., Hemispheric asymmetries in subcortical visual and auditory relay structures in congenital deafness., Eur J Neurosci. 2016 Sep;44(6):2334-9., <https://doi.org/10.1111/ejnj.13340>, Jorge Almeida: jorgealmeida@fpce.uc.pt"
- [22] "Lyness RC, Alvarez I, Sereno MI, MacSweeney M., Microstructural differences in the thalamus and thalamic radiations in the congenitally deaf., Neuroimage. 2014 Oct 15;100:347-57., <https://doi.org/10.1016/j.neuroimage.2014.05.077>, c.rebeccalyness@gmail.com"
- [23] "Karns CM, Stevens C, Dow MW, Schorr EM, Neville HJ., Atypical white-matter microstructure in congenitally deaf adults: A region of interest and tractography study using diffusion-tensor imaging., Hear Res. 2017 Jan;343:72-82., <https://doi.org/10.1016/j.heares.2016.07.008>, ckarns@uoregon.edu"
- [24] "Hribar M, Suput D, Carvalho AA, Battelino S, Vovk A., Structural alterations of brain grey and white matter in early deaf adults., Hear Res. 2014 Dec;318:1-10., <https://doi.org/10.1016/j.heares.2014.09.008>, andrej.vovk@mf.uni-lj.si"
- [25] "Huang L, Zheng W, Wu C, Wei X, Wu X, Wang Y, Zheng H., Diffusion tensor imaging of the auditory neural pathway for clinical outcome of cochlear implantation in pediatric congenital sensorineural hearing loss patients., PLoS One. 2015 Oct 20;10(10):e0140643., <https://doi.org/10.1371/journal.pone.0140643>, hwenb@126.com"
- [26] "Olulade OA, Koo DS, LaSasso CJ, Eden GF., Neuroanatomical profiles of deafness in the context of native language experience., J Neurosci. 2014 Apr 16;34(16):5613-20., <https://doi.org/10.1523/jneurosci.3700-13.2014>, edeng@georgetown.edu"
- [27] "Wu C, Huang L, Tan H, Wang Y, Zheng H, Kong L, Zheng W., Diffusion tensor imaging and MR spectroscopy of microstructural alterations and metabolite concentration changes in the auditory neural pathway of pediatric congenital sensorineural hearing loss patients., Brain Res. 2016 May 15;1639:228-34., <https://doi.org/10.1016/j.brainres.2014.12.025>, hwenb@126.com"
- [28] "Kim E, Kang H, Lee H, Lee HJ, Suh MW, Song JJ, Oh SH, Lee DS., Morphological brain network assessed using graph theory and network filtration in deaf adults., Hear Res. 2014 Sep;315:88-98., <https://doi.org/10.1016/j.heares.2014.06.007>, shaoh@snu.ac.kr; dsl@plaza.snu.ac.kr"
- [29] "Pénicaud S, Klein D, Zatorre RJ, Chen JK, Witcher P, Hyde K, Mayberry RI., Structural brain changes linked to delayed first language acquisition in congenitally deaf individuals., Neuroimage. 2013 Feb 1;66:42-9., <https://doi.org/10.1016/j.neuroimage.2012.09.076>, sidonie.p@gmail.com (S. Pénicaud); denise.klein@mcgill.ca (D. Klein); robert.zatorre@mcgill.ca (R.J. Zatorre); jen-kai.chen@mcgill.ca (J.-K. Chen); krista.hyde@mail.mcgill.ca (K. Hyde); rmayberry@ucsd.edu (R.I. Mayberry)" [30] "Chinnadurai V, Sreedhar CM, Khushu S., Assessment of cochlear nerve deficiency and its effect on normal maturation of auditory tract by diffusion kurtosis imaging and diffusion tensor imaging: A correlational approach., Magn Reson Imaging. 2016 Nov;34(9):1305-1313., <https://doi.org/10.1016/j.mri.2016.07.010>, vijayakumar@inmas.drdo.in; vijayininmas@gmail.com"
- [31] "Kara A, Hakan Ozturk A, Kurtoglu Z, Umit Talas D, Aktekin M, Saygili M, Kanik A., Morphometric comparison of the human corpus callosum in deaf and hearing subjects: An MRI study., J Neuroradiol. 2006 Jun;33(3):158-63., [https://doi.org/10.1016/s0150-9861\(06\)77253-4](https://doi.org/10.1016/s0150-9861(06)77253-4), alevkara@mersin.edu.tr"
- [32] "Xia S, Qi J, Li Q., High-resolution MR study of auditory cortex in prelingual sensorineural hearing loss., Chinese Journal of Medical Imaging Technology. 2008; 24(11):1705-1707., http://www.cjmit.com/cjmit/ch/reader/view_abstract.aspx?flag=1&file_no=20081111&journal_id=cjmit, xiaoshuang77@163.com; cjr.qiji@vip.163.com"
- [33] "Benetti S, Novello L, Maffei C, Rabini G, Jovicich J, Collignon O., White matter connectivity between occipital and temporal regions involved in face and voice processing in hearing and early deaf individuals., Neuroimage. 2018 Oct 1;179:263-274., <https://doi.org/10.1016/j.neuroimage.2018.06.044>, stefania.benetti@unitn.it; olivier.collignon@uclouvain.be"
- [34] "Wang S, Li Y.-H, Zhou Y, Yu C.-S, Xu C.-L, Qin W, Liu Y, Jiang T.-Z., Diffusion tensor imaging observation of brain white matter in congenitally deaf., Chinese Journal of Medical Imaging Technology. 2009; 25(4):585-587., http://www.cjmit.com/cjmit/ch/reader/view_abstract.aspx?flag=1&file_no=20090418&journal_id=cjmit, wang_sh2006@lzu.cn; jiangtz@nlpr.ia.ac.cn"
- [35] "Tae, W.-S. 2015., Reduced gray matter volume of auditory cortical and subcortical areas in congenitally deaf adolescents: A voxel-based morphometric study., Investig Magn Reson Imaging 19, 1-9., <https://doi.org/10.13104/imri.2015.19.1.1>, wstae@kangwon.ac.kr"
- [36] "Feng G, Ingvalson EM, Grieco-Calub TM, Roberts MY, Ryan ME, Birmingham P, Burrowes D, Young NM, Wong PCM., Neural preservation underlies speech improvement from auditory deprivation in young cochlear implant recipients., Proc Natl Acad Sci U S A. 2018 Jan 30;115(5):E1022-E1031., <https://doi.org/10.1073/pnas.1717603115>, p.wong@cuhk.edu.hk"
- [37] "Kumar U, Mishra M., Pattern of neural divergence in adults with prelingual deafness: Based on structural brain analysis., Brain Res. 2018 Jul 23, pii: S0006-8993(18)30405-0., <https://doi.org/10.1016/j.brainres.2018.07.021>, uttam@cbmr.res.in"
- [38] "Leporé N, Vachon P, Lepore F, Chou YY, Voss P, Brun CC, Lee AD, Toga AW, Thompson PM., 3D mapping of brain differences in native signing congenitally and prelingually deaf subjects., Hum Brain Mapp. 2010 Jul;31(7):970-8., <https://doi.org/10.1002/hbm.20910>, nleporé@loni.ucla.edu"
- [39] "Li Y, Ding G, Booth JR, Huang R, Lv Y, Zang Y, He Y, Peng D., Sensitive period for white-matter connectivity of superior temporal cortex in deaf people., Hum Brain Mapp. 2012 Feb;33(2):349-59., <https://doi.org/10.1002/hbm.21215>, Dinggsh@bnu.edu.cn; pdl3507@bnu.edu.cn"
- [40] "Zheng W, Wu C, Huang L, Wu R., Diffusion kurtosis imaging of microstructural alterations in the brains of paediatric patients with congenital sensorineural hearing loss., Sci Rep 2017 May 8. 7:1543., <https://doi.org/10.1038/s41598-017-01263-9>, rhwu@stu.edu.cn"
- [41] "Alfandari D, Vriend C, Heslenfeld DJ, Versfeld NJ, Kramer SE, Zekveld AA., Brain volume differences associated with hearing impairment in adults., Trends Hear. 2018 Jan-Dec;22:1-8., <https://doi.org/10.1177/2331216518763689>, aa.zekveld@vumc.nl"
- [42] "Ponticorvo S, Manara R, Pfeuffer J, Cappiello A, Cuoco S, Pellecchia MT, Saponiero R, Troisi D, Cassandro C, John M, Scarpa A, Cassandro E, Di Salle F, Esposito F., Cortical pattern of reduced perfusion in hearing loss revealed by ASL-MRI., Hum Brain Mapp. 2019 Feb 4., <https://doi.org/10.1002/hbm.24538>, faesposito@unisa.it"
- [43] "Shi B, Yang LZ, Liu Y, Zhao SL, Wang Y, Gu F, Yang Z, Zhou Y, Zhang P, Zhang X., Early-onset hearing loss reorga-

- nizes the visual and auditory network in children without cochlear implantation., *Neuroreport*. 2016 Feb 10;27(3):197-202., <https://doi.org/10.1097/wnr.0000000000000524>, felice828@126.com"
- [44] "Pereira-Jorge MR, Andrade KC, Palhano-Fontes FX, Diniz PRB, Sturzbecher M, Santos AC, Araujo DB., Anatomical and functional MRI changes after one year of auditory rehabilitation with hearing aids., *Neural Plast.* 2018 Sep 10;2018:9303674., <https://doi.org/10.1155/2018/9303674> , draulio@neuro.ufrn.br"
- [45] "Peelle JE, Troiani V, Grossman M, Wingfield A., Hearing loss in older adults affects neural systems supporting speech comprehension., *J Neurosci*. 2011 Aug 31;31(35):12638-43. , <https://doi.org/10.1523/jneurosci.2559-11.2011>, peelle@gmail.com"
- [46] "Ren F, Ma W, Li M, Sun H, Xin Q, Zong W, Chen W, Wang G, Gao F, Zhao B., Gray matter atrophy is associated with cognitive impairment in patients with presbycusis: A comprehensive morphometric study., *Front Neurosci*. 2018 Oct 23;12:744., <https://doi.org/10.3389/fnins.2018.00744>, Fei Gao: feigao6262@163.com; Bin Zhao: qpqoo6262@163.com"
- [47] "Eckert MA, Cute SL, Vaden KI Jr, Kuchinsky SE, Dubno JR., Auditory cortex signs of age-related hearing loss., *J Assoc Res Otolaryngol*. 2012 Oct;13(5):703-13., <https://doi.org/10.1007/s10162-012-0332-5>, eckert@musc.edu"
- [48] "Boyen K, Langers DR, de Kleine E, van Dijk P., Gray matter in the brain: Differences associated with tinnitus and hearing loss., *Hear Res*. 2013 Jan;295:67-78., <https://doi.org/10.1016/j.heares.2012.02.010>, k.boyen@umcg.nl (K. Boyen), d.r.m.langers@umcg.nl, (D.R.M. Langers), e.de.kleine@umcg.nl (E. de Kleine), p.van.dijk@umcg.nl (P. van Dijk)"
- [49] "Luan Y, Wang C, Jiao Y, Tang T, Zhang J, Teng GJ., Prefrontal-temporal pathway mediates the cross-modal and cognitive reorganization in sensorineural hearing loss with or without tinnitus: A multimodal MRI study., *Front Neurosci*. 2019 Mar 12;13:222., <https://doi.org/10.3389/fnins.2019.00222>, gjteng@vip.sina.com"
- [50] "Belkhiria C, Vergara RC, Martín SS, Leiva A, Marcenaro B, Martínez M, Delgado C, Delano PH., Cingulate cortex atrophy is associated with hearing loss in presbycusis with cochlear amplifier dysfunction., *Front Aging Neurosci*. 26 April 2019, <https://doi.org/10.3389/fnagi.2019.00097>, pdelano@med.uchile.cl; phdelano@gmail.com"
- [51] "Uchida Y, Nishita Y, Kato T, Iwata K, Sugiura S, Suzuki H, Sone M, Tange C, Otsuka R, Ando F, Shimokata H, Nakamura A., Smaller hippocampal volume and degraded peripheral hearing among Japanese community dwellers., *Front Aging Neurosci*. 2018 Oct 16;10:319., <https://doi.org/10.3389/fnagi.2018.00319>, yasueu@aichi-med-u.ac.jp"
- [52] "Chen YC, Chen H, Jiang L, Bo F, Xu JJ, Mao CN, Salvi R, Yin X, Lu G, Gu JP., Presbycusis disrupts spontaneous activity revealed by resting-state functional MRI., *Front Behav Neurosci*. 2018 Mar 13;12:44., <https://doi.org/10.3389/fnbeh.2018.00044>, Guangming Lu; cjr.luguangming@vip.163.com; Jian-Ping Gu; cjr.gujianping@vip.163.com"
- [53] "Rigters SC, Bos D, Metselaar M, Roschupkin GV, Baatenburg de Jong RJ, Ikram MA, Vernooij MW, Goedegebure A., Hearing impairment is associated with smaller brain volume in aging., *Front Aging Neurosci*. 2017 Jan 20;9:2, <https://doi.org/10.3389/fnagi.2017.00002> , s.rigters@erasmusmc.nl"
- [54] "Zou Y, Yang Y, Fan W, Yu Q, Wang M, Han P, Ma H., Microstructural alterations in the brains of adults with prelingual sensorineural hearing loss: A diffusion kurtosis imaging study., *Otol Neurol*. 2018 Dec;39(10):e936-e943., <https://doi.org/10.1097/mao.0000000000002000>, cjr.hanping@vip.163.com; 1363191284@qq.com"
- [55] "Smittenaar CR, MacSweeney M, Sereno MI, Schwarzkopf DS., Does congenital deafness affect the structural and functional architecture of primary visual cortex?, *Open Neuroimag J*. 2016 Feb 29;10:1-19., <https://doi.org/10.2174/1874440001610010001>, c.rebeccalyness@gmail.com"
- [56] "Bavelier D, Tomann A, Hutton C, Mitchell T, Corina D, Liu G, Neville H., Visual attention to the periphery is enhanced in congenitally deaf individuals., *J Neurosci*. 2000 Sep 1;20(17):RC93., <https://doi.org/10.1523/JNEUROSCI.20-17-j0001.2000> , daphne@bcs.rochester.edu"
- [57] "Husain FT, Medina RE, Davis CW, Szymko-Bennett Y, Simonyan K, Pajor NM, Horwitz B., Neuroanatomical changes due to hearing loss and chronic tinnitus: a combined VBM and DTI study., *Brain Res*. 2011 Jan 19;1369:74-88., <https://doi.org/10.1016/j.brainres.2010.10.095>, husainf@illinois.edu"
- [58] "Xu XM, Jiao Y, Tang TY, Zhang J, Lu CQ, Salvi R, Teng GJ., Sensorineural hearing loss and cognitive impairments: Contributions of thalamus using multiparametric MRI., *J Magn Reson Imaging*. 2019 Jan 29., <https://doi.org/10.1002/jmri.26665>, gjteng@seu.edu.cn"
- [59] "Profant O, Škoch A, Balogová Z, Tintéra J, Hlinka J, Syka J., Diffusion tensor imaging and MR morphometry of the central auditory pathway and auditory cortex in aging. Diffusion tensor imaging and MR morphometry of the central auditory pathway and auditory cortex in aging., *Neuroscience*. 2014 Feb 28;260:87-97., <https://doi.org/10.1016/j.neuroscience.2013.12.010>, profant@biomed.cas.cz"
- [60] "Lin FR, Ferrucci L, An Y, Goh JO, Doshi J, Metter EJ, Davatzikos C, Kraut MA, Resnick SM., Association of hearing impairment with brain volume changes in older adults., *Neuroimage*. 2014 Apr 15;90:84-92., <https://doi.org/10.1016/j.neuroimage.2013.12.059>, flin1@jhmi.edu"
- [61] "Eckert MA, Kuchinsky SE, Vaden KI, Cute SL, Spampinato MV, Dubno JR., White matter hyperintensities predict low frequency hearing in older adults., *J Assoc Res Otolaryngol*. 2013 Jun;14(3):425-33., <https://doi.org/10.1007/s10162-013-0381-4>, eckert@musc.edu"
- [62] "Rigters SC, Cremers LGM, Ikram MA, van der Schroeff MP, de Groot M, Roschupkin GV, Niessen WJN, Baatenburg de Jong RJ, Goedegebure A, Vernooij MW., White-matter microstructure and hearing acuity in older adults: a population-based cross-sectional DTI study., *Neurobiol Aging*. 2018 Jan;61:124-131., <https://doi.org/10.1016/j.neurobiolaging.2017.09.018>, s.rigters@erasmusmc.nl"
- [63] "Qian ZJ, Chang PD, Moonis G, Lalwani AK., A novel method of quantifying brain atrophy associated with age-related hearing loss., *Neuroimage Clin*. 2017 Jul 24;16:205-209., <https://doi.org/10.1016/j.nicl.2017.07.021>, anil.lalwani@columbia.edu"
- [64] "Ma W, Li M, Gao F, Zhang X, Shi L, Yu L, Zhao B, Chen W, Wang G, Wang X., DTI analysis of presbycusis using voxel-based analysis., *AJR Am J Neuroradiol*. 2016 Nov;37(11):2110-2114., <https://doi.org/10.3174/ajnr.A4870>, wgb7932596@hotmail.com"

Unilateral hearing loss (total n=8)

- VBM studies
 1. Fan et al. Otol Neurotol. 2015 Dec;36(10):1622-7. (Unilateral SNHL adult mixed cause) -VBM -SPM
 2. Yang et al. Hear Res. 2014 Oct;316:37-43. (Right unilateral SHNL adult) -SPM – VBM
 3. Wang et al. Sci Rep. 2016 May 13;6:25811.(Adult acquired unilateral) SPM -VBM
- DTI
 1. Wu et al. AJNR Am J Neuroradiol. 2009 Oct;30(9):1773-7. (Congenital Unilateral deaf children) - DTI-Studio
 2. Lin et al. J Magn Reson Imaging. 2008 Sep;28(3):598-603. (Bilateral and unilateral SNHL Adult) - DTI-Studio
 3. Rachakonda et al. Front Syst Neurosci. 2014 May 26;8:87. (Unilateral left and right, adolescent) – Not indicated
 4. Wu et al. Audiol Neurotol. 2009;14(4):248-53. (Unilateral mixed left/right SNHL mixed congenital/unknown adult)-DTI Studio
 5. Vos et al. Hear Res. 2015 May;323:1-8. (Unilateral mixed left and right SNHL adult) – DTI Tractography - ExploreDTI

Signed differential mapping (SDM)

Seed-based d Mapping (formerly “Signed Differential Mapping”):

> <https://www.sdmproject.com/>

1. Radua J, Mataix-Cols D. Voxel-wise meta-analysis of grey matter changes in obsessive-compulsive disorder. Br J Psychiatry. 2009; 195:393–402.
2. Radua J, van den Heuvel OA, Surguladze S, Mataix-Cols D. Meta-analytical comparison of voxel based morphometry studies in obsessive-compulsive disorder vs other anxiety disorders. Arch Gen Psychiatry. 2010; 67:701–711.

Table 9: SDM: congenital

MNI.coordinate	SDM.Z	P	Voxels	Description	Direction
-8,52,-20	4.350	0.0000068	916	Left gyrus rectus, BA 11	positive
-16,-100,-6	3.835	0.0000628	950	Left calcarine fissure / surrounding cortex, BA 17	positive
-22,-38,60	3.621	0.0001470	755	(undefined), BA 3	positive
26,-76,38	3.187	0.0007187	508	Right superior occipital gyrus, BA 19	positive
30,-32,56	3.494	0.0002378	457	Right postcentral gyrus, BA 3	positive
-8,38,12	3.387	0.0003530	419	Left anterior cingulate / paracingulate gyri, BA 32	positive
-4,-28,32	2.901	0.0018615	399	Left median cingulate / paracingulate gyri, BA 23	positive
62,2,10	2.817	0.0024230	319	Right rolandic operculum, BA 6	positive
14,-44,-10	3.679	0.0001172	259	Right cerebellum, hemispheric lobule IV / V, BA 30	positive
-8,-52,-8	2.704	0.0034276	287	Left cerebellum, hemispheric lobule IV / V, BA 18	positive
-26,-92,20	3.424	0.0003090	240	Left middle occipital gyrus, BA 18	positive
8,-72,22	2.994	0.0013756	102	Corpus callosum	positive
-42,-36,22	2.463	0.0068921	70	Left superior temporal gyrus, BA 48	positive
-56,10,30	2.664	0.0038628	52	Left precentral gyrus, BA 44	positive
-18,40,30	2.625	0.0043344	36	Corpus callosum	positive
44,-4,-10	1.938	0.0263297	39	Right superior temporal gyrus	positive
-32,-16,-12	2.134	0.0164014	35	Corpus callosum	positive
62,-32,-6	2.029	0.0212226	33	Right middle temporal gyrus, BA 21	positive
36,-22,-14	2.677	0.0037128	24	Right hippocampus, BA 20	positive
6,-34,56	1.959	0.0250691	21	Right paracentral lobule	positive
-26,20,-16	2.194	0.0141032	19	Left frontal orbito-polar tract	positive
-22,40,36	1.988	0.0234269	8	Left superior frontal gyrus, dorsolateral, BA 9	positive
34,-68,-46	1.865	0.0311240	7	Right cerebellum, hemispheric lobule VIIIB	positive
-36,-10,-42	1.762	0.0390477	2	Left inferior temporal gyrus, BA 20	positive
-18,42,40	1.660	0.0484373	2	Left superior frontal gyrus, dorsolateral, BA 9	positive
52,2,-4	1.673	0.0471951	1	Right superior temporal gyrus, BA 38	positive
-20,46,36	1.670	0.0475018	1	Left superior frontal gyrus, dorsolateral, BA 9	positive
52,-14,-10	1.655	0.0489883	1	Right superior temporal gyrus, BA 22	positive
8,-54,-38	-2.751	0.0029747	714	Right cerebellum, hemispheric lobule IX	negative
-50,-16,-14	-3.909	0.0000463	521	Left middle temporal gyrus, BA 20	negative
42,12,-34	-3.013	0.0012935	323	Right temporal pole, middle temporal gyrus, BA 20	negative
-6,26,44	-3.092	0.0009937	214	Left superior frontal gyrus, medial, BA 8	negative
-48,-52,40	-2.485	0.0064724	223	Left inferior parietal (excluding supramarginal and angular) gyri, BA 40	negative
-44,8,-30	-2.333	0.0098195	190	Left temporal pole, middle temporal gyrus, BA 20	negative
16,-12,-10	-2.861	0.0021141	164	Right cortico-spinal projections	negative
38,-22,36	-3.305	0.0004744	149	Right superior longitudinal fasciculus III	negative
46,-58,42	-3.349	0.0004056	141	Right angular gyrus, BA 39	negative
-20,-54,12	-3.587	0.0001674	109	Corpus callosum	negative
-36,32,18	-3.168	0.0007666	123	Left inferior frontal gyrus, triangular part, BA 48	negative
22,36,48	-4.063	0.0000243	103	Right superior frontal gyrus, dorsolateral, BA 9	negative
-46,-6,-26	-2.997	0.0013640	97	Left inferior network, inferior longitudinal fasciculus	negative
-4,-32,22	-2.655	0.0039663	100	Corpus callosum	negative
-14,-66,-32	-2.564	0.0051706	68	(undefined)	negative
-30,-58,-58	-2.242	0.0124691	60	Left cerebellum, hemispheric lobule VIII	negative
28,42,28	-2.263	0.0118076	52	Right middle frontal gyrus, BA 46	negative
-46,-70,-46	-2.622	0.0043685	37	Left cerebellum, crus II	negative
26,-12,-2	-2.269	0.0116403	42	Right cortico-spinal projections	negative
4,-54,18	-2.683	0.0036445	31	Right precuneus, BA 30	negative
-54,-26,26	-2.386	0.0085091	28	Left superior longitudinal fasciculus III	negative
44,12,54	-2.203	0.0137867	25	Right middle frontal gyrus, BA 9	negative
44,6,20	-2.171	0.0149726	24	Right superior longitudinal fasciculus III	negative
10,-70,40	-1.972	0.0242994	23	Right precuneus, BA 7	negative
-40,-48,58	-2.064	0.0195199	17	Left inferior parietal (excluding supramarginal and angular) gyri, BA 40	negative
-30,-66,-48	-1.896	0.0289586	18	Left cerebellum, hemispheric lobule VIII	negative
0,-66,-10	-1.927	0.0269926	11	Cerebellum, vermic lobule VI	negative
34,-10,50	-1.989	0.0233668	10	Right superior longitudinal fasciculus II	negative
-2,26,-10	-1.831	0.0335253	9	Left anterior cingulate / paracingulate gyri, BA 11	negative
12,-80,48	-1.879	0.0301139	7	Right precuneus, BA 7	negative
60,-44,32	-1.917	0.0275989	7	Right supramarginal gyrus, BA 40	negative

Table 10: SDM: congenital... continuation

MNI.coordinate	SDM.Z	P	Voxels	Description	Direction
24,-26,4	-1.898	0.0288799	7	Corpus callosum	negative
18,32,28	-1.950	0.0255769	4	Corpus callosum	negative
-26,-4,-16	-1.954	0.0253757	4	Left amygdala, BA 34	negative
-44,6,28	-1.778	0.0377381	4	Left inferior frontal gyrus, opercular part, BA 44	negative
40,-18,24	-1.931	0.0267345	3	Right superior longitudinal fasciculus III	negative
4,-66,-16	-1.760	0.0392402	3	Cerebellum, vermic lobule VI	negative
56,-38,24	-1.697	0.0448450	3	Right supramarginal gyrus, BA 48	negative
-42,4,22	-1.716	0.0430821	3	Left superior longitudinal fasciculus III	negative
-10,32,-10	-1.785	0.0371427	2	Left anterior cingulate / paracingulate gyri, BA 11	negative
-56,-46,38	-1.738	0.0411224	2	Left inferior parietal (excluding supramarginal and angular) gyri, BA 40	negative
42,-16,-10	-1.696	0.0449376	2	Right inferior network, inferior longitudinal fasciculus	negative
10,-80,38	-1.674	0.0471122	2	Right cuneus cortex, BA 19	negative
-32,-8,-28	-1.870	0.0307359	1	Left inferior network, inferior longitudinal fasciculus	negative
-18,-42,8	-1.828	0.0338045	1	Corpus callosum	negative
-24,-2,-28	-1.803	0.0357051	1	Left amygdala, BA 28	negative
-30,-52,-8	-1.784	0.0372359	1	Left fusiform gyrus, BA 37	negative
-18,-36,-8	-1.782	0.0373835	1	Left median network, cingulum	negative
-30,-64,10	-1.738	0.0410686	1	Corpus callosum	negative
-24,-32,-14	-1.723	0.0424798	1	Left median network, cingulum	negative
10,-82,44	-1.679	0.0466105	1	Right cuneus cortex, BA 19	negative
20,-6,-20	-1.666	0.0478409	1	Right hippocampus, BA 28	negative
34,28,40	-1.654	0.0490536	1	Right middle frontal gyrus, BA 9	negative

Table 11: SDM: acquired

MNI.coordinate	SDM.Z	P	Voxels	Description	Direction
60,-24,16	3.668	0.0001223	651	Right superior temporal gyrus, BA 42	positive
52,-60,4	2.650	0.0040274	109	Right middle temporal gyrus, BA 37	positive
-44,-10,6	-2.782	0.0027017	858	Left rolandic operculum, BA 48	negative
6,-34,34	-1.853	0.0319374	65	Right median cingulate / paracingulate gyri, BA 23	negative
-54,-30,16	-1.663	0.0481477	1	Left superior temporal gyrus, BA 42	negative

Table 12: SDM: pediatric

MNI.coordinate	SDM.Z	P	Voxels	Description	Direction
-6,-32,32	3.238	0.0006011	586	Left median network, cingulum	positive
26,-78,36	3.087	0.0010125	471	Right superior occipital gyrus, BA 19	positive
-10,52,-2	2.958	0.0015498	144	Left superior frontal gyrus, medial orbital, BA 10	positive
-18,-98,-6	2.835	0.0022947	131	Left calcarine fissure / surrounding cortex, BA 18	positive
6,-36,56	2.455	0.0070484	138	Right paracentral lobule	positive
-2,42,8	2.298	0.0107808	90	Left anterior cingulate / paracingulate gyri, BA 32	positive
-2,42,-22	2.094	0.0181222	26	Left gyrus rectus, BA 11	positive
-2,46,-26	1.726	0.0421527	1	Left gyrus rectus, BA 11	positive
10,52,-16	1.645	0.0499467	1	Corpus callosum	positive
46,-54,42	-3.111	0.0009324	269	Right inferior parietal (excluding supramarginal and angular) gyri, BA 40	negative
-48,-22,0	-3.096	0.0009812	211	Corpus callosum	negative
52,-24,2	-1.825	0.0340229	9	Corpus callosum	negative
-44,-16,-16	-1.789	0.0368080	6	Left inferior network, inferior longitudinal fasciculus	negative

Table 13: SDM: adult

MNI.coordinate	SDM.Z	P	Voxels	Description	Direction
58,-2,-10	2.524	0.0057985	301	Right superior temporal gyrus, BA 21	positive
-22,-36,60	2.796	0.0025855	288	Left postcentral gyrus, BA 3	positive
44,12,-34	-2.342	0.0095819	84	Right temporal pole, middle temporal gyrus, BA 20	negative
-38,34,18	-2.212	0.0134751	30	Left inferior frontal gyrus, triangular part, BA 45	negative
-44,6,-30	-1.906	0.0283524	23	Left middle temporal gyrus, BA 20	negative
-58,-20,-14	-1.773	0.0380803	6	Left middle temporal gyrus, BA 21	negative

Table 14: SDM: AgedAdult

MNI.coordinate	SDM.Z	P	Voxels	Description	Direction
58,-16,6	3.210	0.0006627	1782	Right superior temporal gyrus, BA 48	positive
54,-60,4	3.121	0.0009015	461	Right middle temporal gyrus	positive
16,-74,40	2.492	0.0063471	198	Right precuneus, BA 19	positive
14,-8,-8	2.328	0.0099693	36	Right cortico-spinal projections	positive
-10,42,-20	2.097	0.0180048	29	Left gyrus rectus, BA 11	positive
36,-44,-14	1.823	0.0341623	7	Right inferior network, inferior longitudinal fasciculus	positive
42,16,30	1.828	0.0337837	6	Right inferior frontal gyrus, opercular part, BA 44	positive
-4,-60,38	1.683	0.0462278	2	Left precuneus	positive
48,-10,-12	1.677	0.0467685	1	Right superior temporal gyrus, BA 48	positive
38,14,28	1.659	0.0485649	1	Right inferior frontal gyrus, opercular part, BA 48	positive
50,-16,-10	1.646	0.0498625	1	Right middle temporal gyrus, BA 48	positive
-32,-6,12	-1.738	0.0411015	6	Left insula, BA 48	negative
-32,-10,6	-1.736	0.0412629	4	(undefined), BA 48	negative
-34,-10,16	-1.717	0.0430003	3	Left insula, BA 48	negative
-28,-14,10	-1.691	0.0454556	3	Left striatum	negative

Table 15: SDM: GM

MNI.coordinate	SDM.Z	P	Voxels	Description	Direction
62,-12,8	3.709	0.0001041	1093	Right superior temporal gyrus, BA 22	positive
-4,-90,8	2.378	0.0087125	198	Left calcarine fissure / surrounding cortex, BA 18	positive
22,-74,40	2.735	0.0031158	127	Right superior occipital gyrus, BA 7	positive
-10,-32,36	2.402	0.0081576	123	Left median network, cingulum	positive
-6,42,-20	2.746	0.0030164	100	Corpus callosum	positive
54,-62,4	2.426	0.0076259	58	Right middle temporal gyrus, BA 37	positive
0,-36,54	1.807	0.0353866	5	Left paracentral lobule	positive
-8,-96,-2	1.655	0.0489485	1	Left calcarine fissure / surrounding cortex, BA 17	positive
-4,24,44	-2.476	0.0066513	41	Left superior frontal gyrus, medial, BA 8	negative

Table 16: SDM: WM

MNI.coordinate	SDM.Z	P	Voxels	Description	Direction
62,-14,-18	2.769	0.0028142	586	Right middle temporal gyrus, BA 21	positive
-22,-36,60	2.695	0.0035164	258	Left postcentral gyrus, BA 3	positive
10,38,10	2.847	0.0022033	142	Right median network, cingulum	positive
-14,56,-2	2.255	0.0120670	19	Corpus callosum	positive
44,-4,-10	1.788	0.0369088	6	Right superior temporal gyrus	positive
-50,-16,-14	-2.681	0.0036704	456	Left middle temporal gyrus, BA 20	negative
6,-64,-42	-2.665	0.0038518	240	Cerebellum, vermic lobule VIII	negative
-14,-64,-30	-3.205	0.0006742	176	(undefined)	negative
44,12,-34	-2.435	0.0074469	78	Right temporal pole, middle temporal gyrus, BA 20	negative
-38,34,18	-2.416	0.0078490	40	Left inferior frontal gyrus, triangular part, BA 45	negative
-2,-30,22	-2.348	0.0094253	39	Corpus callosum	negative
-38,-16,18	-1.811	0.0350648	4	Left rolandic operculum, BA 48	negative

Table 17: ALE report of first 10 clusters

Cluster Number	\$Volume mm^3\$	WC.x	WC.y	WC.z	Extrema value	x	y	z	Label
1	592	-43.2	-22.8	8.1	0.007556	-50.0	-20.0	8.0	Left Cerebrum.Temporal Lobe.Superior Temporal Gyrus.Gray Matter.Brodmann area 13
1	592	-43.2	-22.8	8.1	0.007331	-43.6	-21.6	9.2	Left Cerebrum.Temporal Lobe.Superior Temporal Gyrus.Gray Matter.Brodmann area 13
1	592	-43.2	-22.8	8.1	0.007112	-40.4	-25.8	7.3	Left Cerebrum.Temporal Lobe.Superior Temporal Gyrus.Gray Matter.Brodmann area 13
2	584	44.9	-21.6	5.3	0.007556	44.0	-20.0	4.0	Right Cerebrum.Sub-lobar.Insula.Gray Matter.Brodmann area 13
2	584	44.9	-21.6	5.3	0.007331	44.7	-22.0	3.3	Right Cerebrum.Sub-lobar.Insula.Gray Matter.Brodmann area 13
2	584	44.9	-21.6	5.3	0.007112	44.9	-22.5	6.5	Right Cerebrum.Sub-lobar.Superior Temporal Gyrus.Gray Matter.Brodmann area 22
3	272	41.1	-25.6	12.9	0.007331	39.0	-26.0	14.0	Right Cerebrum.Sub-lobar.Insula.Gray Matter.Brodmann area 13
3	272	41.1	-25.6	12.9	0.007112	42.0	-25.5	12.5	Right Cerebrum.Temporal Lobe.Transverse Temporal Gyrus.Gray Matter.Brodmann area 41
4	256	25.1	-14.7	20.4	0.007331	24.5	-14.5	20.0	Right Cerebrum.Sub-lobar.Lentiform Nucleus.Gray Matter.Putamen
4	256	25.1	-14.7	20.4	0.007112	26.0	-15.0	21.0	Right Cerebrum.Sub-lobar.Thalamus.Gray Matter.*
5	240	-17.6	-58.4	-16.3	0.007331	-14.0	-56.0	-15.0	Left Cerebellum.Anterior Lobe.Culmen.Gray Matter.*
5	240	-17.6	-58.4	-16.3	0.007112	-19.5	-59.5	-17.0	Left Cerebellum.Anterior Lobe.Culmen.Gray Matter.*
6	240	53.2	-20.6	0.8	0.007112	53.2	-20.6	0.8	Right Cerebrum.Temporal Lobe.Superior Temporal Gyrus.Gray Matter.Brodmann area 22
7	232	-49.5	-5.9	-8.4	0.007331	-50.0	-7.0	-8.0	Left Cerebrum.Temporal Lobe.Superior Temporal Gyrus.Gray Matter.Brodmann area 22
7	232	-49.5	-5.9	-8.4	0.007112	-48.0	-2.7	-11.3	Left Cerebrum.Temporal Lobe.Superior Temporal Gyrus.Gray Matter.Brodmann area 22
7	232	-49.5	-5.9	-8.4	0.006901	-51.0	-9.0	-4.0	Left Cerebrum.Temporal Lobe.Superior Temporal Gyrus.Gray Matter.Brodmann area 22
8	224	-1.9	-36.1	-8.0	0.007556	-6.0	-36.0	-8.0	Left Cerebellum.Anterior Lobe.Culmen.Gray Matter.*
8	224	-1.9	-36.1	-8.0	0.007331	2.0	-35.0	-8.0	Left Cerebellum.Anterior Lobe.Culmen.Gray Matter.*
8	224	-1.9	-36.1	-8.0	0.007112	-2.0	-37.0	-8.0	Left Cerebellum.Anterior Lobe.Culmen.Gray Matter.*
9	208	30.9	-38.4	16.5	0.007556	32.0	-36.0	16.0	Right Cerebrum.Sub-lobar.Caudate.Gray Matter.Caudate Tail
9	208	30.9	-38.4	16.5	0.007112	31.0	-42.0	17.0	Right Cerebrum.Sub-lobar.Caudate.Gray Matter.Caudate Tail
10	192	57.5	-36.3	23.3	0.007340	54.0	-36.0	22.0	Right Cerebrum.Sub-lobar.Insula.Gray Matter.Brodmann area 13
10	192	57.5	-36.3	23.3	0.007234	60.0	-38.0	24.0	Right Cerebrum.Temporal Lobe.Superior Temporal Gyrus.Gray Matter.Brodmann area 13

Anatomic Likelihood Estimation

Fox PT, Lancaster JL. Mapping context and content: the BrainMap model. Nat Rev Neurosci. 2002 Apr;3(4):319-21.

> <http://www.brainmap.org/ale/>
> <http://www.brainmap.org/scribe/>

Table 15. ALE report of first 10 clusters: WC: weighted center.

Multi-Level Kernel Density Analysis (mKDA): Wager Methods

<https://github.com/canlab/Canlab MKDA MetaAnalysis>

Definitions for mKDA

- 1) Cluster Definitions (KDA documentation of Wager's scripts)
- 2) Clusters in yellow - these are the clusters that surpass the height-corrected threshold.

Table 18: mKDA report

Contrasts	Folder	Height threshold clusters	p<0.001 clusters	p<0.01 clusters	p<0.05 clusters	Description
Study column in file	currAnalysis_study_contrast	2	2	6	0	Clusters found significant in both hemispheres, but very small
Uniform (all contrasts one)	currAnalysis_uniform_contrast	95	0	0	0	All clusters found significant and appear in final result
Study contrast subanalyses	Folder (in studycontrast_subanalysis)	NA	NA	NA	NA	Description
Increase	currAnalysis_study_increase	2	0	0	0	One cluster in both hemispheres
Increase, left	currAnalysis_study_increase_left	0	2	0	0	One small cluster in the left hemisphere
Increase, left, GM	currAnalysis_study_increase_left_GM	0	0	0	0	No significant clusters found
Increase, left, WM	currAnalysis_study_increase_left_WM	3	0	0	0	One tiny cluster in the left hemisphere
Increase, right	currAnalysis_study_increase_right	1	0	0	0	Two clusters in the right hemisphere
Increase, right, GM	currAnalysis_study_increase_right_GM	1	0	0	0	Two small clusters in the right hemisphere
Increase, right, WM	currAnalysis_study_increase_right_WM	3	0	2	0	Multiple clusters in both hemispheres
Decrease	currAnalysis_study_decrease	1	0	0	0	1 (2?) tiny clusters in left hemisphere
Decrease, left	currAnalysis_study_decrease_left	0	0	0	0	No significant clusters found
Decrease, left, GM	currAnalysis_study_decrease_left_GM	1	0	0	0	Tiny cluster in left hemisphere
Decrease, left, WM	currAnalysis_study_decrease_left_WM	1	3	1	0	Small clusters in left hemisphere
Decrease, right	currAnalysis_study_decrease_right	2	0	0	0	Tiny cluster in right hemisphere
Decrease, right, GM	currAnalysis_study_decrease_right_GM	0	0	0	0	No significant clusters found
Decrease, right, WM	currAnalysis_study_decrease_right_WM	2	0	0	0	Small clusters in left hemisphere
VBM	currAnalysis_study_vbm	1	1	0	0	Small clusters in left hemisphere
DTI	currAnalysis_study_DTI	2	0	0	0	Cluster in both
GM	currAnalysis_study_GM	0	0	0	0	No significant clusters found
Increase, GM	currAnalysis_study_increase_GM	0	0	0	0	No significant clusters found
Decrease, GM	currAnalysis_study_decrease_GM	0	0	0	0	No significant clusters found
WM	currAnalysis_study_WM	2	0	0	0	Cluster in both
Increase, WM	currAnalysis_study_increase_WM	3	0	2	0	Clusters in both hemispheres
Decrease, WM	currAnalysis_study_decrease_WM	1	0	0	0	Very tiny cluster in left
Left	currAnalysis_study_left	2	0	0	0	Clusters in left
Left, GM	currAnalysis_study_left_GM	0	0	0	0	No significant clusters found
Left, WM	currAnalysis_study_left_WM	3	4	0	0	Clusters in left
Right	currAnalysis_study_right	1	0	0	0	Two clusters in the right hemisphere
Right, GM	currAnalysis_study_right_GM	0	0	0	0	No significant clusters found
Right, WM	currAnalysis_study_right_WM	2	3	0	0	Clusters in right

- 3) Clusters in orange - these are incremental clusters that pass the most stringent extent-based threshold ($p < .001$) that are not within 10 mm of the clusters for the height-based threshold.
- 4) Clusters in red - these are incremental clusters that pass the medium extent-based threshold ($p < .01$) that are not within 10 mm of the clusters for the height-corrected and stringent extent-corrected thresholds.
- 5) Clusters in purple - these are incremental clusters that pass the lenient extent-based threshold ($p < .05$) that are not within 10 mm of the clusters for the height-corrected, as well as the stringent and medium extent-corrected thresholds.

Table mKDA report: Color of clusters in images: YELLOW, ORANGE, RED and PURPLE

The following cluster definitions used by Wager's scripts are briefly summarized (see SI for extended analysis). Yellow indicates clusters surpass the height-corrected threshold and orange, red and purple clusters are not within 10 mm of the clusters for the height-corrected. Further, orange indicates clusters pass the most stringent extent-based threshold ($p < .001$), red indicates clusters that pass the medium extent-based threshold ($p < .01$) and purple indicates clusters pass the lenient extent-based threshold ($p < .05$). The primary mKDA analyses were done for acquired and congenital separately and combined. Additional analyses are found in the SI.

Cluster comparisons list

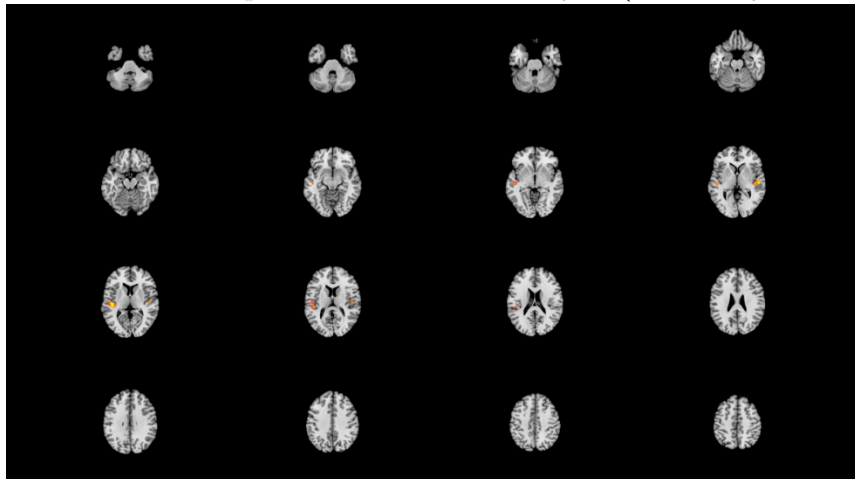
The following mKDA specific analyses were conducted. If no significant clusters were found, no image map was produced.

1. Cluster: Specific ROI cluster analysis
2. Cluster: All MNI Coordinate mapping
3. Cluster: Increase (all increase)
 - (a) Cluster: Increase left (all left)
 - i. Cluster: Increase left GM
 - ii. Cluster: Increase left WM

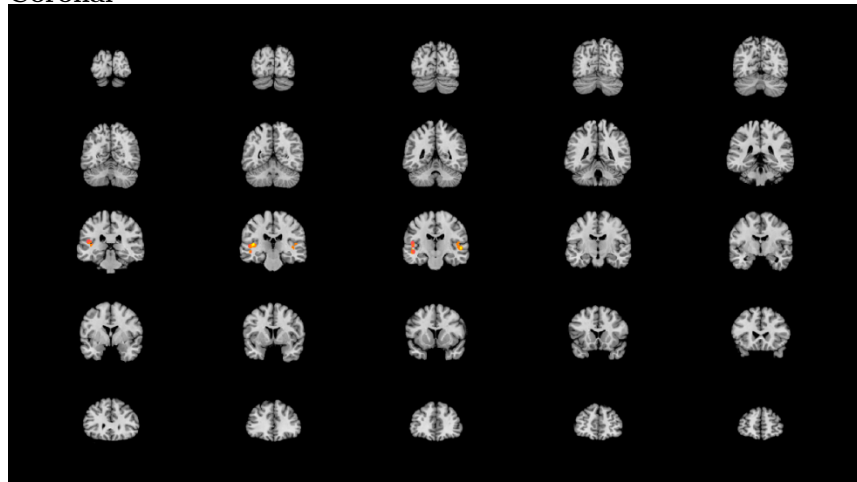
- (b) Cluster: Increase right (all right)
 - i. Cluster: Increase right GM
 - ii. Cluster: Increase right WM)
- 4. Cluster: Decrease (all decrease)
 - (a) Cluster: Decrease left (all left)
 - i. Cluster: Decrease left GM
 - ii. Cluster: Decrease left WM)
 - (b) Cluster: Decrease right (all right)
 - i. Cluster: Decrease right GM
 - ii. Cluster: Decrease right WM
- 5. Cluster: All VBM (only VBM)
- 6. Cluster: ALL DTI (Only DTI)
- 7. Cluster: ALL GM (irrespective of increase or decrease)
 - (a) Cluster: GM increase
 - (b) Cluster: GM decrease
- 8. Cluster: All WM (irrespective of increase or decrease)
 - (a) Cluster: WM increase
 - (b) Cluster: WM decrease
- 9. Cluster: All Left
 - (a) Cluster: All left GM (to match regression figure panel)
 - (b) Cluster: All left WM (to match regression figure panel)
- 10. Cluster: All right
 - (a) Cluster: All right GM (to match regression figure panel)
 - (b) Cluster: All right WM (to match regression figure panel)

The important information for results is contained in the cl variable in the Activation_clusters.mat file. This gives you a variable with 4 fields or cells, and within a cell is information about the regions (clusters/brain blobs) that pass the height threshold (referred to as cl{1}), the $p < .001$ threshold (referred to as cl{2}), the $p < .01$ threshold (referred to as cl{3}), and the $p < .05$ threshold (referred to as cl{4}), respectively.

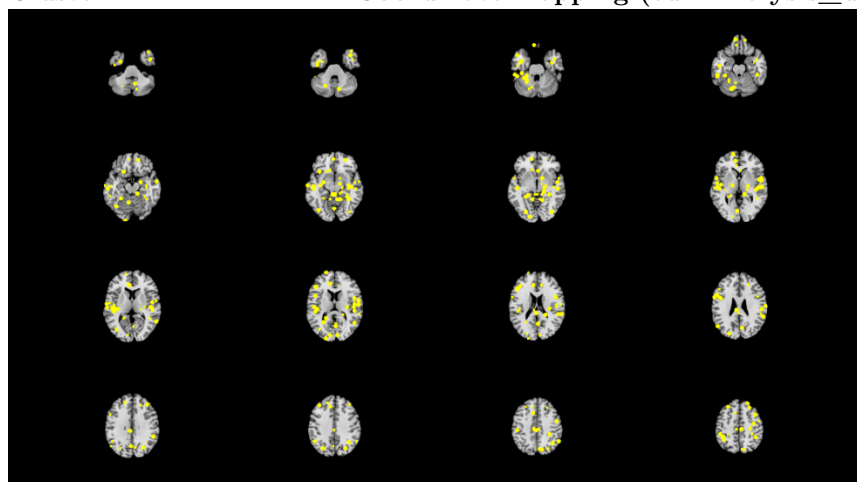
Cluster mKDA: Specific ROI cluster analysis (currAnalysis study contrast) Axial



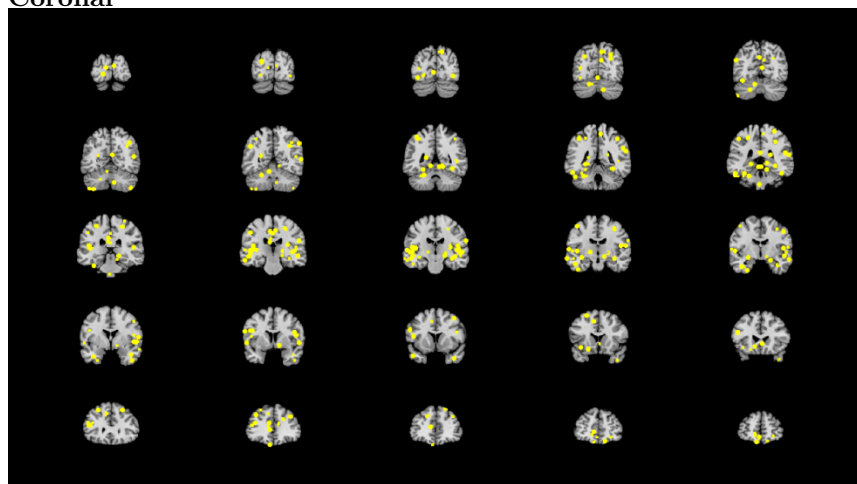
Coronal



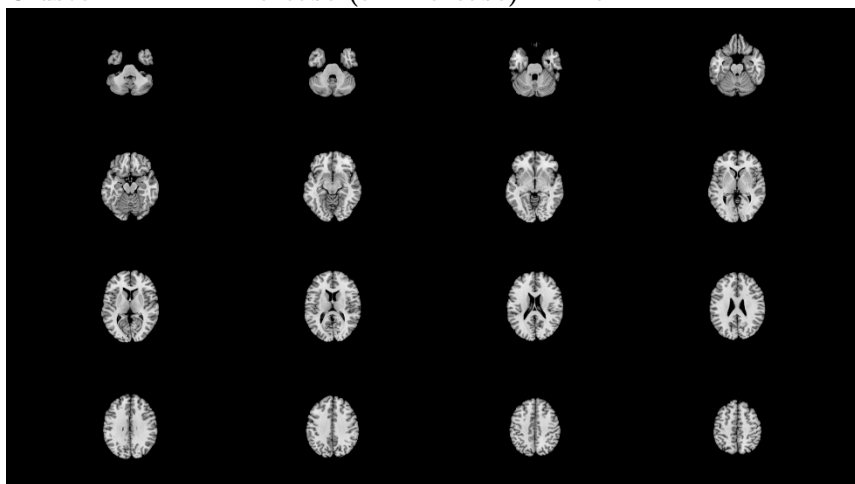
Cluster mKDA: All MNI Coordinate mapping (currAnalysis_uniform_contrast) Axial



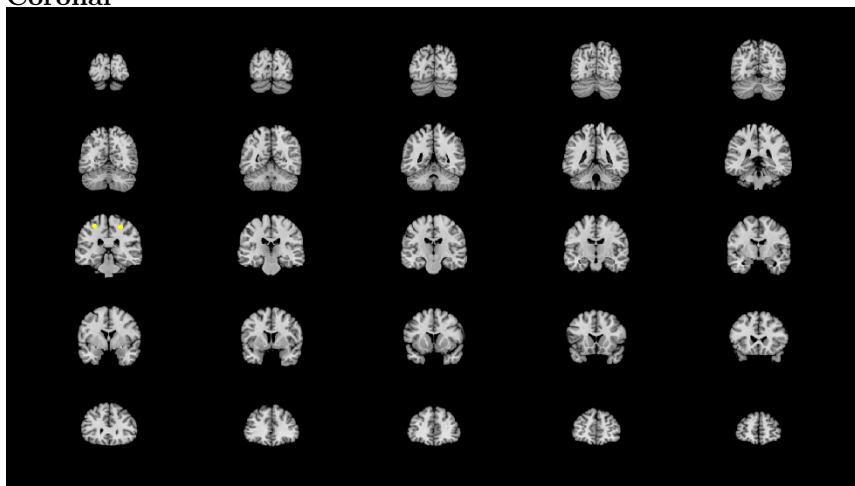
Coronal



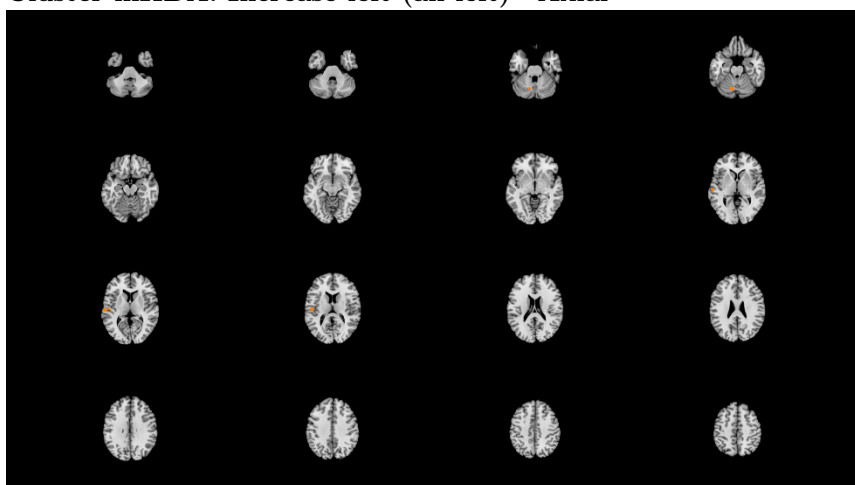
Cluster mKDA: Increase (all increase) Axial



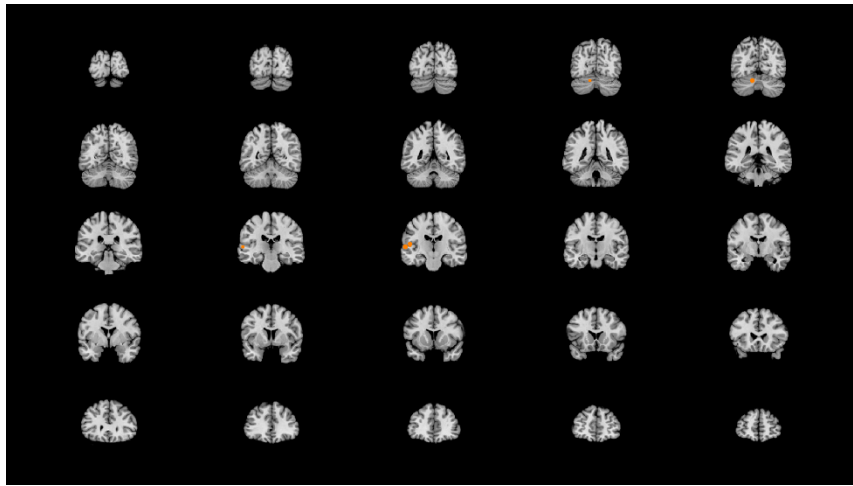
Coronal



Cluster mKDA: Increase left (all left) Axial

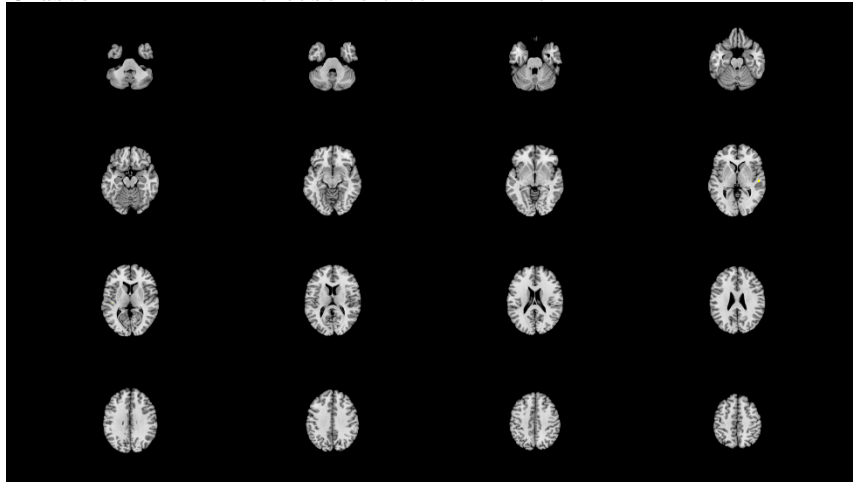


Coronal

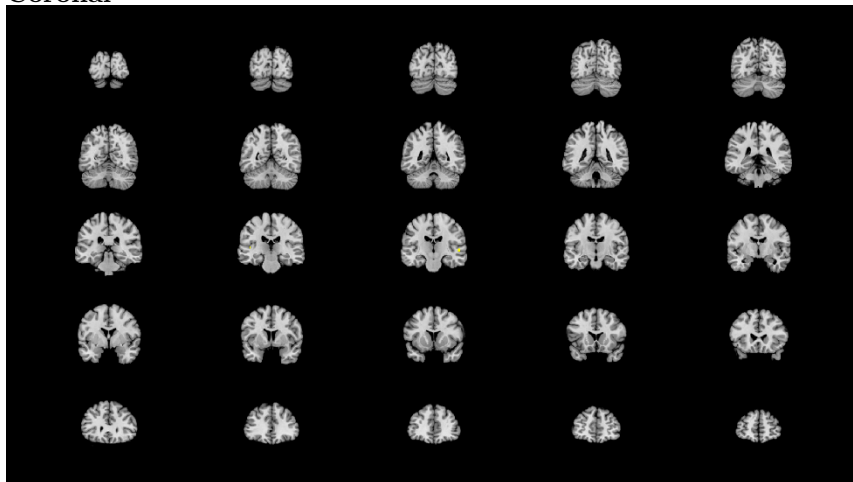


Cluster mKDA: Increase left GM No significant clusters found. No image map produced.

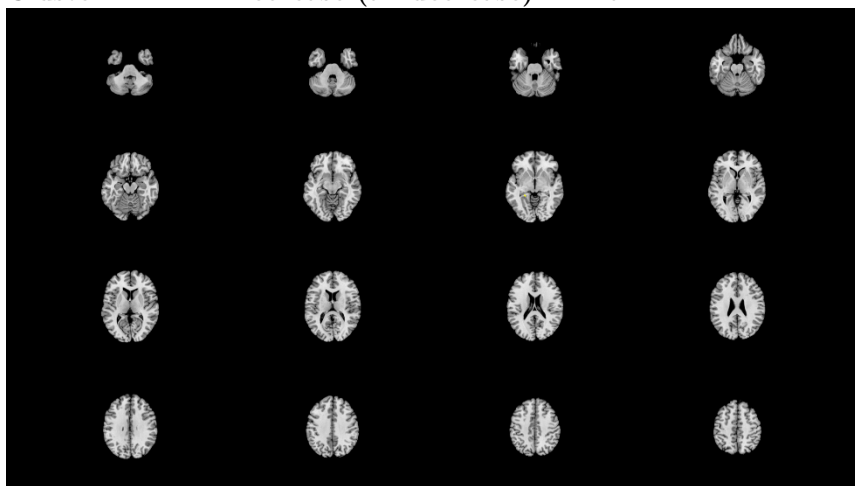
Cluster mKDA: Increase left WM Axial



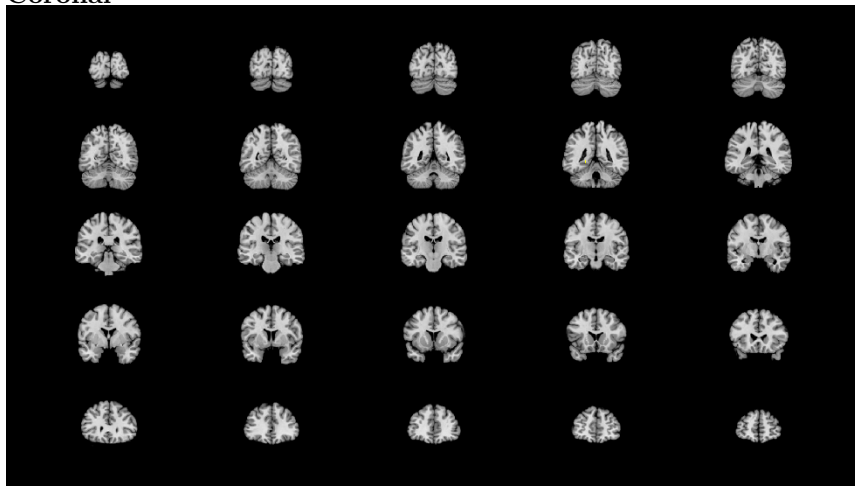
Coronal



Cluster mKDA: Decrease (all decrease) Axial

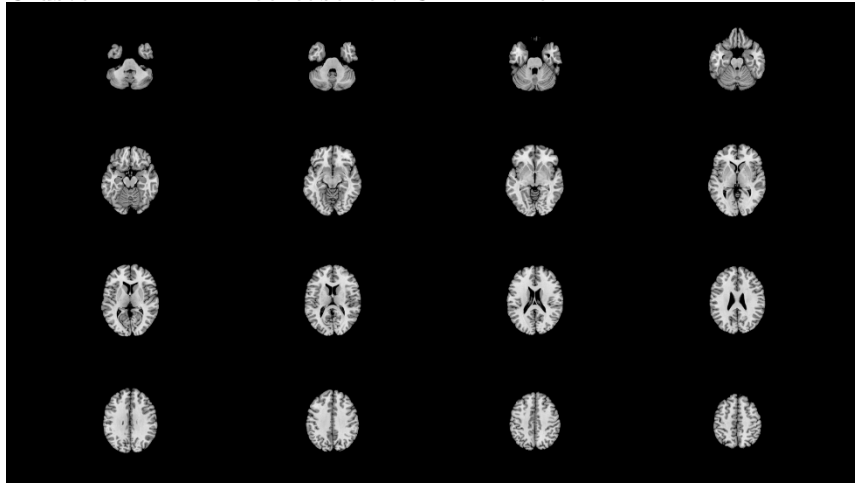


Coronal

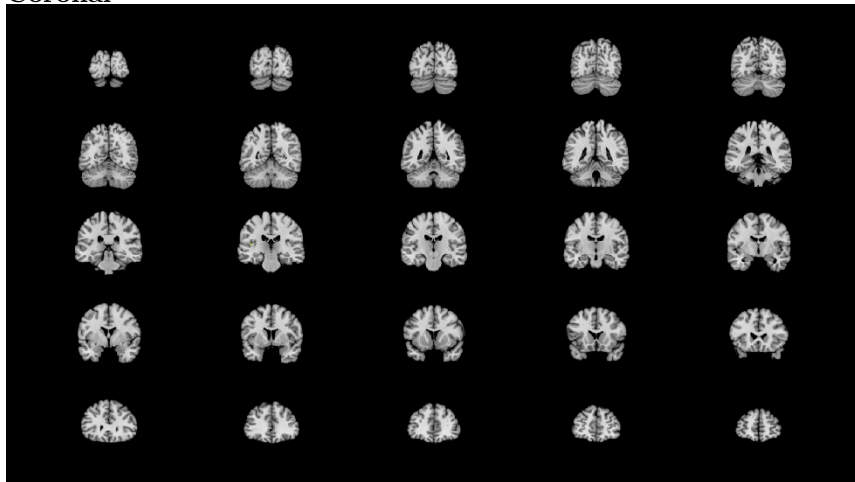


Cluster mKDA: Decrease left (all left) No significant clusters found. No image map produced.

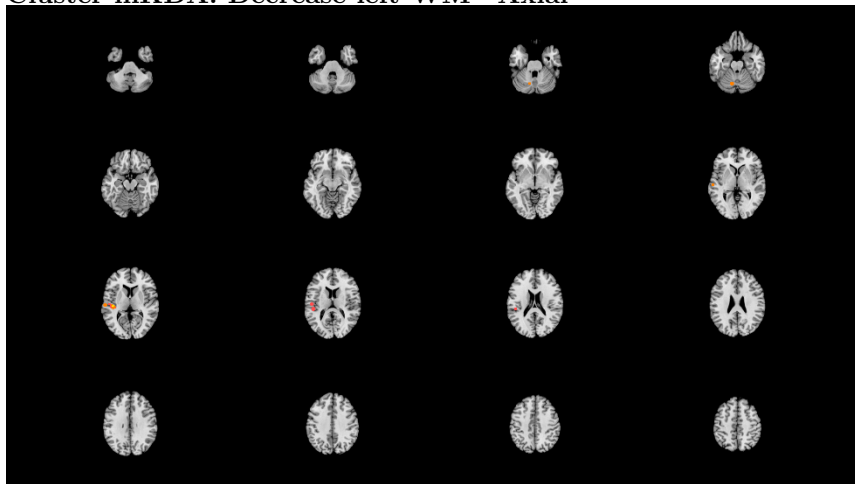
Cluster mKDA: Decrease left GM Axial



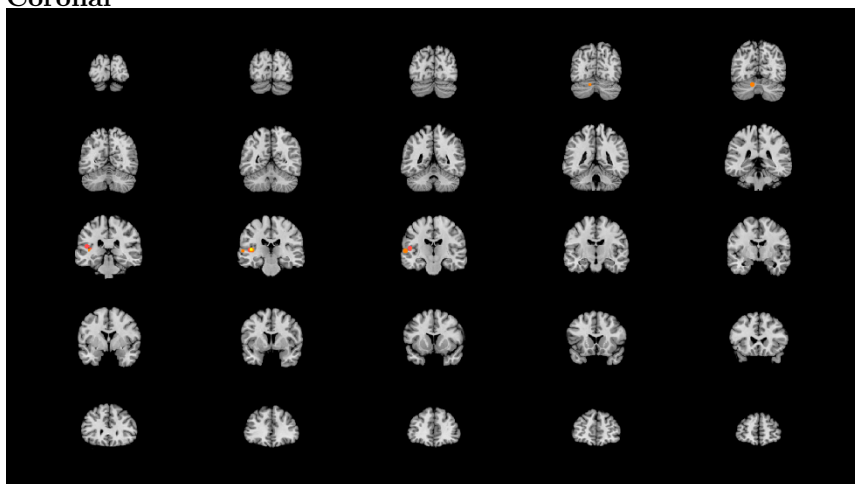
Coronal



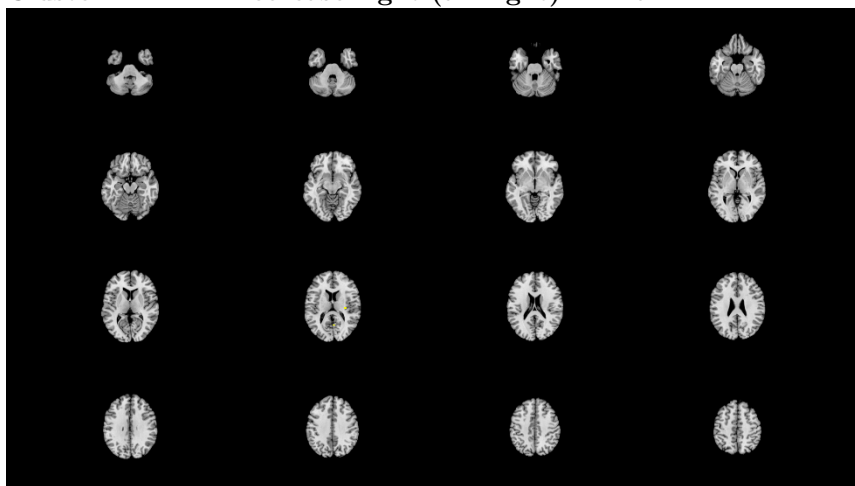
Cluster mKDA: Decrease left WM Axial



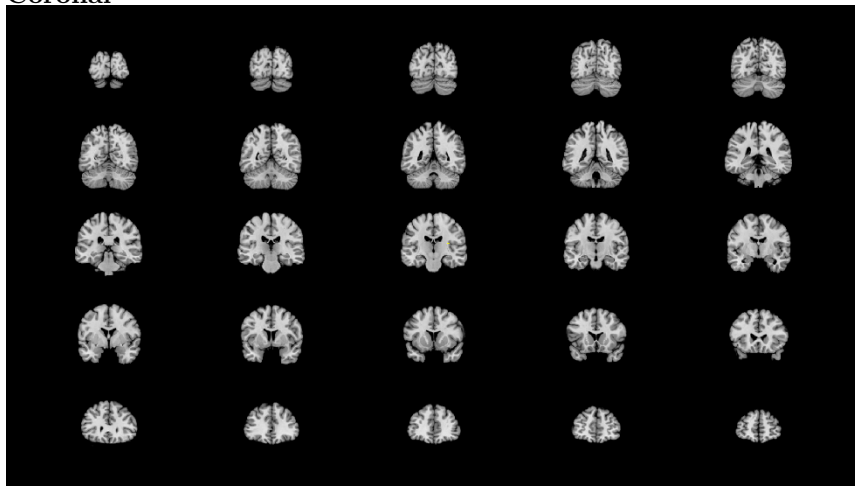
Coronal



Cluster mKDA: Decrease right (all right) Axial

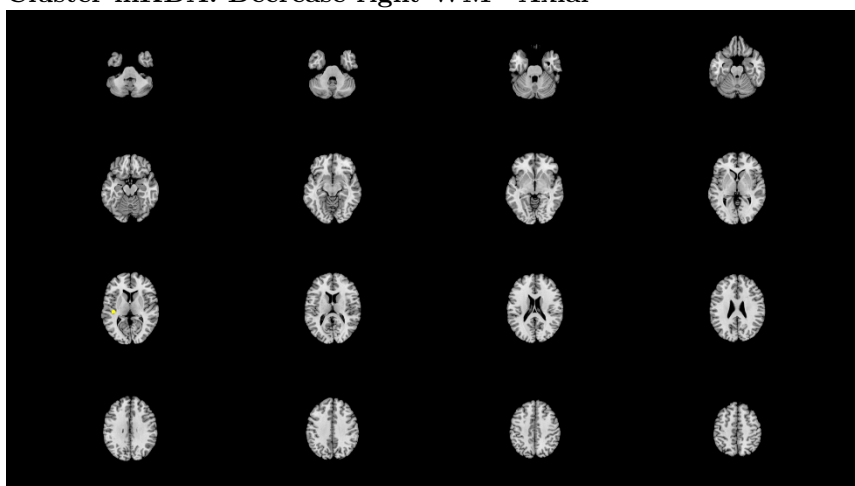


Coronal

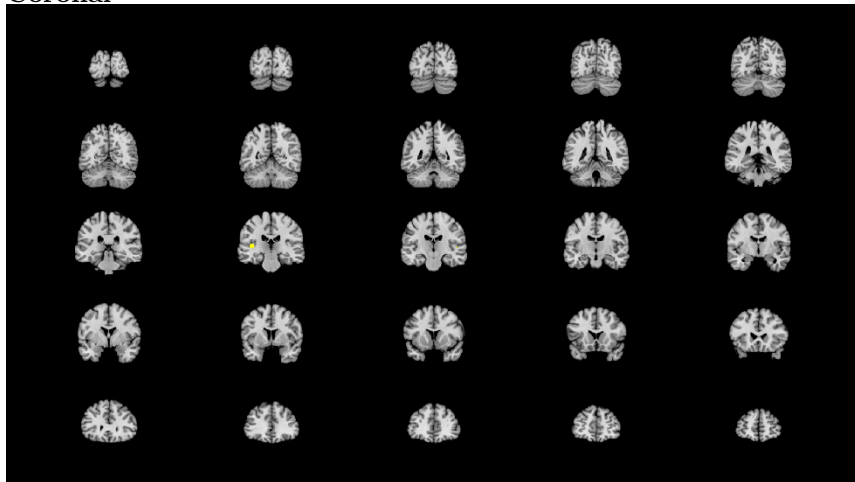


Cluster mKDA: Decrease right GM No significant clusters found. No image map produced.

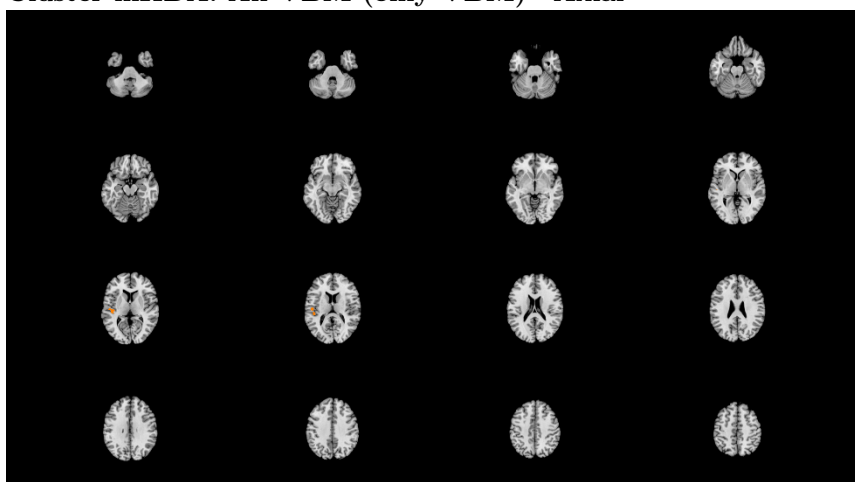
Cluster mKDA: Decrease right WM Axial



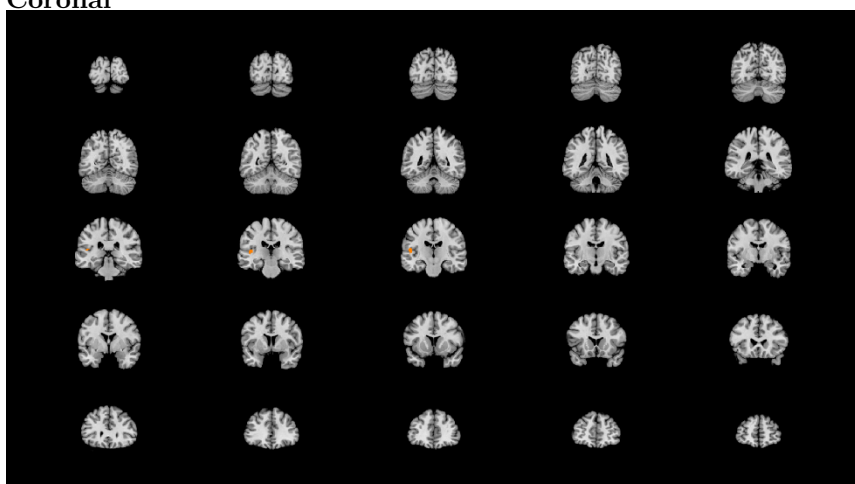
Coronal



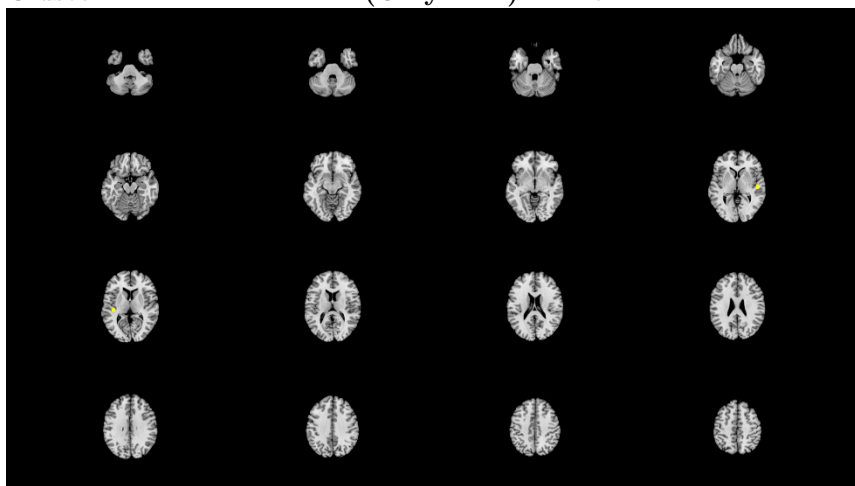
Cluster mKDA: All VBM (only VBM) Axial



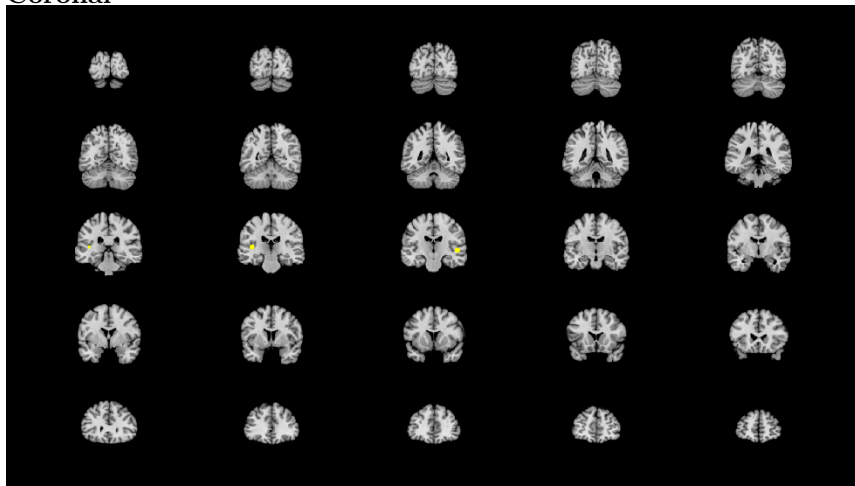
Coronal



Cluster mKDA: ALL DTI (Only DTI) Axial



Coronal

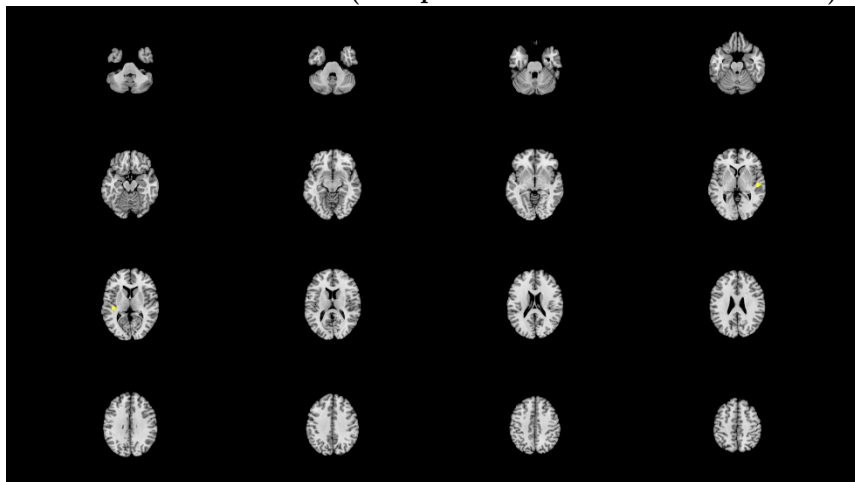


Cluster mKDA: ALL GM (irrespective of increase or decrease) No significant clusters found. No image map produced.

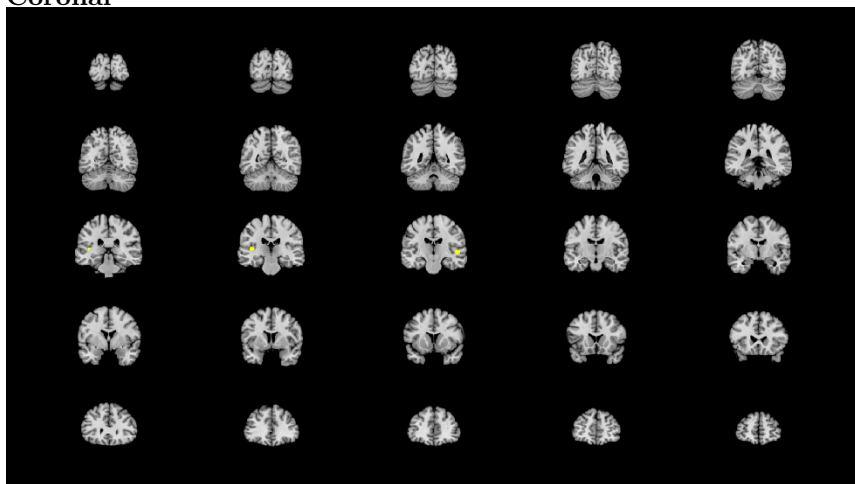
Cluster mKDA: GM increase No significant clusters found. No image map produced.

Cluster mKDA: GM decrease No significant clusters found. No image map produced.

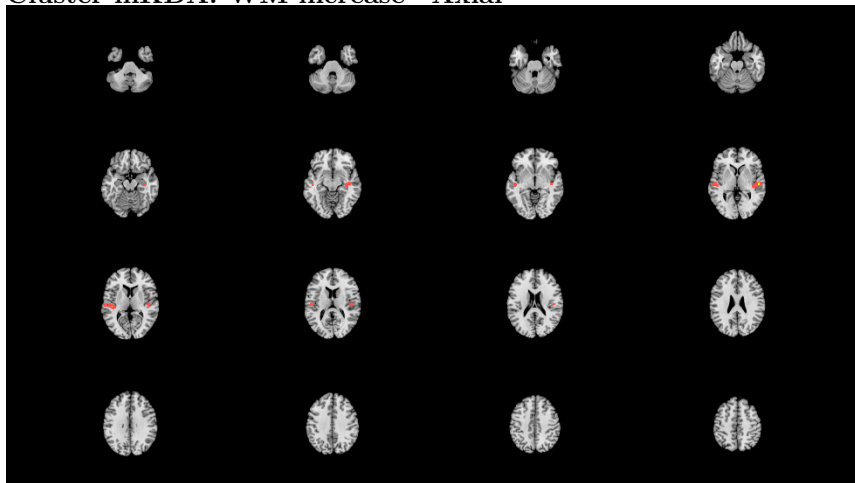
Cluster mKDA: All WM (irrespective of increase or decrease) Axial



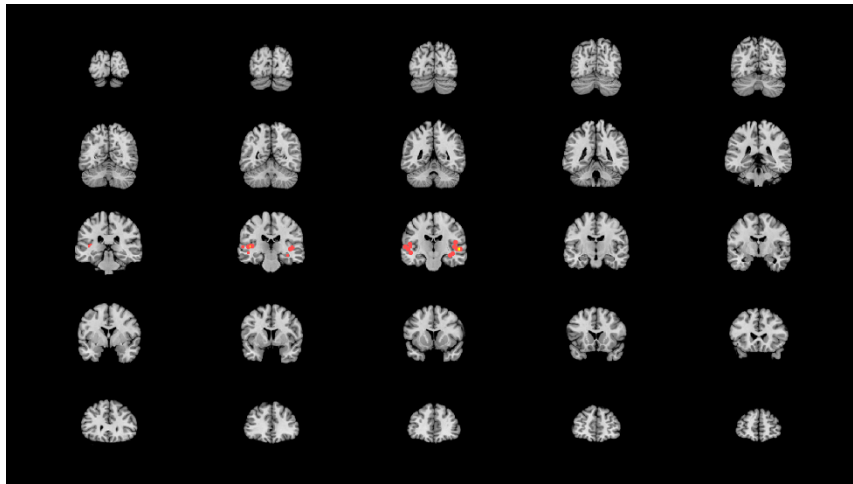
Coronal



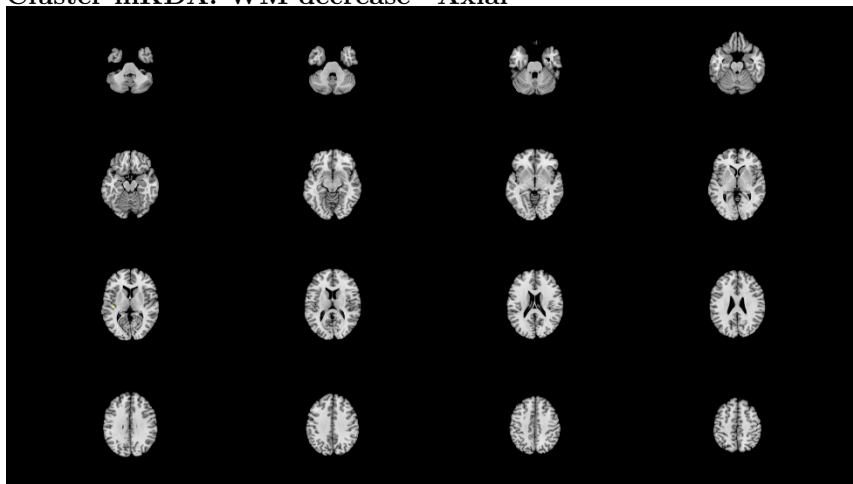
Cluster mKDA: WM increase Axial



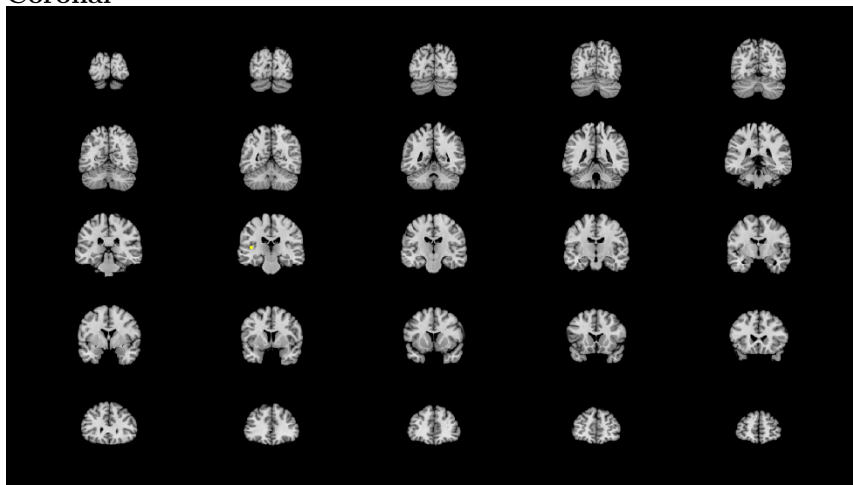
Coronal



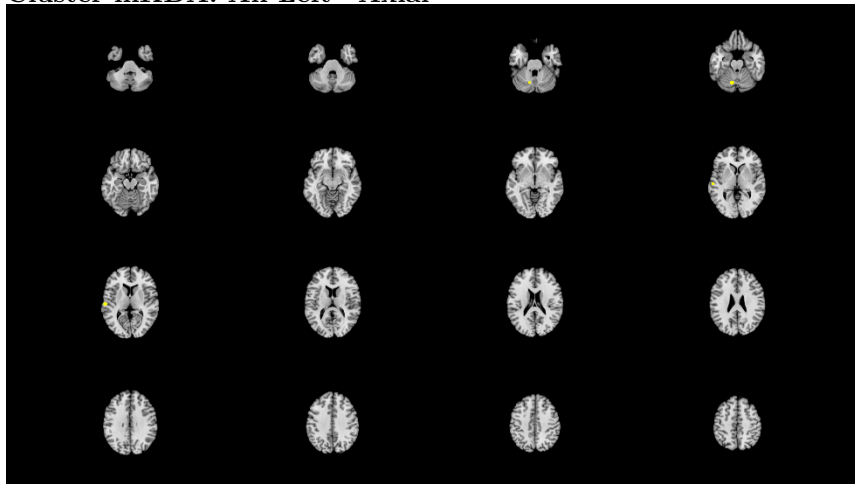
Cluster mKDA: WM decrease Axial



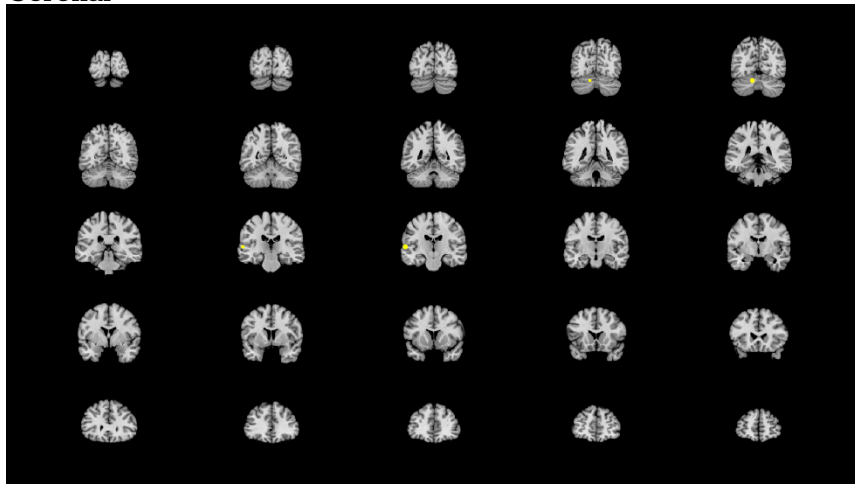
Coronal



Cluster mKDA: All Left Axial

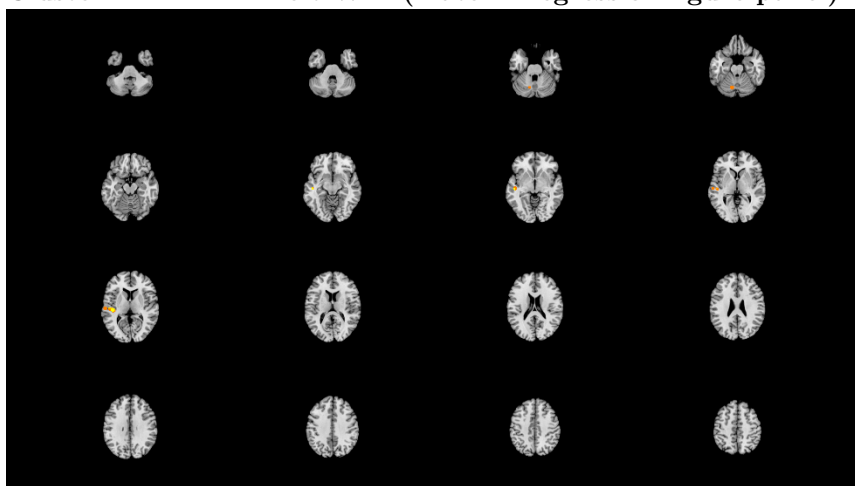


Coronal

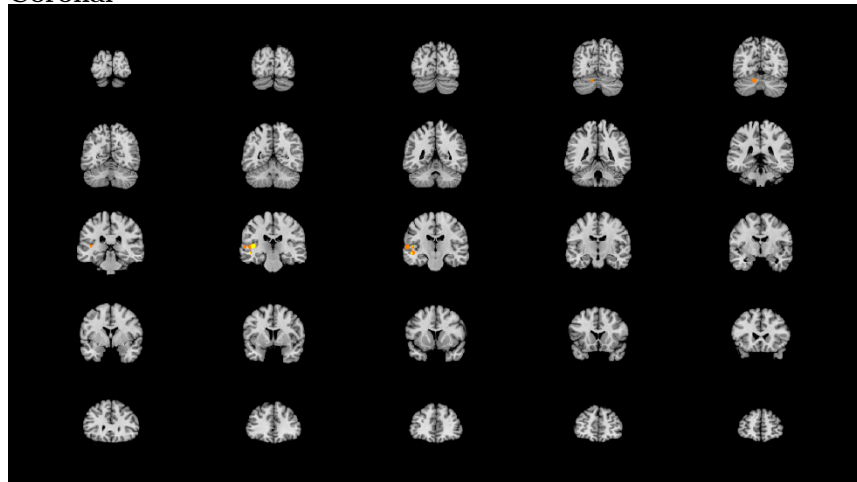


Cluster mKDA: All left GM (match - regression figure panel) No significant clusters found. No image map produced.

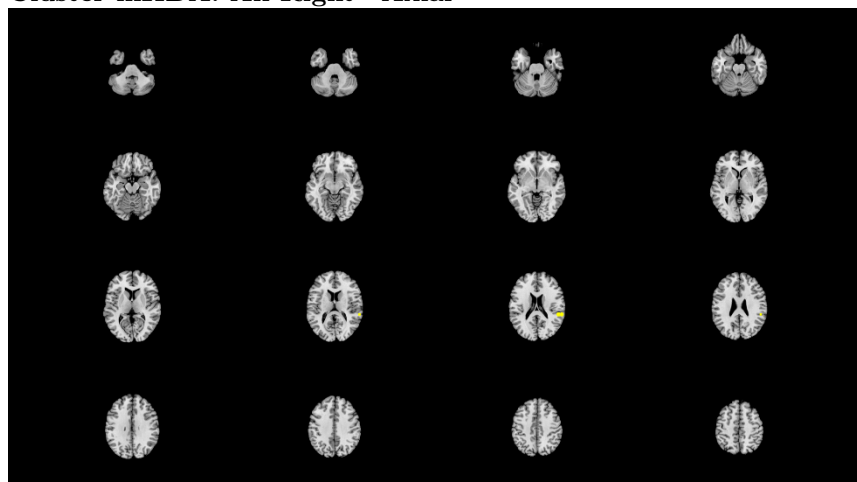
Cluster mKDA: All left WM (match - regression figure panel) Axial



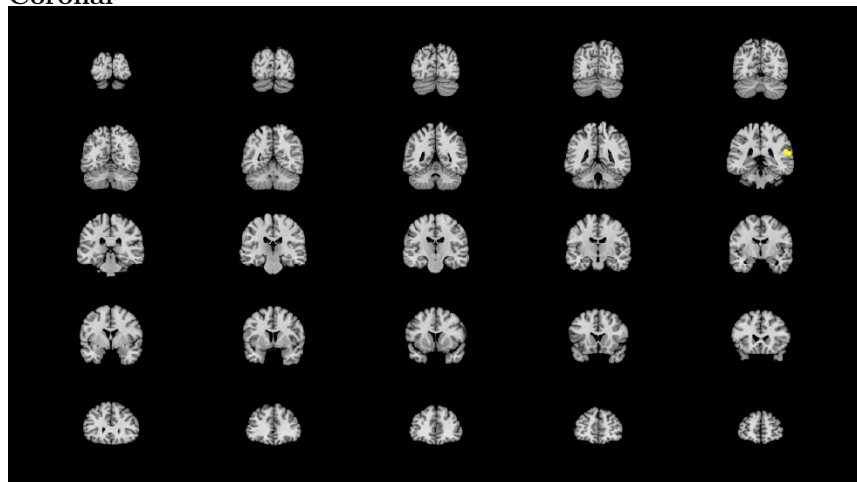
Coronal



Cluster mKDA: All Right Axial

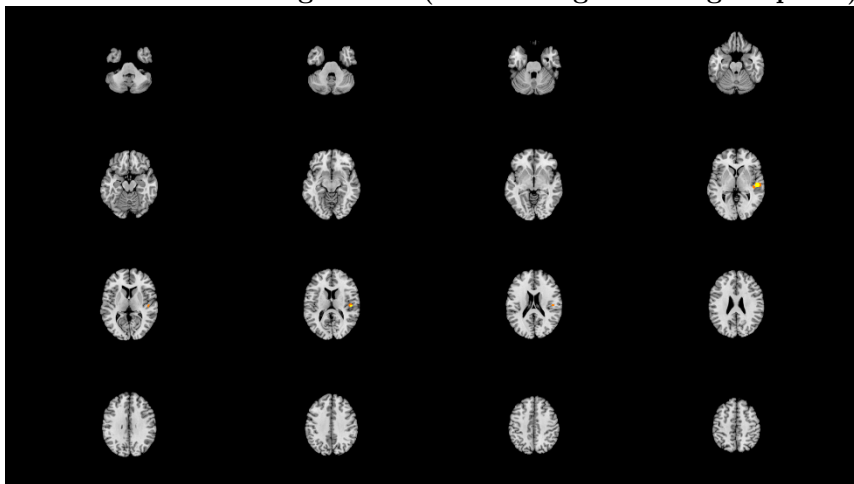


Coronal

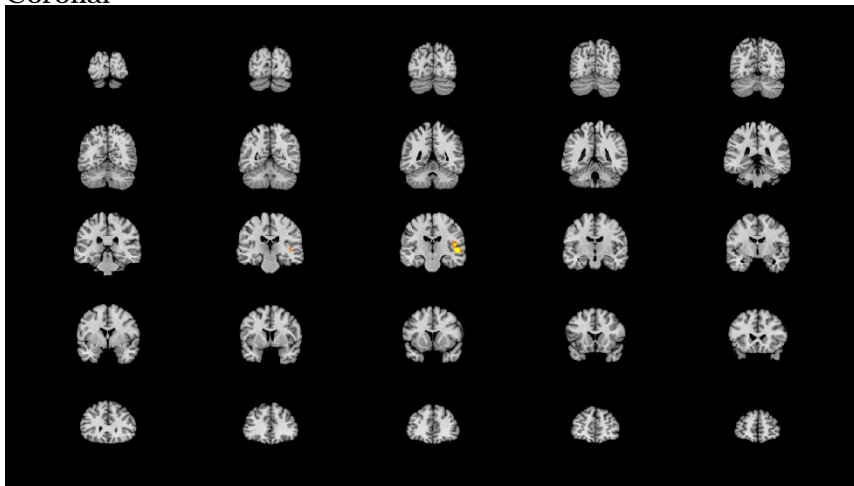


Cluster mKDA: All right GM (match - regression figure panel) No significant clusters found. No image map produced.

Cluster mKDA: All right WM (match - regression figure panel) Axial

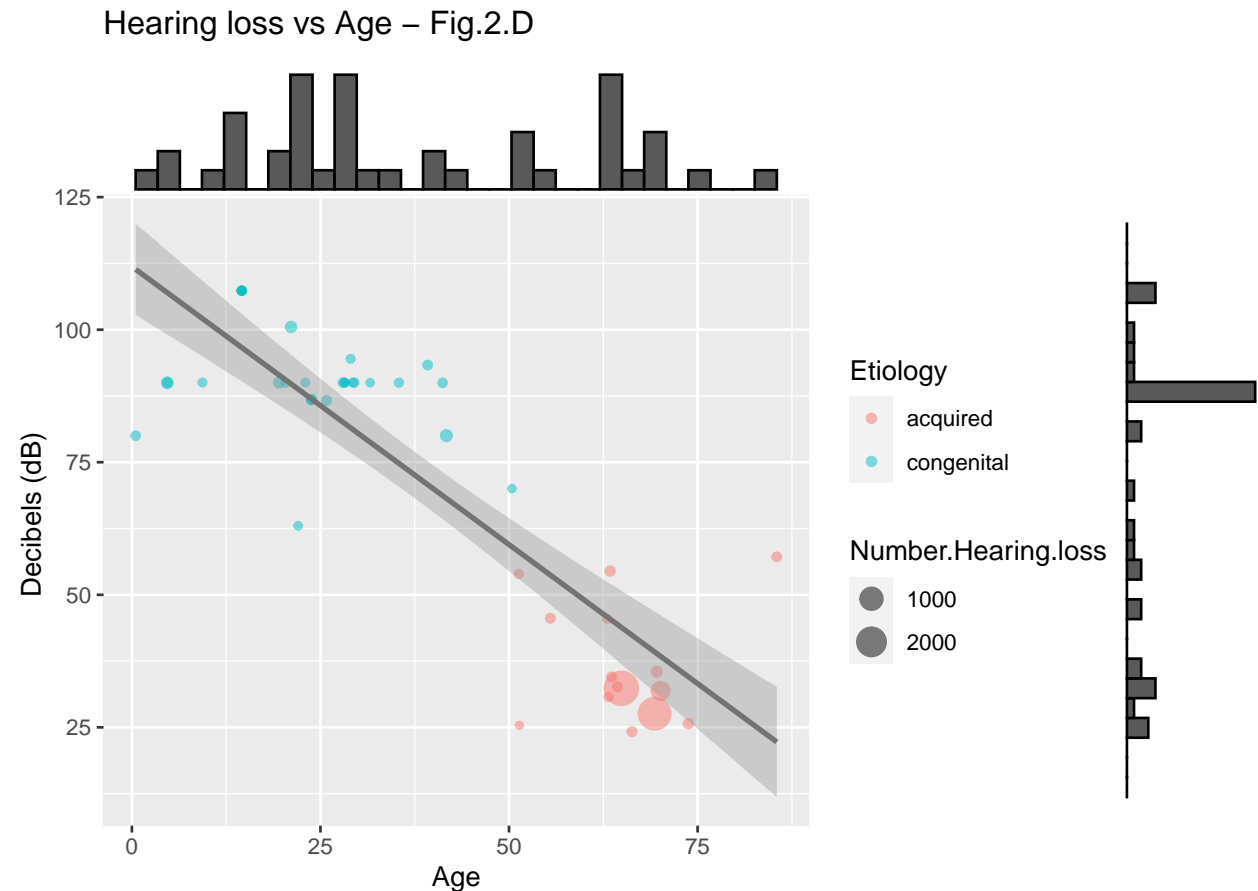


Coronal

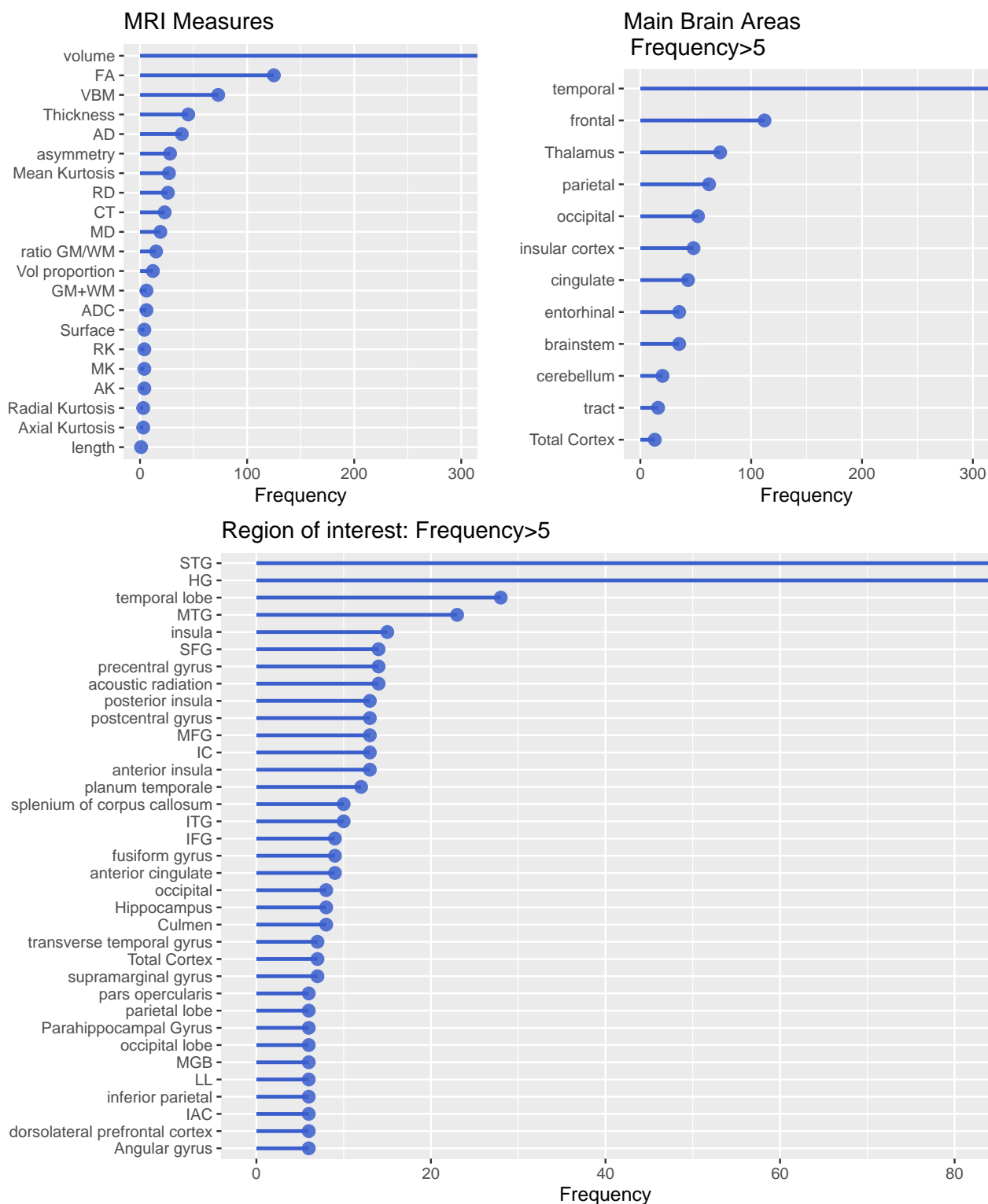


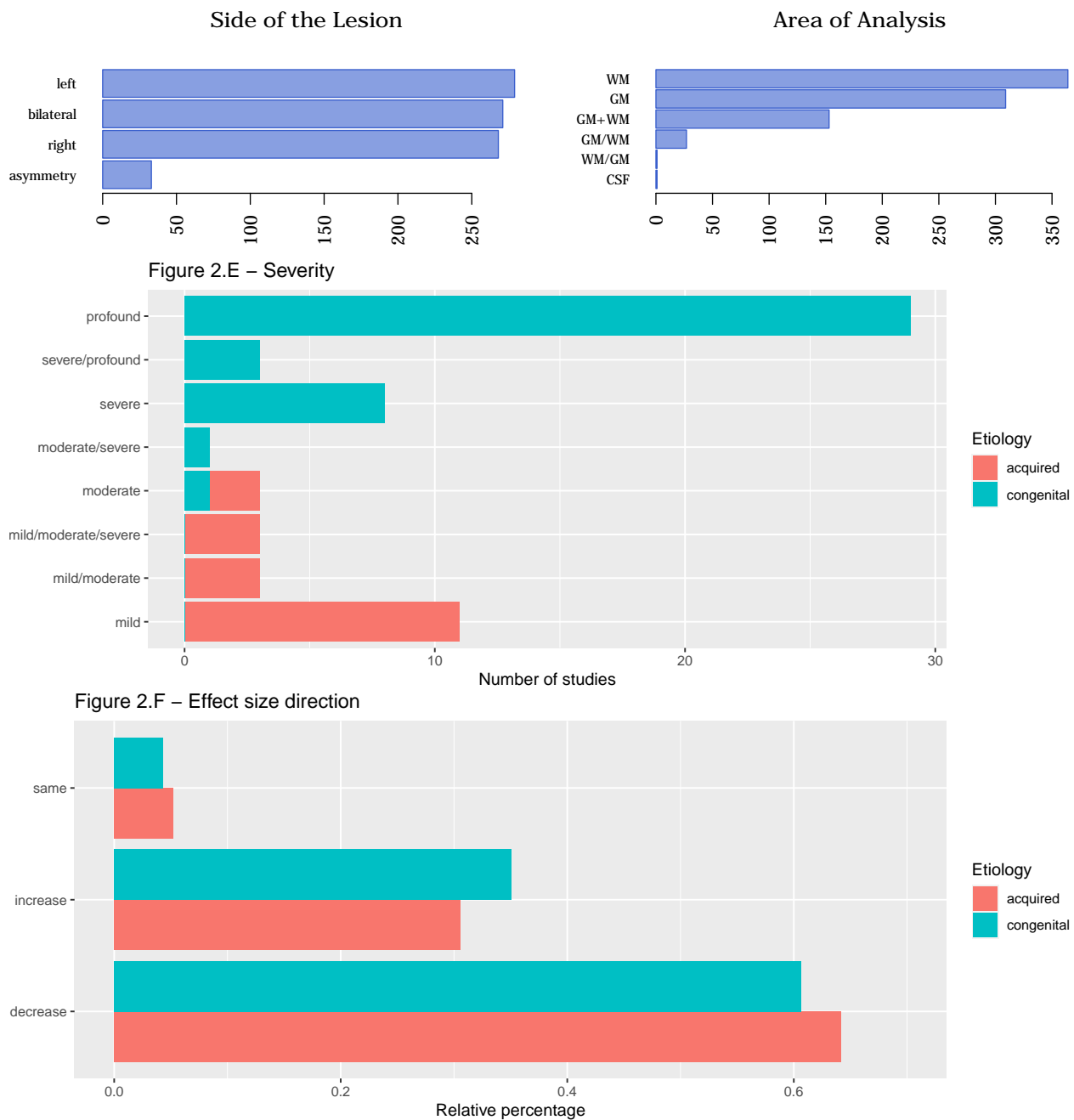
Studies characteristics

Relation between hearing loss (dB) and age (Figure 2.D)



Studies characteristics (Figure 2.E, 2.F)





Brain structure (GM, WM) and MRI measures

Highlights

- Most of the studies that measured Gray matter focus on cortical changes (volume, thickness and VBM).
- White matter studies are more heterogeneous in their measurements.
- Diffusion tensor (DT) derived measurements are the most frequent in white matter, followed by volume.
- It is harder to interpret a meta-analysis of multiple white matter measurements because its effect varies widely in different directions. The measurements derived from DT have the most differences.

We conduct our meta-analysis using the **TWO** most frequent measurements for gray and white matter. We use *volume* for GM and *fractional anisotropy* for WM.

Further meta regressions can be found in the supplementary material.

Gray Matter

- thickness
- VBM

White Matter integrity

- mean diffusivity MD
- radial diffusivity RD
- axial diffusivity AD
- mean kurtosis

White Matter volume

- thickness (I am unsure how they did this)
- VBM
- volume

Bilatereal - GM volume

- WM volume
- WM fractional anisotropy

Frequency table: Brain structure (GM, WM) and MRI measures

Table 19: Matter vs measure (continued below)

	AD	ADC	AK	asymmetry	Axial Kurtosis	CT	FA	GM+WM
GM	0	0	2	9	0	23	8	0
WM	39	6	2	8	3	0	117	0

Table 20: Table continues below

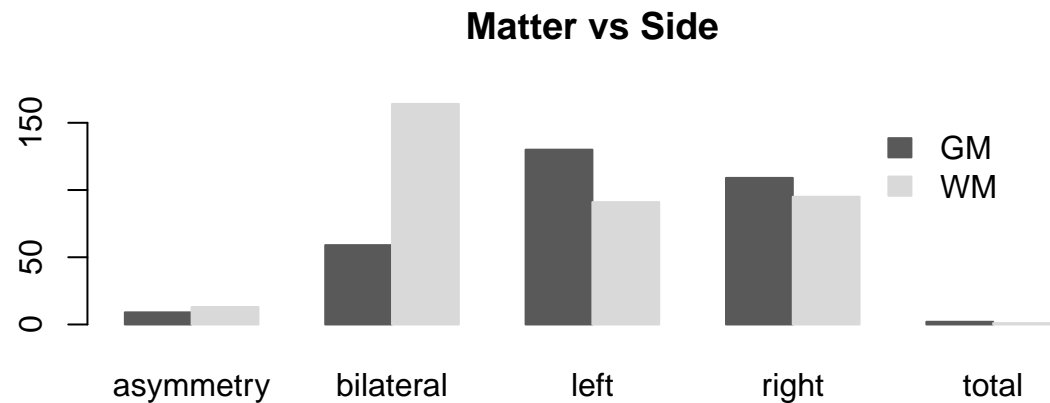
	length	MD	Mean Kurtosis	MK	Radial Kurtosis	ratio GM/WM	RD
GM	0	2	0	2	0	0	0
WM	1	17	27	2	3	0	26

	RK	Surface	Thickness	VBM	Vol proportion	volume
GM	2	4	14	43	6	194
WM	2	0	10	16	6	79

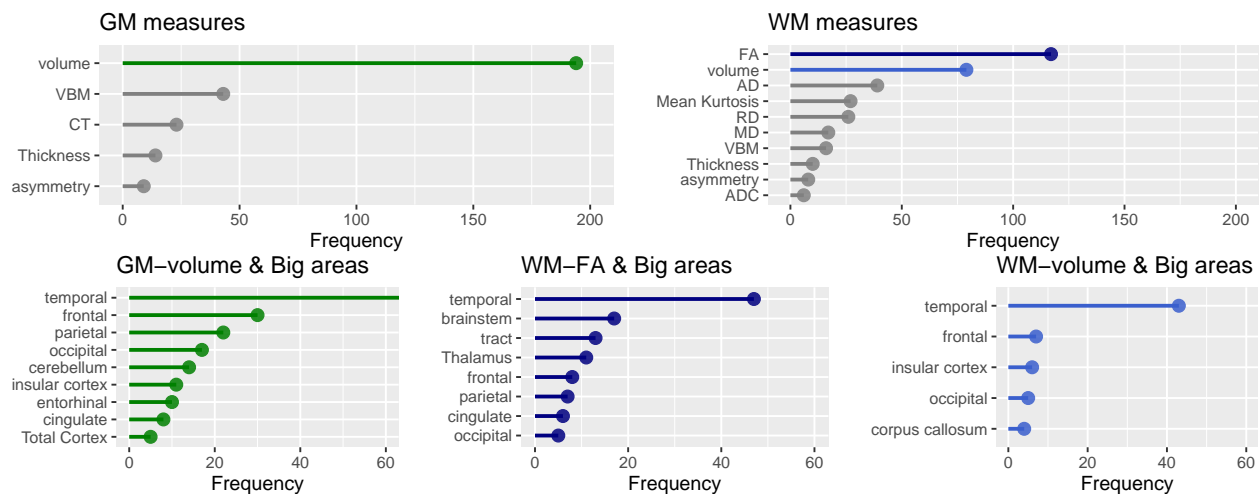
Table 22: Matter vs Side

	asymmetry	bilateral	left	right	total
GM	9	59	130	109	2
WM	13	164	91	95	1

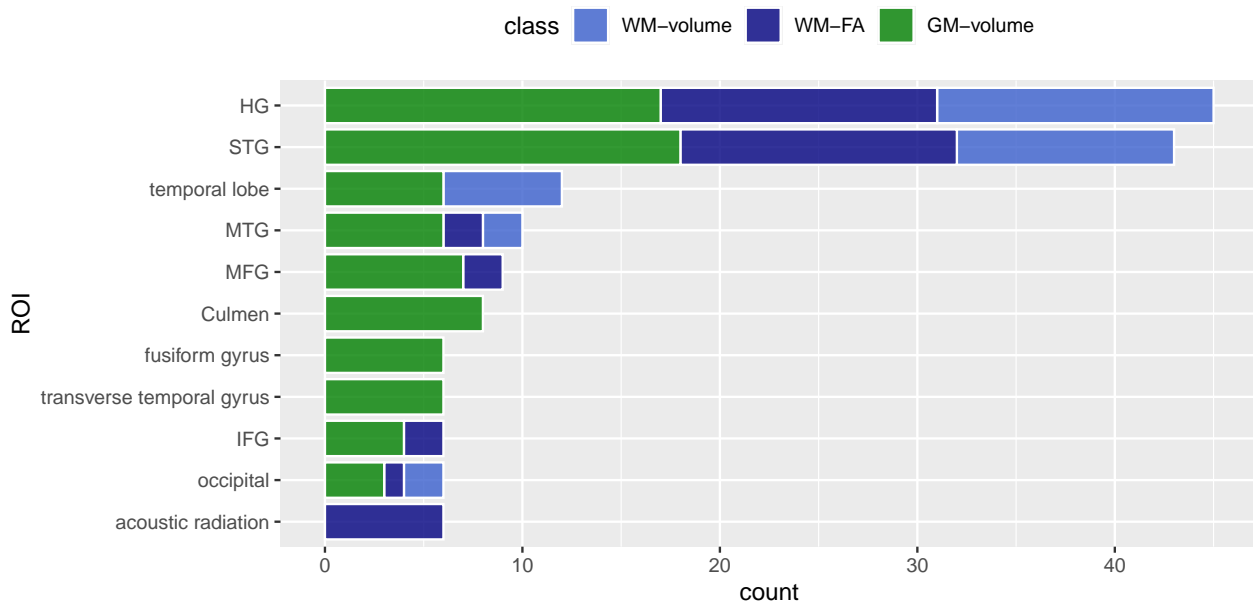
Brain structure (GM, WM) and side



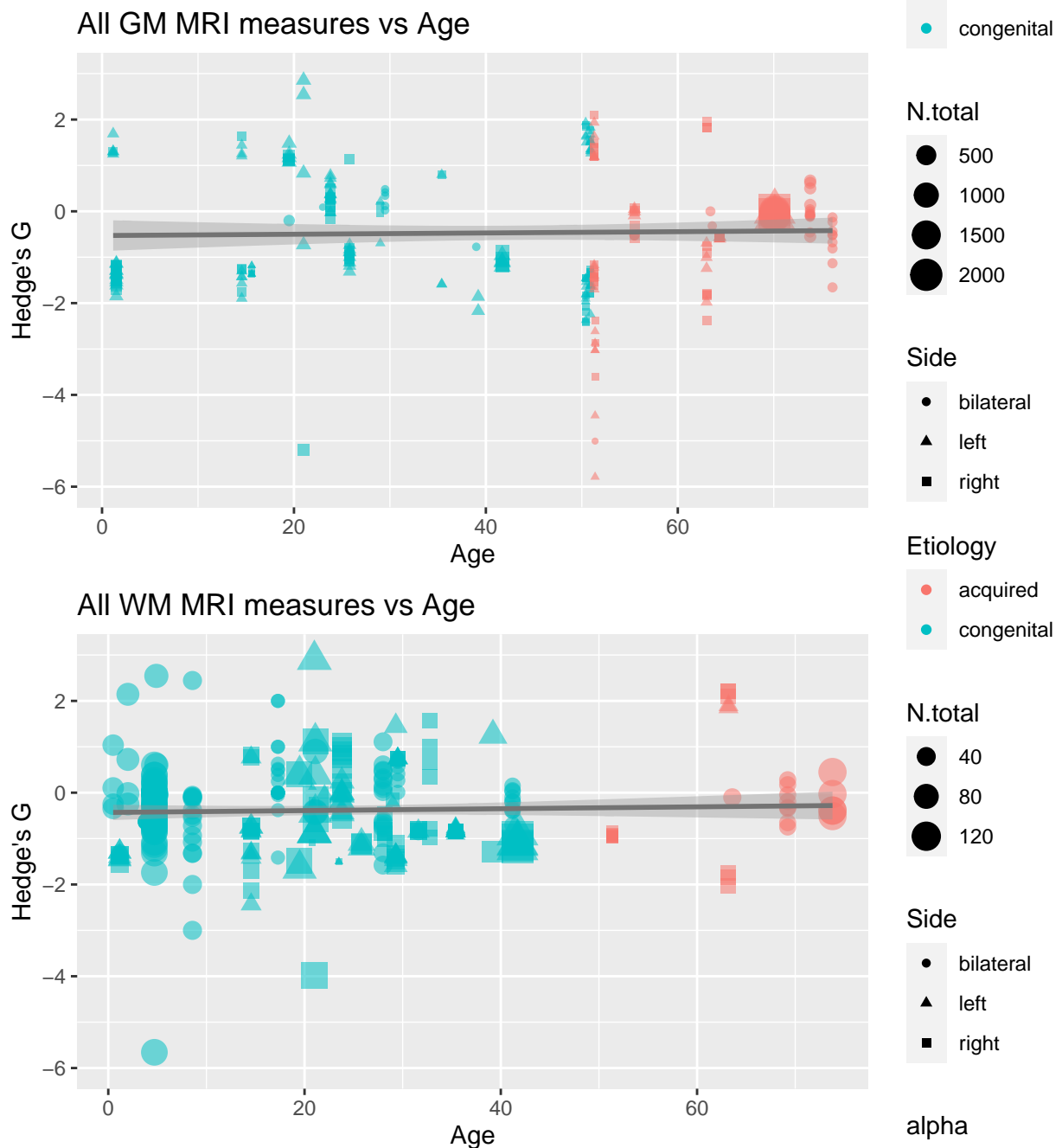
Studies characteristics (Figure 2.A, 2.B): Brain structure (GM, WM) by MRI measure (volume and FA)



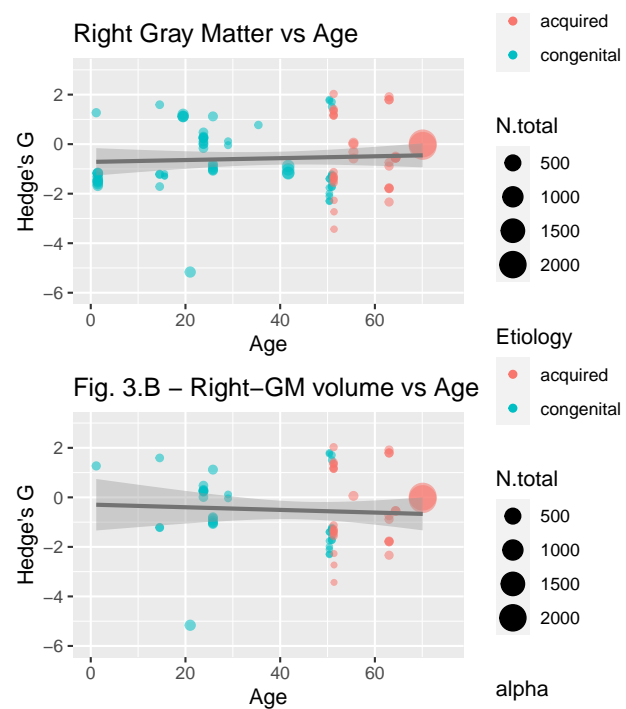
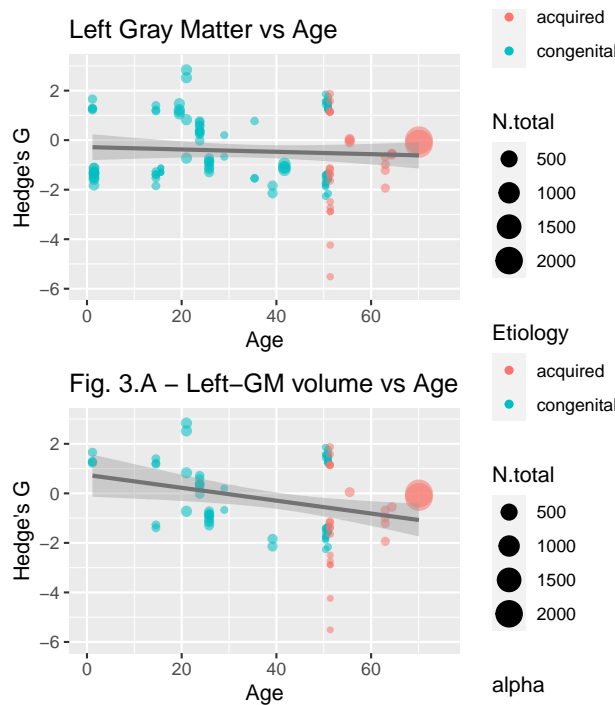
MRI measures by ROI (Figure 2.C)



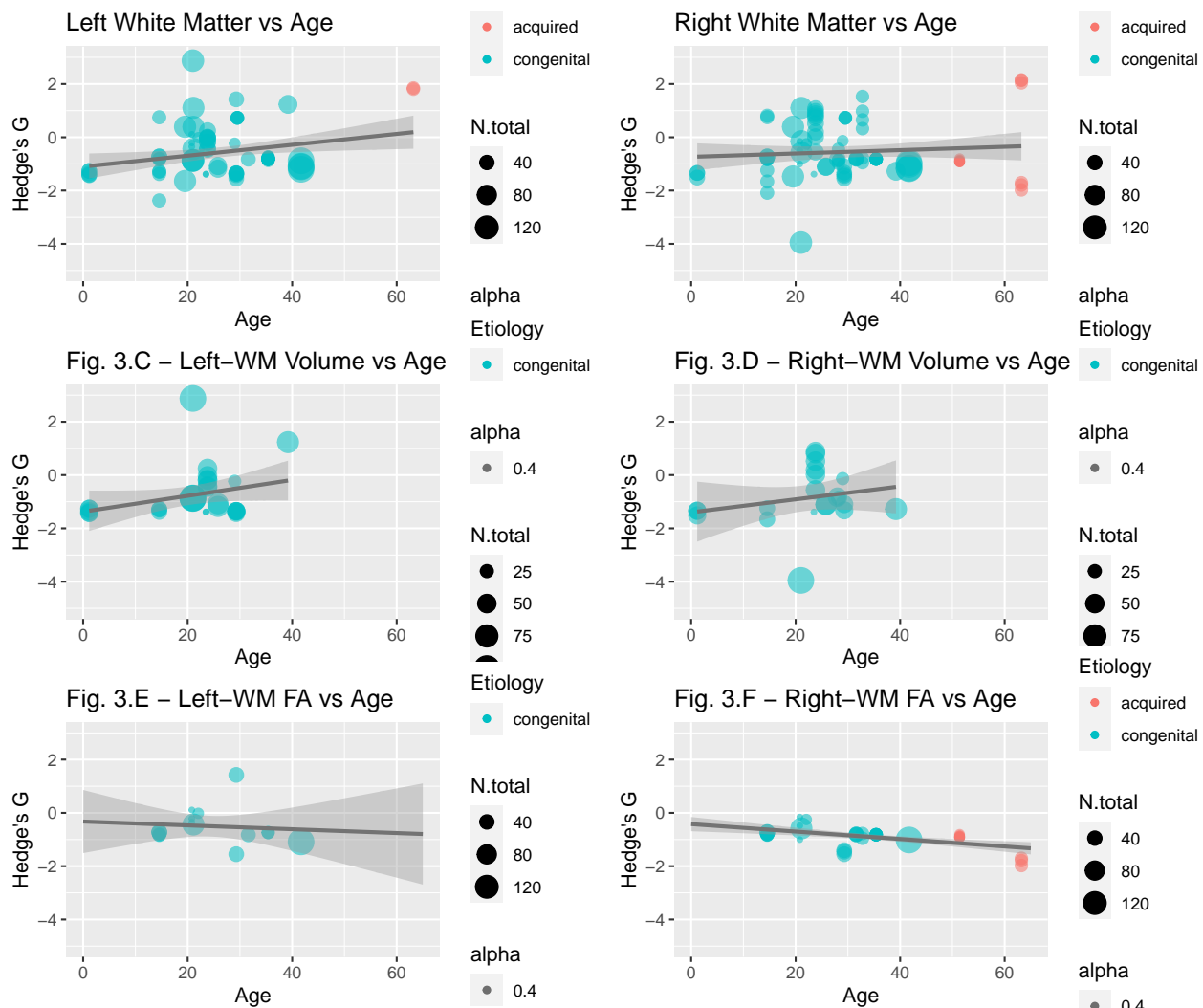
Relations of all MRI measurements of GM and WM with age



Gray matter relation with Age by volume (Figures 3.A and 3.B)



White matter relation with Age by volume and FA (Figures 3.C, 3.D and 3.F)



Gray and White matter relation with Age by asymmetry

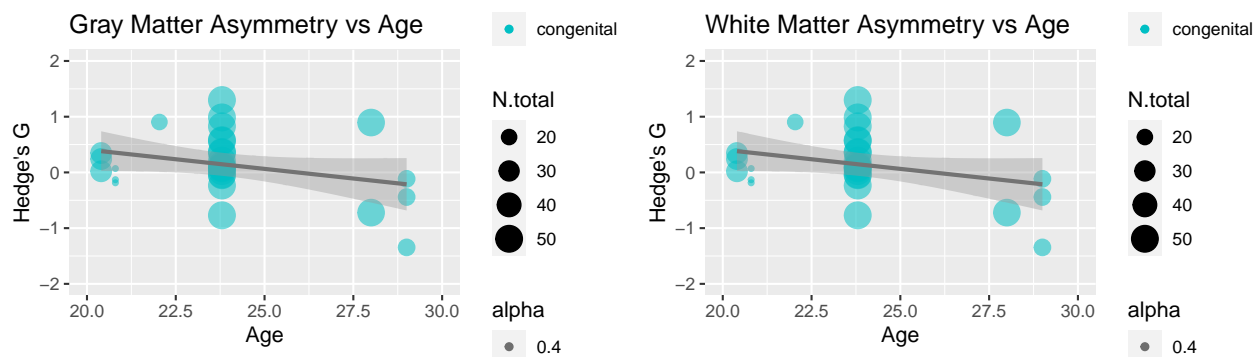
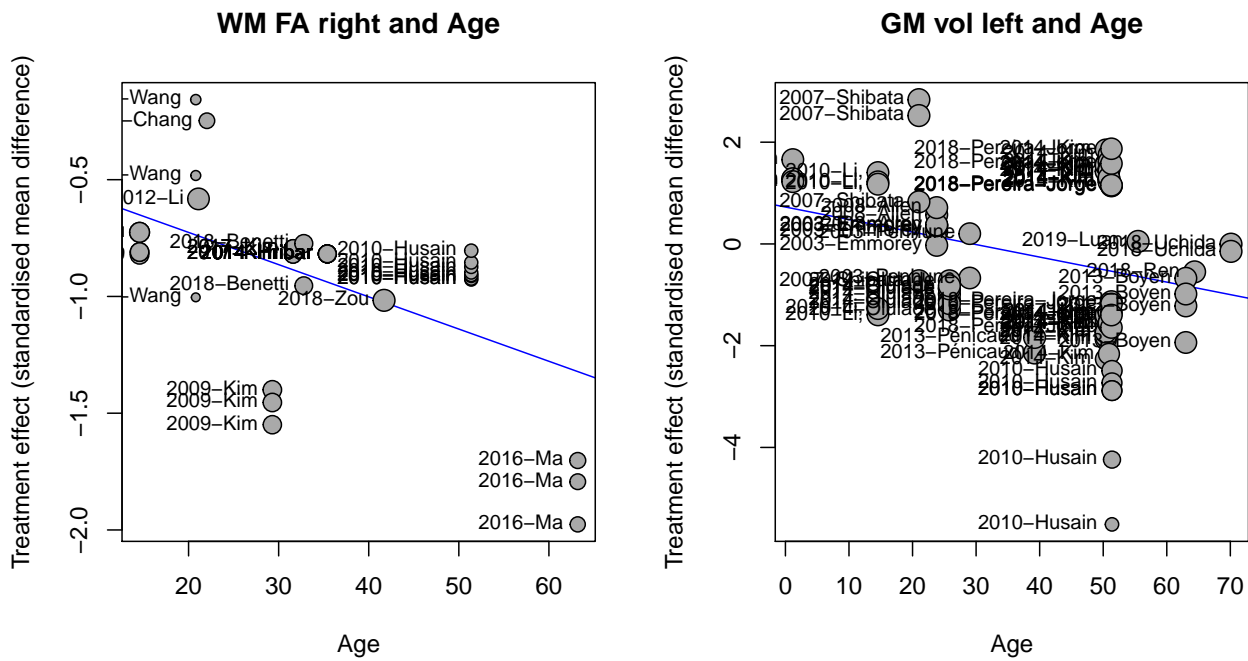


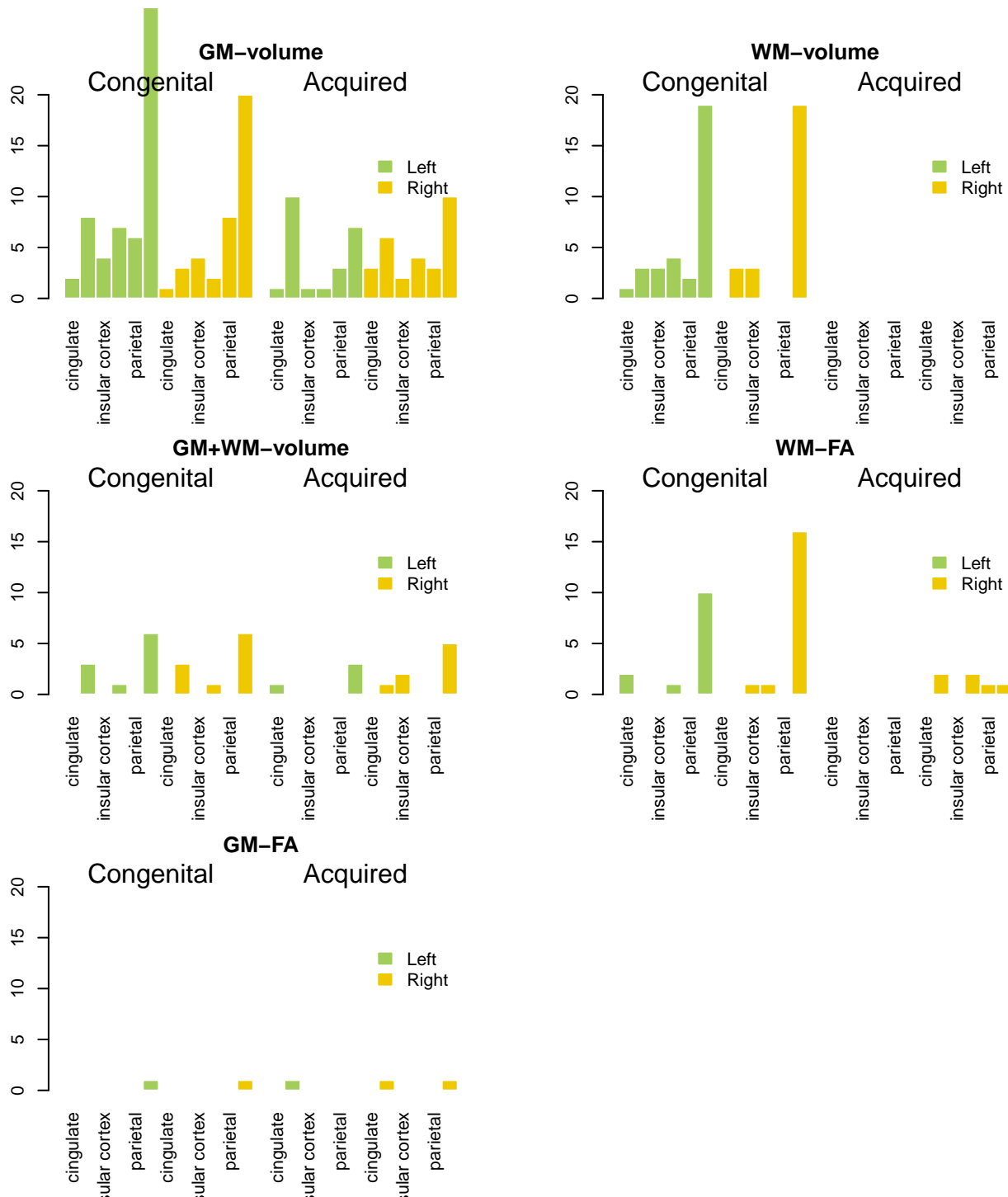
Table of estimates and meta-regression: WM and GM relation with age by MRI measures (volume and FA)

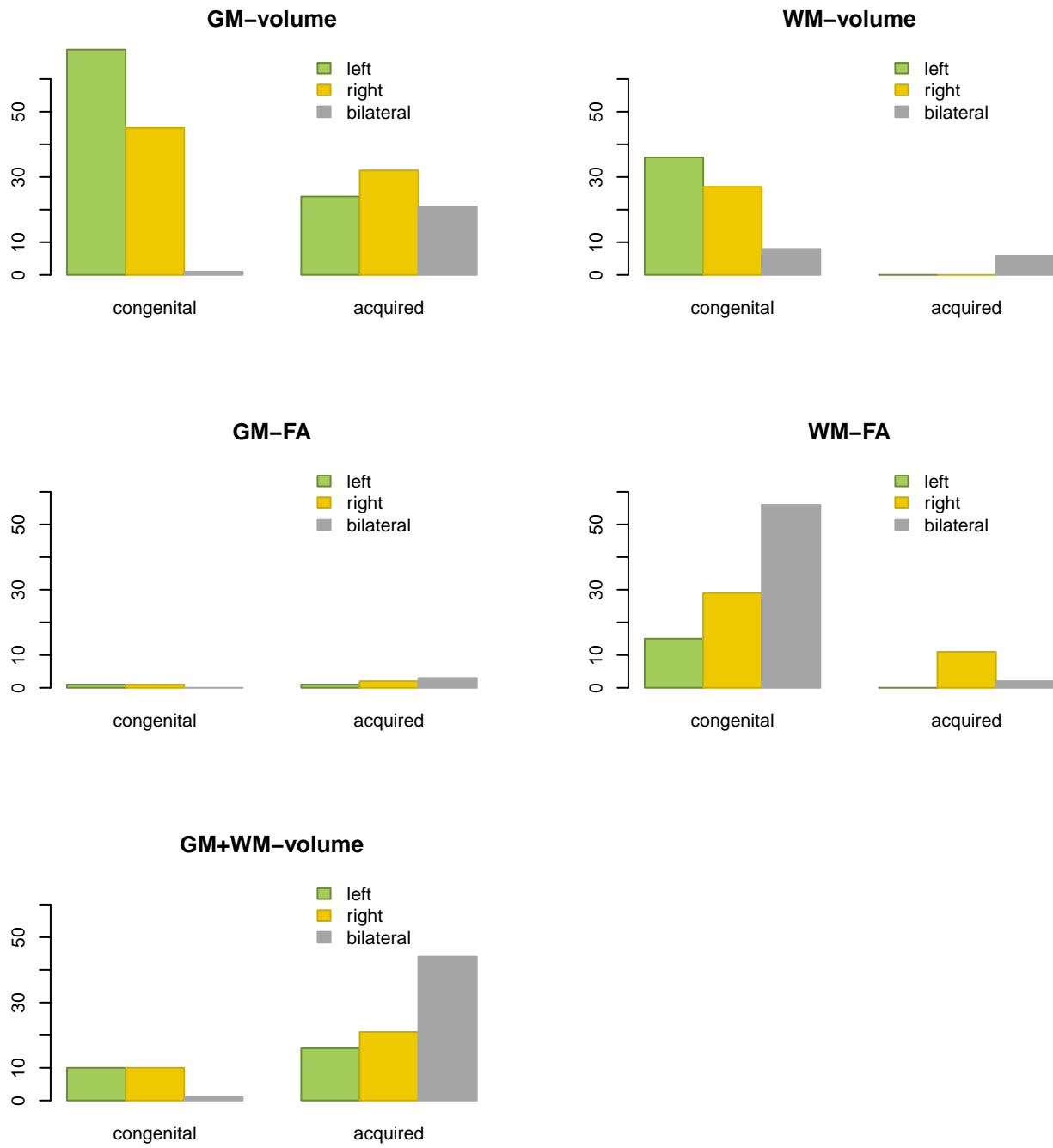
Model	r	p-value	t.stat	df
GM.vol.L	-0.27	0.0103	-2.62	85
WM.vol.L	0.26	0.1687	1.41	28
WM.fa.L	-0.09	0.7393	-0.34	13
GM.vol.R	-0.07	0.5343	-0.62	69
WM.vol.R	0.23	0.316	1.03	19
WM.fa.R	-0.55	2e-04	-4.04	38



Meta-regression

Included variables by Etiology, Brain matter and MRI measure



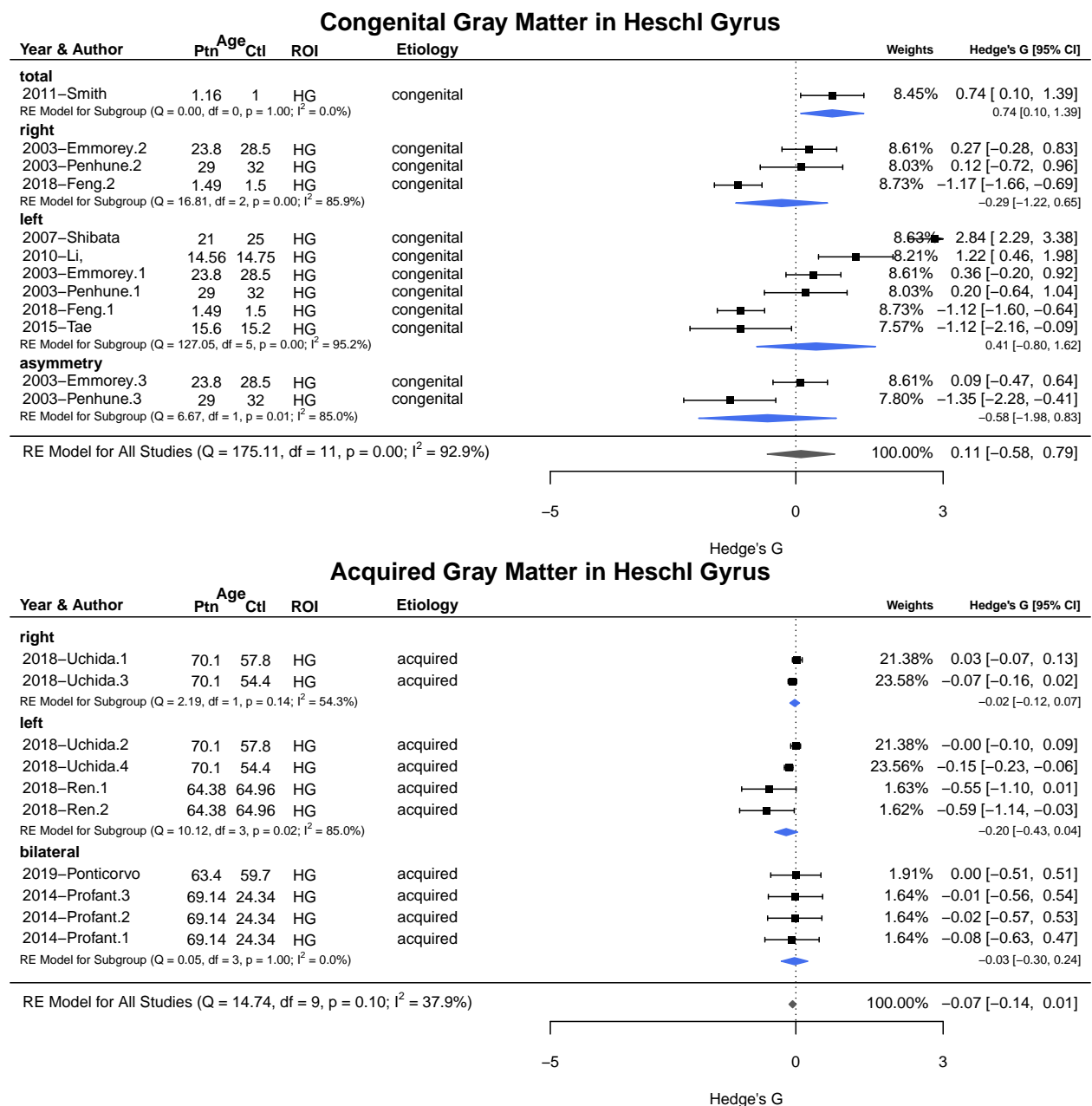


Meta-regressions of Gray Matter in the Heschl Gyrus

Random effects model no intercept covariated by etiology and age

Table 24: Gray Matter in Heschl Gyrus

	HedgeG	se	zval	ci.lo	ci.up	pval
Acquired	-1.81	1.638	-1.105	-5.021	1.4	0.2691
Congenital	-0.3122	0.488	-0.6398	-1.269	0.6442	0.5223
HL.age	0.02455	0.02373	1.034	-0.02197	0.07106	0.301



Meta-regressions of Gray Matter in Congenital by severity and side (volume and VBM)

Random effects model no intercept covariated by severity and age

Table 25: Congenital Gray Matter by severity

	HedgeG	se	zval	ci.lo	ci.up	pval
bilateral.profound	0.464	0.5432	0.8541	-0.6007	1.529	0.393
left.moderate/severe	-1.376	0.3607	-3.815	-2.083	-0.669	0.0001363
left.profound	0.3106	0.3396	0.9145	-0.355	0.9761	0.3605
left.severe	0.2423	0.4758	0.5092	-0.6902	1.175	0.6106
left.severe/profound	1.371	0.61	2.248	0.1757	2.567	0.02457
right.moderate/severe	-1.39	0.3783	-3.675	-2.132	-0.6488	0.0002379
right.profound	-0.1366	0.3964	-0.3446	-0.9136	0.6404	0.7304
right.severe	-0.1626	0.462	-0.352	-1.068	0.7429	0.7248
right.severe/profound	1.282	1.218	1.052	-1.106	3.67	0.2927
total.severe	0.436	1.227	0.3552	-1.97	2.842	0.7225
total.severe/profound	0.7545	1.213	0.622	-1.623	3.132	0.5339
H1.age	-0.01079	0.01055	-1.023	-0.03147	0.009885	0.3063

Congenital - Meta-regressions of Gray Matter Volume

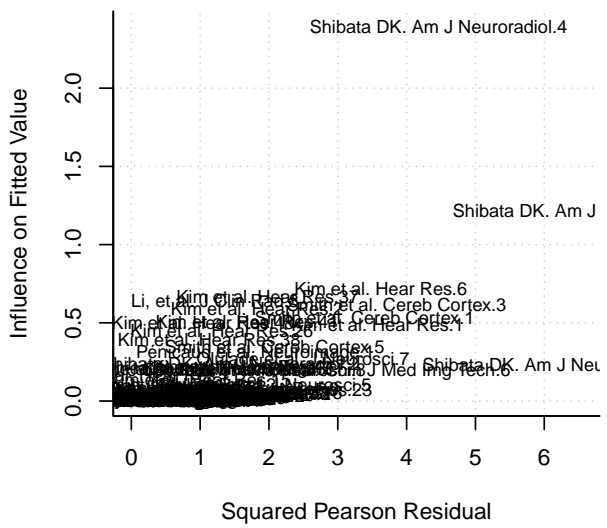
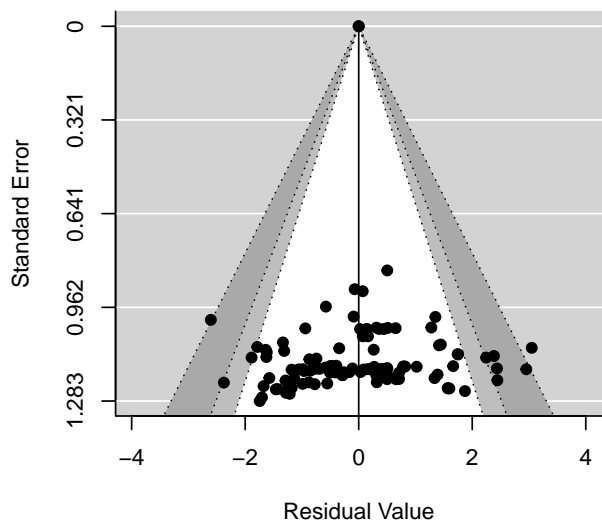
Random effects model no intercept covariated by Big area

Table 26: REM by big area- Congenital - Gray Matter Volume

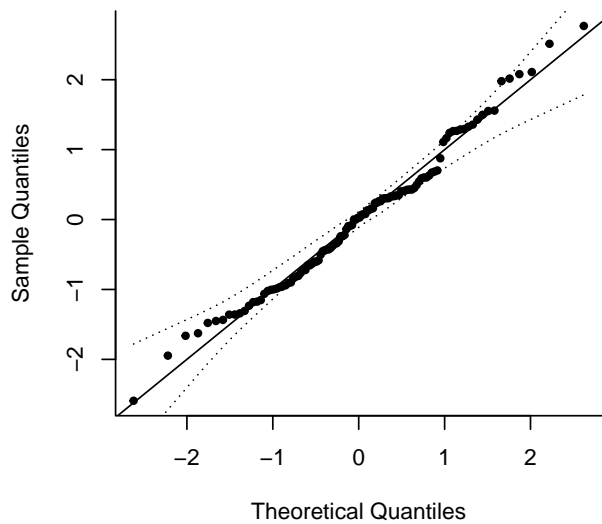
	HedgeG	se	zval	ci.lo	ci.up	pval	N
left cerebellum	0.9013104	0.3734628	2.4133872	0.1693367	1.6332841	0.0158050	11
left cingulate	1.4999543	0.9036636	1.6598593	-0.2711937	3.2711023	0.0969428	2
left frontal	-0.5879845	0.4467854	-1.3160334	-1.4636677	0.2876988	0.1881628	8
left insular cortex	0.0628005	0.6065046	0.1035449	-1.1259267	1.2515276	0.9175305	4
left occipital	-0.5251523	0.4566856	-1.1499207	-1.4202396	0.3699351	0.2501765	7
left parietal	-0.8874850	0.5149084	-1.7235784	-1.8966869	0.1217169	0.0847840	6
left temporal	-0.1159681	0.2235026	-0.5188668	-0.5540252	0.3220890	0.6038537	30
left Thalamus	1.2815547	1.2134567	1.0561191	-1.0967766	3.6598861	0.2909138	1
right cerebellum	1.6815703	0.7283834	2.3086335	0.2539651	3.1091754	0.0209639	3
right cingulate	-0.8017506	1.1929769	-0.6720588	-3.1399424	1.5364411	0.5015462	1
right entorhinal	0.0586466	0.6339350	0.0925119	-1.1838432	1.3011364	0.9262913	4
right frontal	-2.5593121	0.7143293	-3.5828186	-3.9593717	-1.1592525	0.0003399	3
right insular cortex	-0.1339176	0.5980210	-0.2239346	-1.3060172	1.0381821	0.8228082	4
right occipital	-1.7301425	0.8957245	-1.9315566	-3.4857303	0.0254452	0.0534143	2
right parietal	-1.1125014	0.4445211	-2.5026964	-1.9837468	-0.2412560	0.0123251	8
right temporal	-0.5427415	0.2729266	-1.9885987	-1.0776678	-0.0078152	0.0467455	20

Table 27: Congenital - Gray Matter Volume

Test	Estimates
Mixed-effect model:	k= 114 : tau ² = 1.35 (SE= 0.22) I ² = 91.08 %, H ² = 11.21
Residual heterogeneity:	QE(df= 98)= 1048.28 , p.val= 7.08528565862191e-159
Test of moderators (big areas):	QM(df= 16)= 48.63 p.val= 3.78635028624703e-05



Congenital – GM Volume



Acquired - Meta-regressions of Gray Matter by Volume

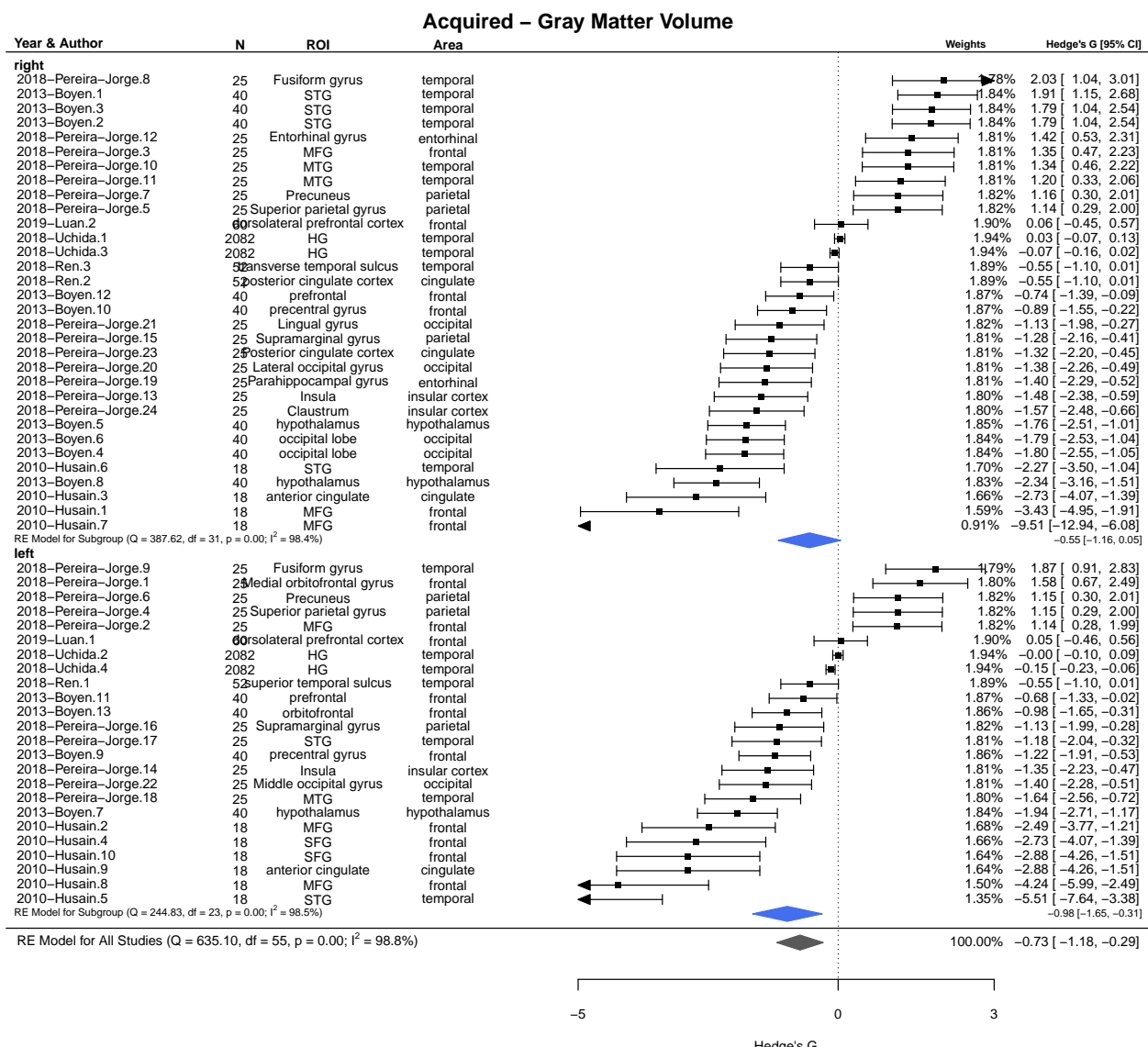
Random effects model no intercept covariated by Big area

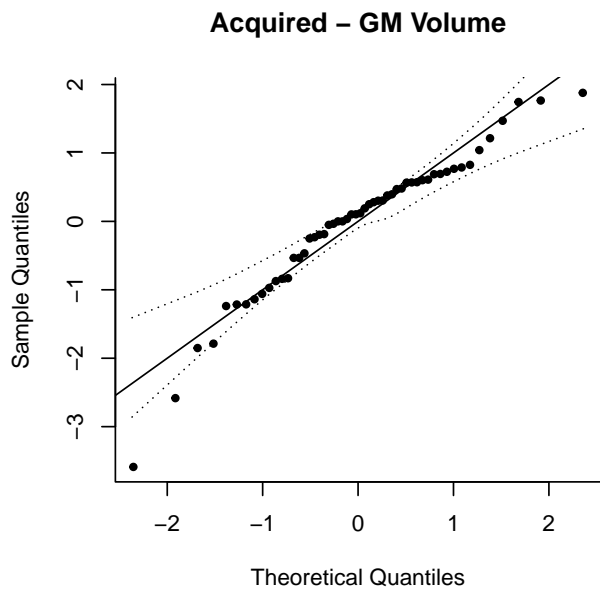
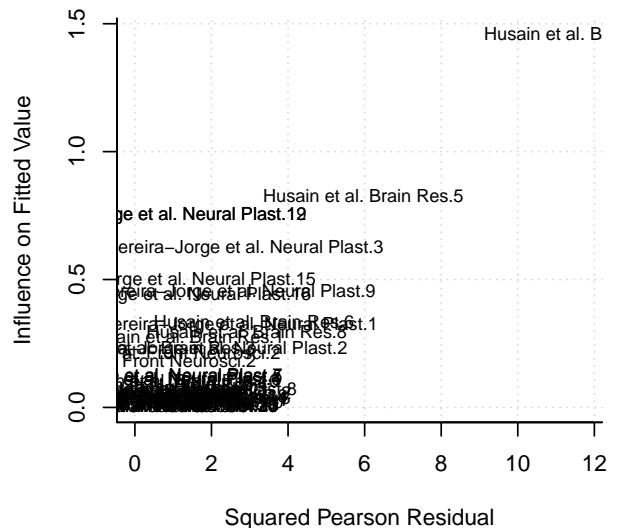
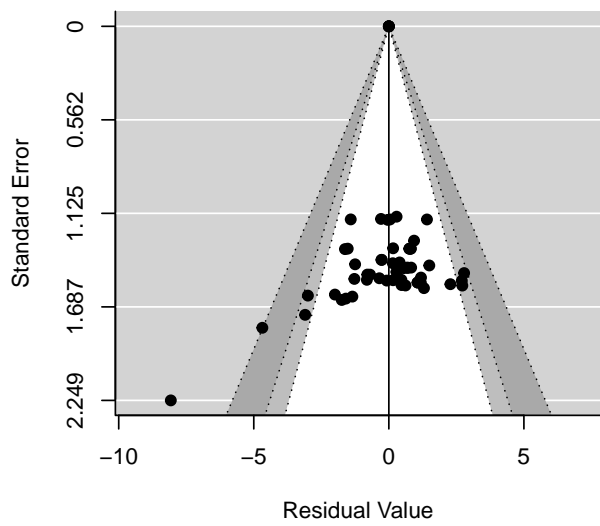
Table 28: REM by big area - Acquired - Gray Matter Volume

	HedgeG	se	zval	ci.lo	ci.up	pval	N
left cingulate	-2.8834593	1.7275069	-1.6691449	-6.269311	0.5023920	0.0950887	1
left frontal	-1.1400688	0.5267737	-2.1642479	-2.172526	-0.1076114	0.0304453	10
left hypothalamus	-1.9371568	1.6261099	-1.1912828	-5.124274	1.2499600	0.2335426	1
left insular cortex	-1.3534702	1.6409912	-0.8247883	-4.569754	1.8628133	0.4094918	1
left occipital	-1.3978319	1.6417994	-0.8514023	-4.615700	1.8200359	0.3945459	1
left parietal	0.3896201	0.9454302	0.4121088	-1.463389	2.2426292	0.6802597	3
left temporal	-0.8301541	0.6236257	-1.3311735	-2.052438	0.3921299	0.1831319	7
right cingulate	-1.4826100	0.9540207	-1.5540648	-3.352456	0.3872362	0.1201690	3
right entorhinal	0.0070725	1.1610972	0.0060912	-2.268636	2.2827812	0.9951399	2
right frontal	-1.4376558	0.7012092	-2.0502524	-2.812001	-0.0633111	0.0403398	6
right hypothalamus	-2.0470474	1.1513226	-1.7779963	-4.303598	0.2095035	0.0754045	2
right insular cortex	-1.5245544	1.1626676	-1.3112555	-3.803341	0.7542323	0.1897714	2
right occipital	-1.5236790	0.8157812	-1.8677544	-3.122581	0.0752228	0.0617963	4
right parietal	0.3405078	0.9458955	0.3599846	-1.513413	2.1944289	0.7188586	3
right temporal	0.7270216	0.5141240	1.4140977	-0.280643	1.7346863	0.1573332	10

Table 29: Acquired - Gray Matter Volume

Test	Estimates
Mixed-effect model:	k= 56 : tau^2= 2.49 (SE= 0.6) I^2= 98.57 %, H^2= 70.1
Residual heterogeneity:	QE(df= 41)= 412.31 , p.val= 8.01499990705428e-63
Test of moderators (big areas):	QM(df= 15)= 29.35 p.val= 0.014479351188099





Congenital - White Matter by VOLUME

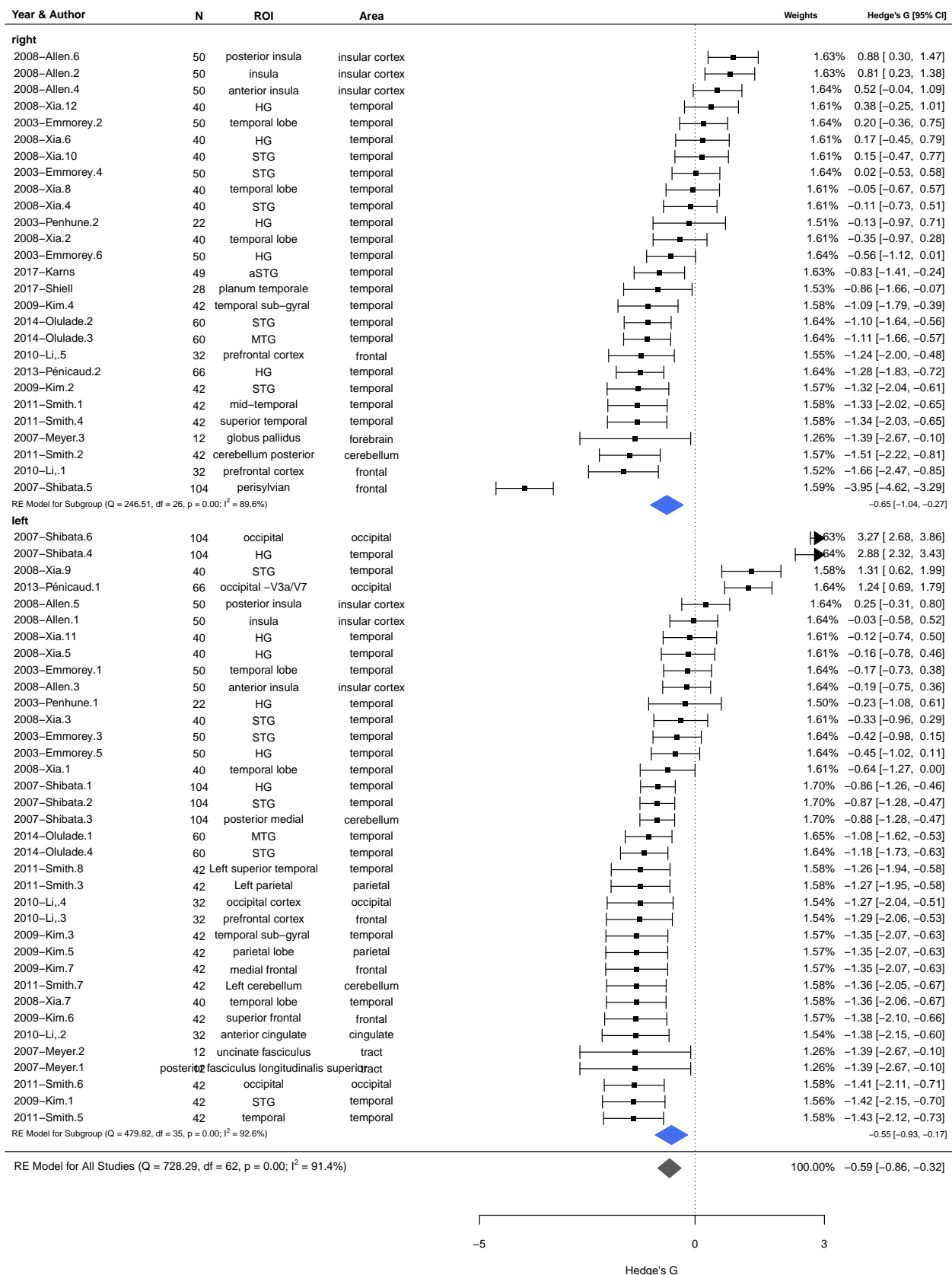
Random effects model no intercept covariated by Big area

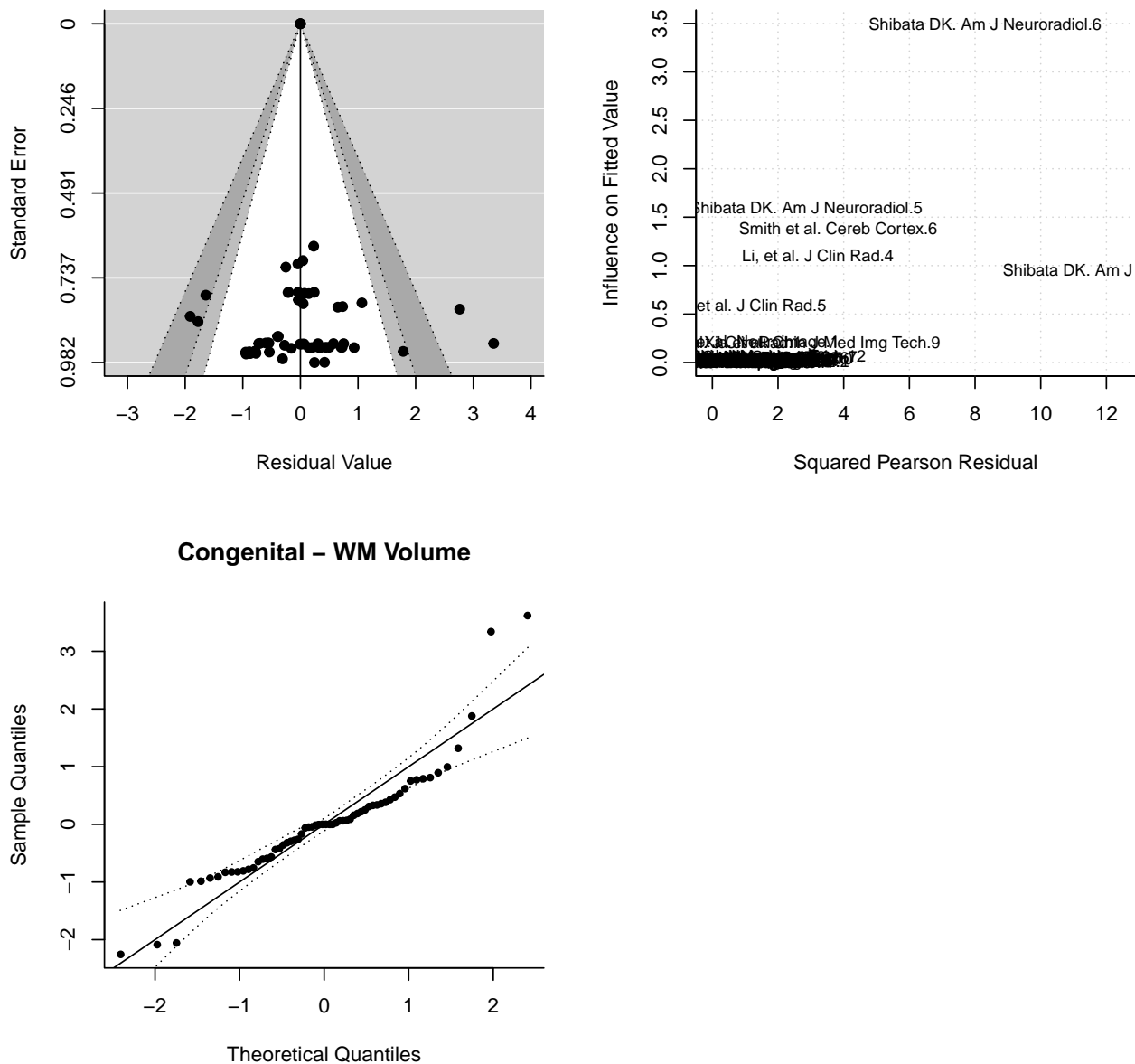
Table 30: REM by big area - Congenital - White Matter Volume

	HedgeG	se	zval	ci.lo	ci.up	pval	N
left cerebellum	-1.1070810	0.6745058	-1.6413217	-2.4290881	0.2149260	0.1007306	2
left cingulate	-1.3786454	0.9926110	-1.3889080	-3.3241272	0.5668365	0.1648607	1
left frontal	-1.3402379	0.5684006	-2.3579110	-2.4542825	-0.2261933	0.0183781	3
left insular cortex	0.0079129	0.5504384	0.0143756	-1.0709265	1.0867523	0.9885303	3
left occipital	0.5024402	0.4846477	1.0367123	-0.4474518	1.4523323	0.2998699	4
left parietal	-1.3081390	0.6914333	-1.8919238	-2.6633233	0.0470452	0.0585011	2
left temporal	-0.4780484	0.2210575	-2.1625524	-0.9113131	-0.0447837	0.0305756	19
left tract	-1.3856308	0.7930734	-1.7471658	-2.9400261	0.1687645	0.0806086	2
right cerebellum	-1.5134943	0.9788737	-1.5461589	-3.4320516	0.4050629	0.1220662	1
right forebrain	-1.3856308	1.1215752	-1.2354328	-3.5838777	0.8126162	0.2166695	1
right frontal	-2.3098509	0.5696811	-4.0546382	-3.4264054	-1.1932964	0.0000502	3
right insular cortex	0.7369857	0.5521197	1.3348296	-0.3451490	1.8191204	0.1819321	3
right temporal	-0.5528945	0.2217554	-2.4932631	-0.9875270	-0.1182620	0.0126575	19

Table 31: Congenital White Matter Volume

Test	Estimates
Mixed-effect model:	k= 63 : tau ² = 0.83 (SE= 0.19) I ² = 89.36 %, H ² = 9.4
Residual heterogeneity:	QE(df= 50)= 462.69 , p.val= 3.35220276992225e-68
Test of moderators (big areas):	QM(df= 13)= 50.92 p.val= 2.07007590853841e-06

Congenital White Matter Volume



Acquired - White Matter by VOLUME (ONLY BILATERAL)

Not enough values for the Random effects model no intercept covariated by Big area and Side (left or right)

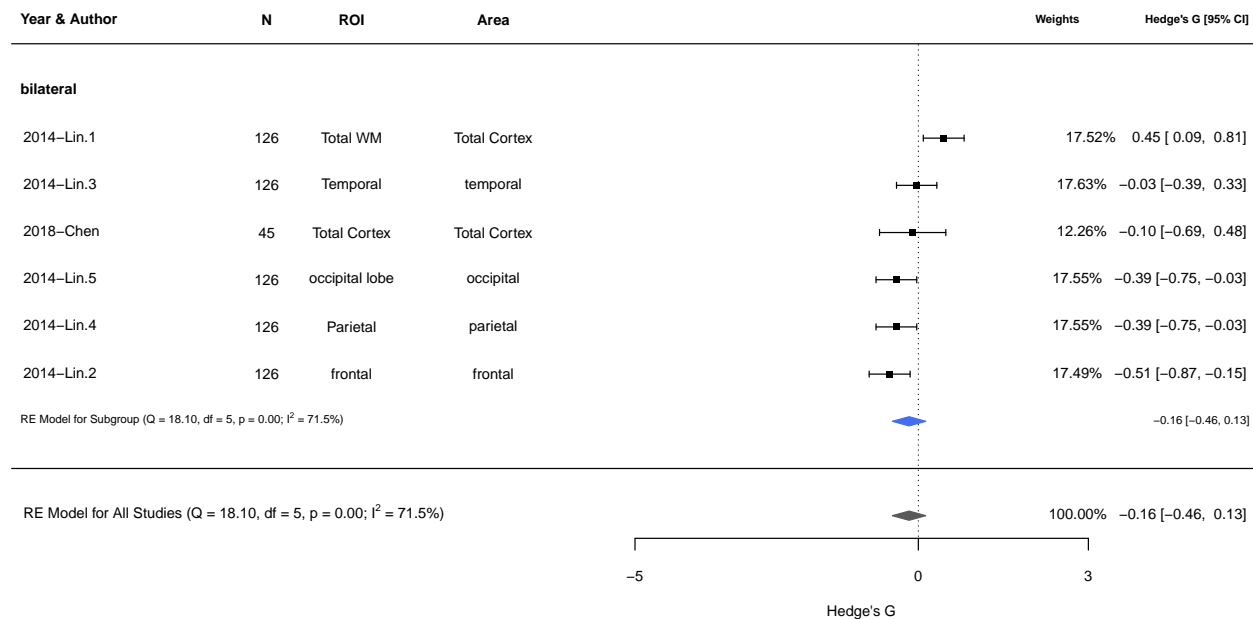
Table 32: REM by big area - Acquired White Matter Volume

	HedgeG	se	zval	ci.lo	ci.up	pval	N
bilateral frontal	-0.5069091	0.3500431	-1.4481334	-1.1929809	0.1791627	0.1475797	1
bilateral occipital	-0.3876364	0.3494280	-1.1093454	-1.0725027	0.2972300	0.2672812	1
bilateral parietal	-0.3876364	0.3494280	-1.1093454	-1.0725027	0.2972300	0.2672812	1
bilateral temporal	-0.0298182	0.3485651	-0.0855455	-0.7129932	0.6533569	0.9318277	1
bilateral Total Cortex	0.2239473	0.2691216	0.8321415	-0.3035214	0.7514160	0.4053291	2

Table 33: acquired White Matter Volume

Test	Estimates
Mixed-effect model:	k= 6 : tau^2 = 0.09 (SE= 0.21) I^2= 59.05 %, H^2= 2.44
Residual heterogeneity:	QE(df= 1)= 2.44 , p.val= 0.118106312179678
Test of moderators (big areas):	QM(df= 5)= 5.26 p.val= 0.385192885534552

Acquired White Matter Volume



Nothing is significant

Congenital - White Matter by FA fractional anisotropy

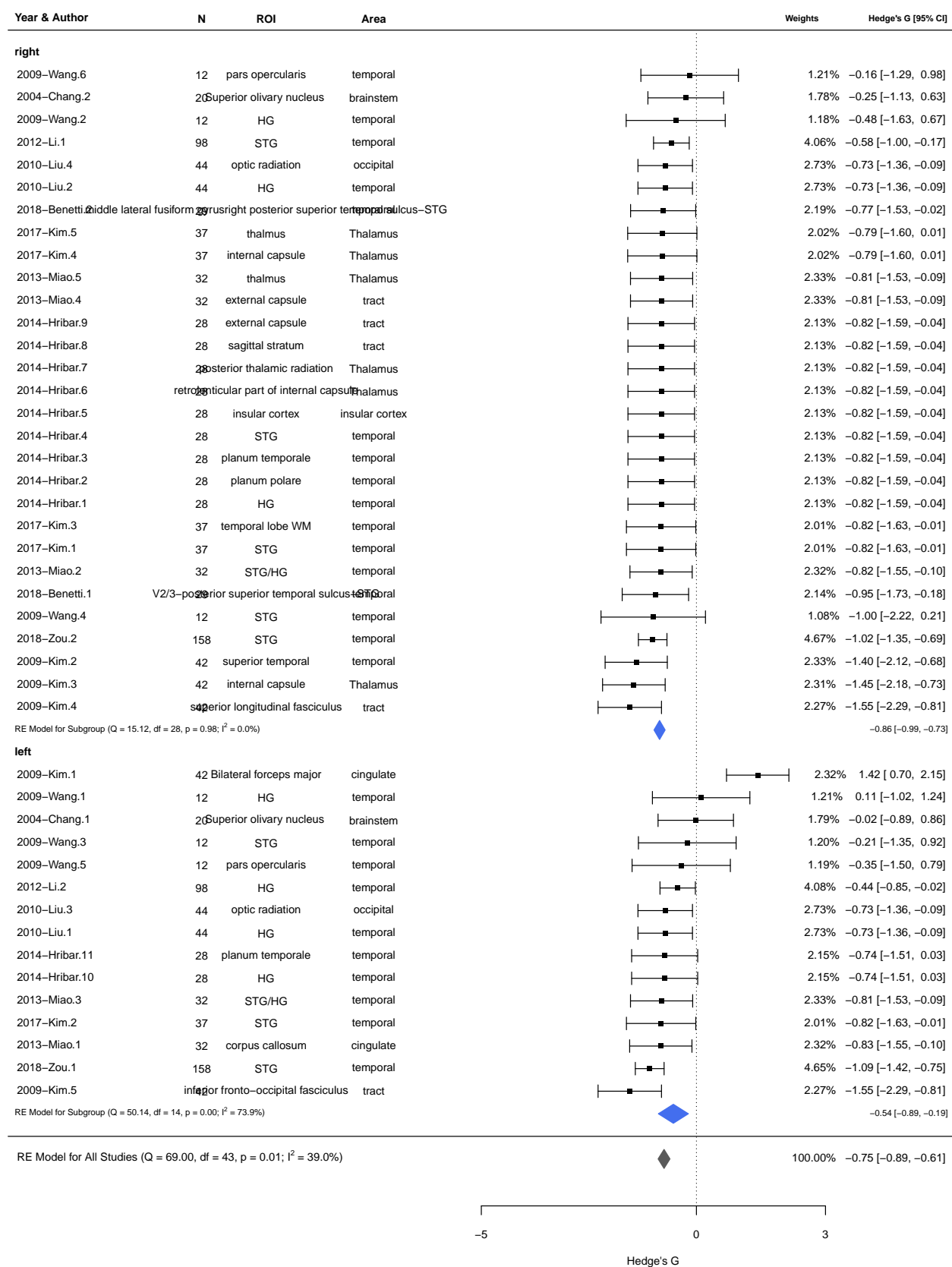
Random effects model no intercept covariated by Big area

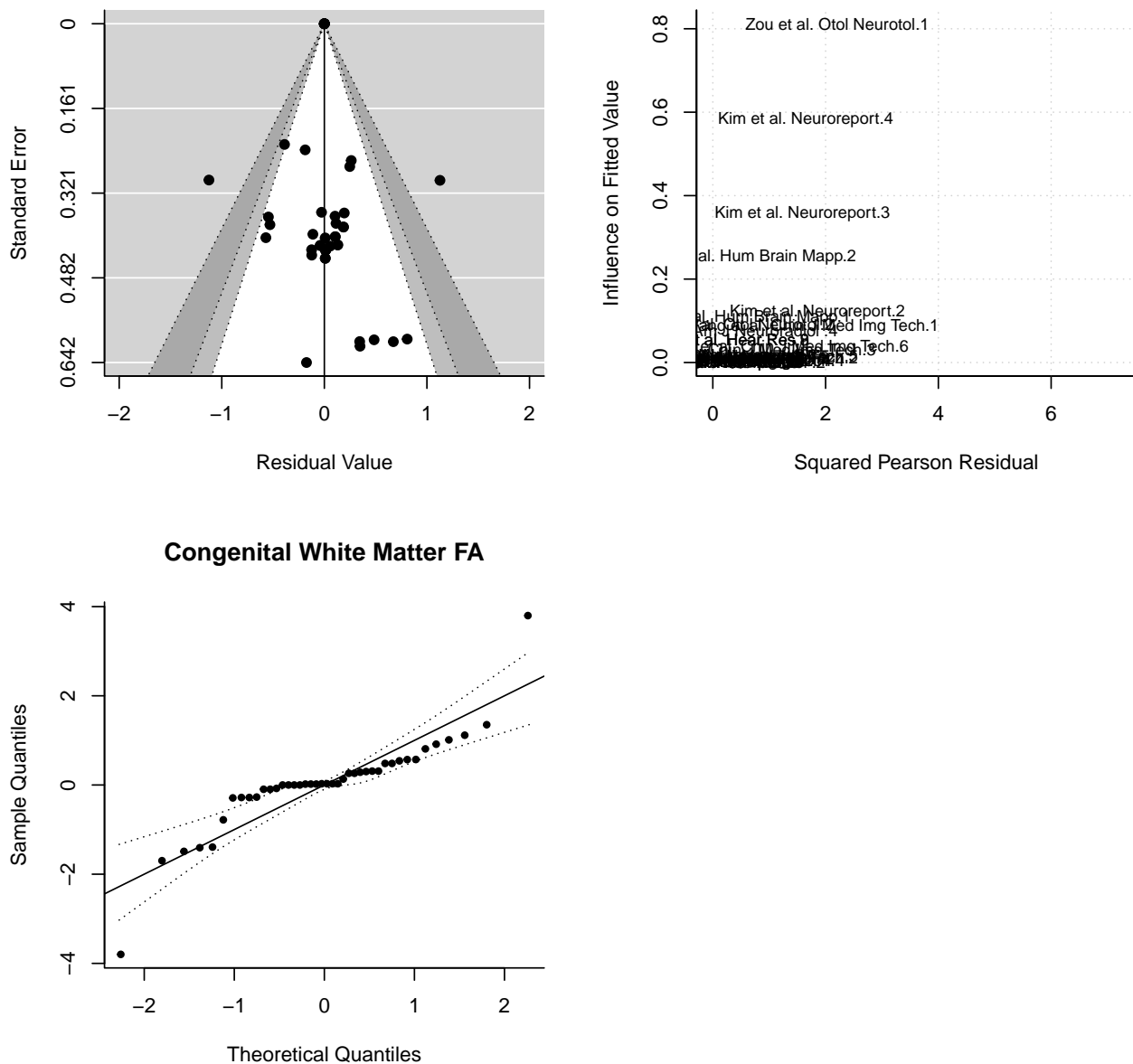
Table 34: REM by big area - Congenital White Matter FA

	HedgeG	se	zval	ci.lo	ci.up	pval	N
left brainstem	-0.0155675	0.4891077	-0.0318283	-0.9742009	0.9430660	0.9746090	1
left cingulate	0.2970009	0.2964912	1.0017190	-0.2841112	0.8781129	0.3164793	2
left occipital	-0.7254299	0.3790761	-1.9136787	-1.4684055	0.0175457	0.0556612	1
left temporal	-0.6980338	0.1264916	-5.5184183	-0.9459528	-0.4501147	0.0000000	10
left tract	-1.5493057	0.4250056	-3.6453770	-2.3823013	-0.7163100	0.0002670	1
right brainstem	-0.2475694	0.4908382	-0.5043809	-1.2095945	0.7144557	0.6139937	1
right insular cortex	-0.8177670	0.4415169	-1.8521760	-1.6831242	0.0475902	0.0640005	1
right occipital	-0.7254299	0.3790761	-1.9136787	-1.4684055	0.0175457	0.0556612	1
right temporal	-0.8298372	0.1035639	-8.0128036	-1.0328187	-0.6268557	0.0000000	16
right Thalamus	-0.9238373	0.1788955	-5.1641181	-1.2744659	-0.5732086	0.0000002	6
right tract	-1.0039894	0.2156391	-4.6558783	-1.4266343	-0.5813446	0.0000032	4

Table 35: Congenital White Matter FA

Test	Estimates
Mixed-effect model:	k = 44 : tau^2 = 0.04 (SE = 0.04) I^2 = 24.12 %, H^2 = 1.32
Residual heterogeneity:	QE(df = 33) = 40.58, p.val = 0.17085782139714
Test of moderators (big areas):	QM(df = 11) = 168.31 p.val = 2.63258401967927e-30

Congenital White Matter FA



Acquired - White Matter by FA fractional anisotropy (ONLY RIGHT)

Random effects model no intercept covariated by Big area

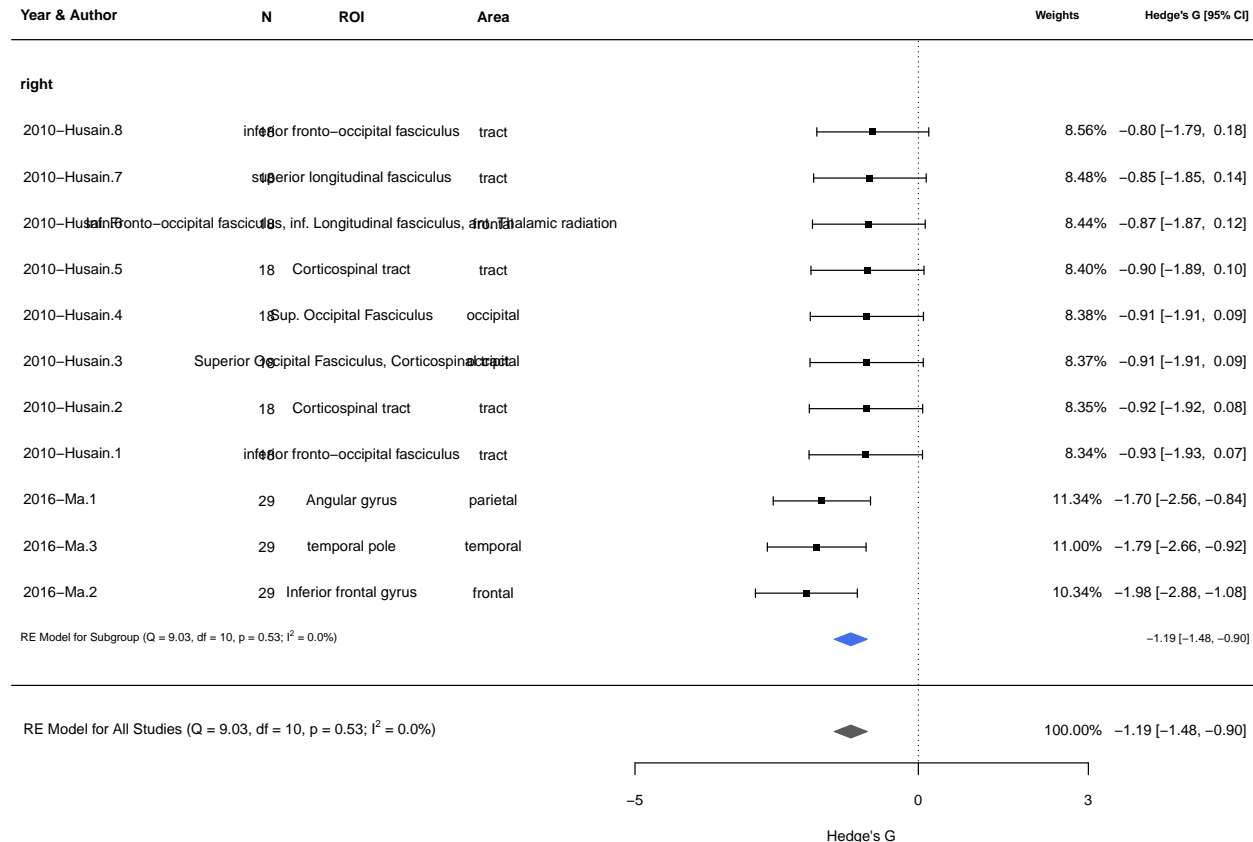
Table 36: REM by big area - Acquired White Matter FA

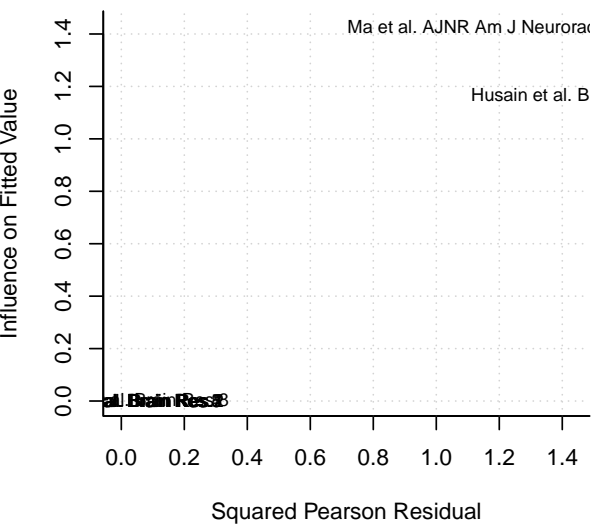
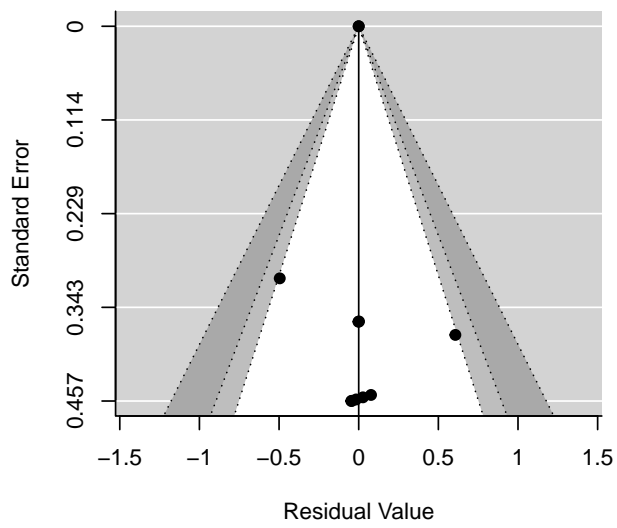
	HedgeG	se	zval	ci.lo	ci.up	p.val	N
right frontal	-1.4804586	0.3403176	-4.350226	-2.147469	-0.8134483	0.0000136	2
right occipital	-0.9104754	0.3603273	-2.526801	-1.616704	-0.2042469	0.0115107	2
right parietal	-1.7025869	0.4379232	-3.887866	-2.560901	-0.8442731	0.0001011	1
right temporal	-1.7933682	0.4445829	-4.033822	-2.664735	-0.9220018	0.0000549	1
right tract	-0.8811554	0.2271998	-3.878328	-1.326459	-0.4358519	0.0001052	5

Table 37: acquired White Matter FA

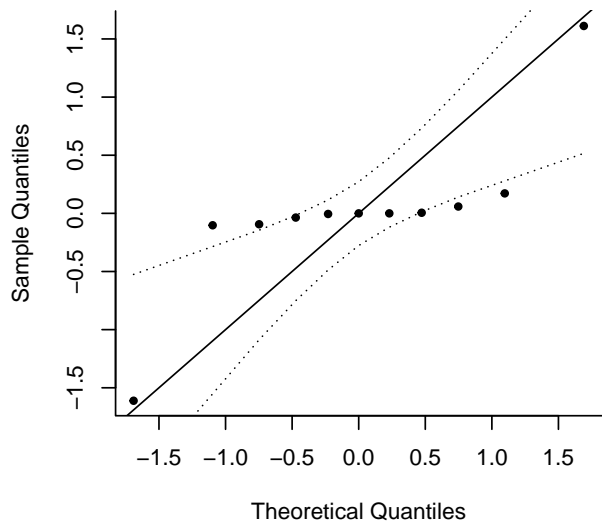
Test	Estimates
Mixed-effect model:	k= 11 : tau^2= 0 (SE= 0.15) I^2= 0 %, H^2= 1
Residual heterogeneity:	QE(df= 6)= 2.64 , p.val= 0.852507484101014
Test of moderators (big areas):	QM(df= 5)= 71.74 p.val= 4.45450158997401e-14

acquired White Matter FA



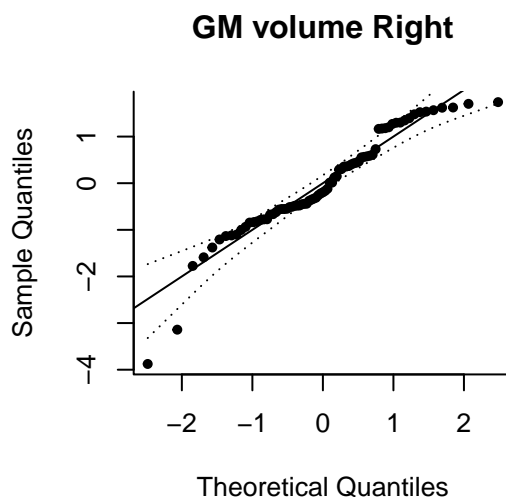
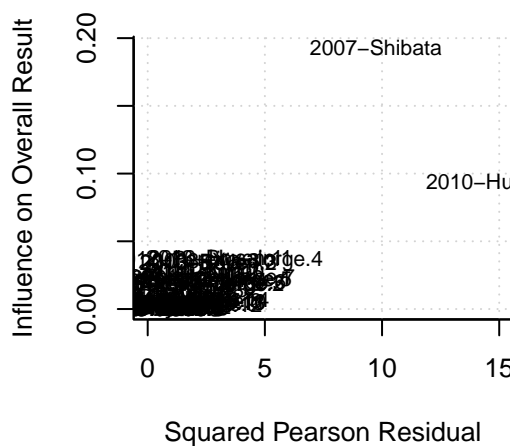
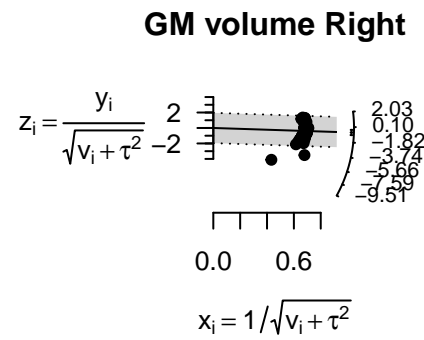
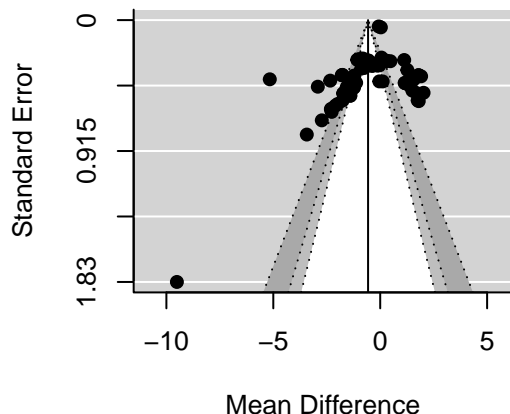


acquired White Matter FA

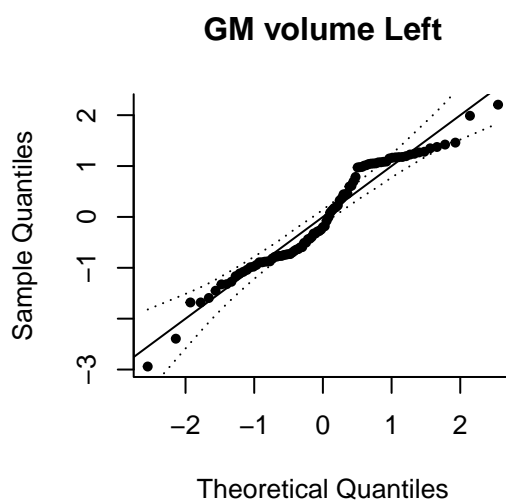
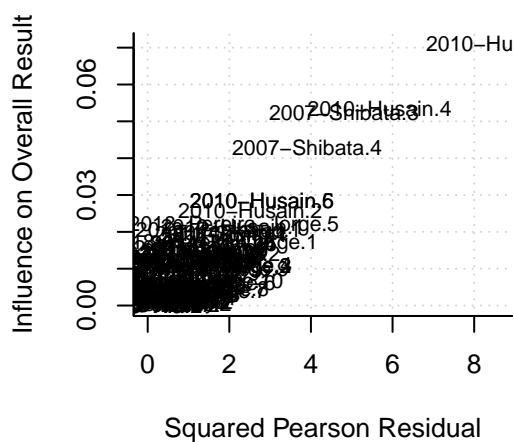
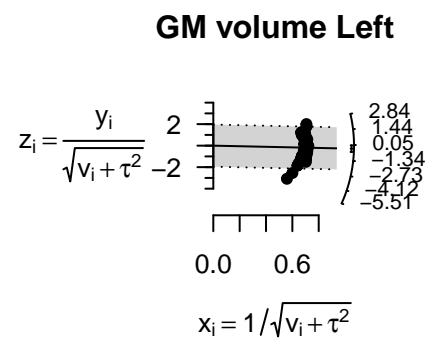
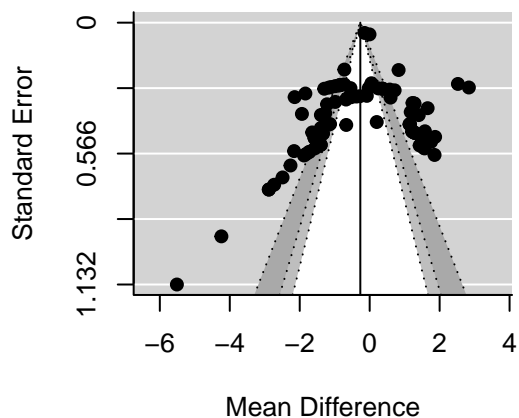


Supplementary material: heterogeneity per model

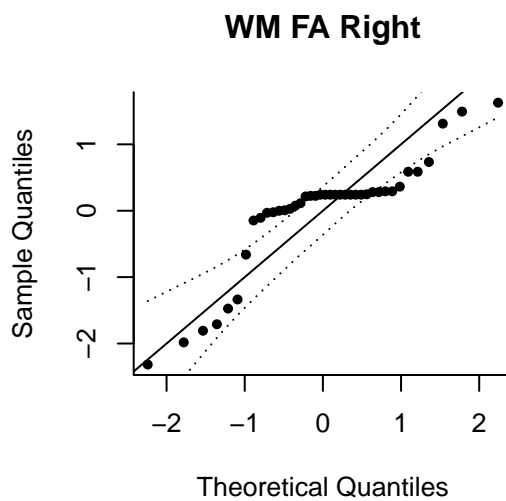
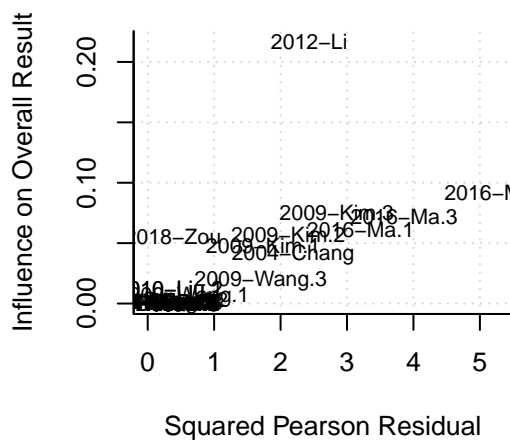
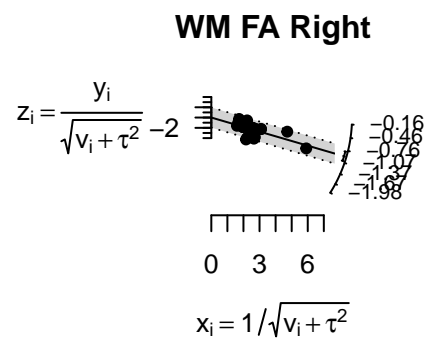
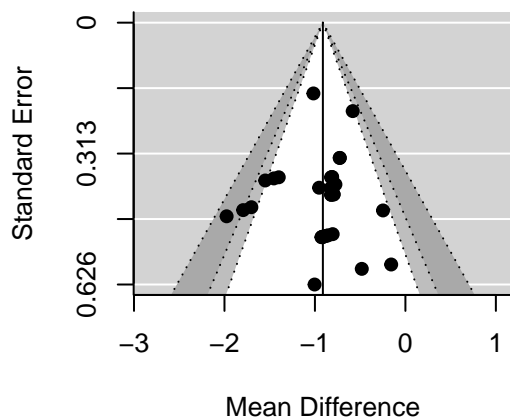
Heterogeneity: GM volume Right



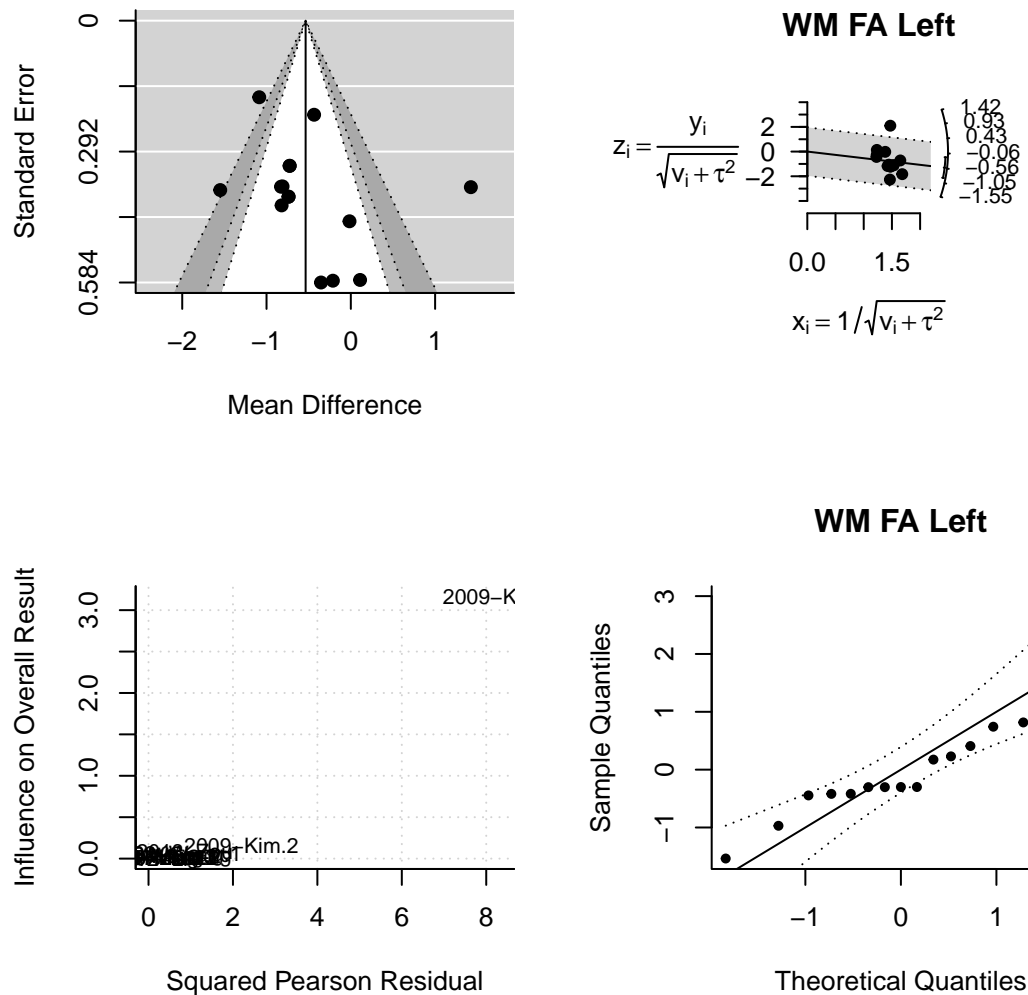
Heterogeneity: GM volume Left



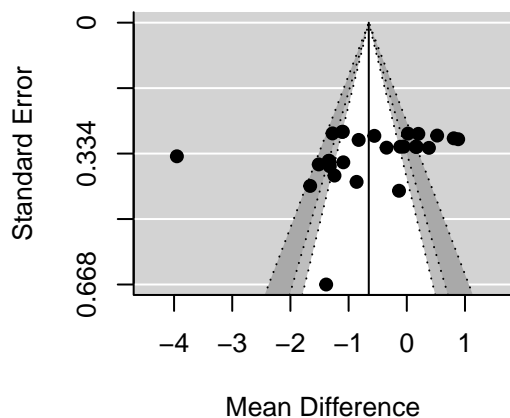
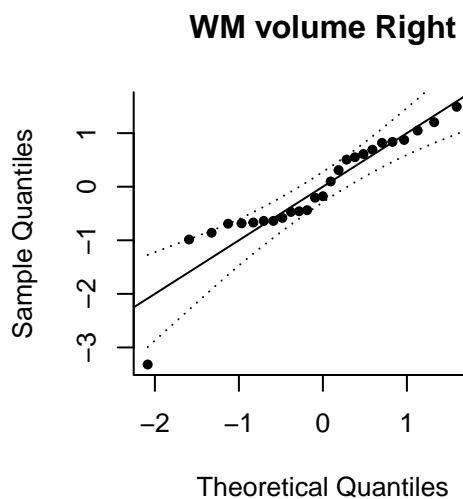
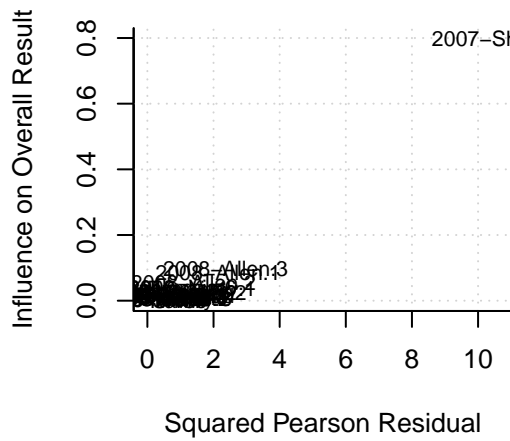
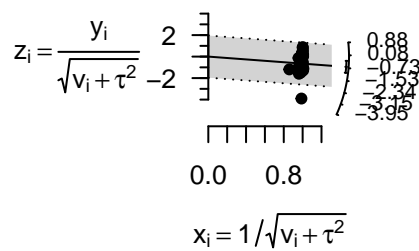
Heterogeneity: WM FA Right



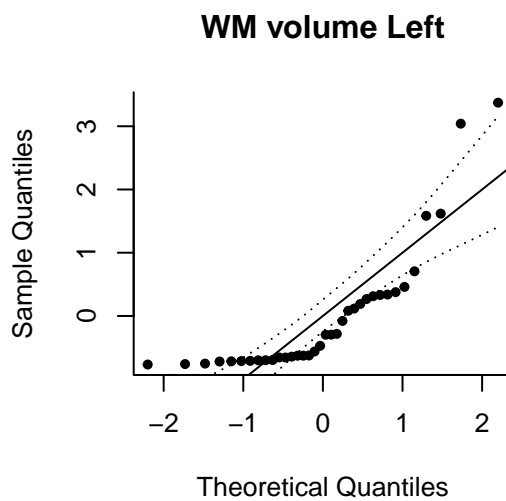
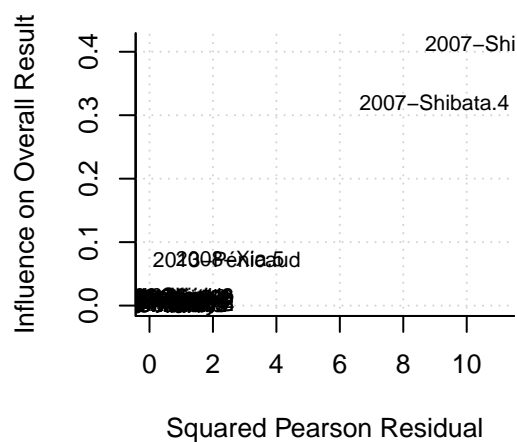
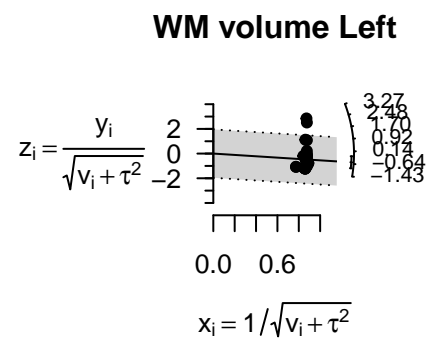
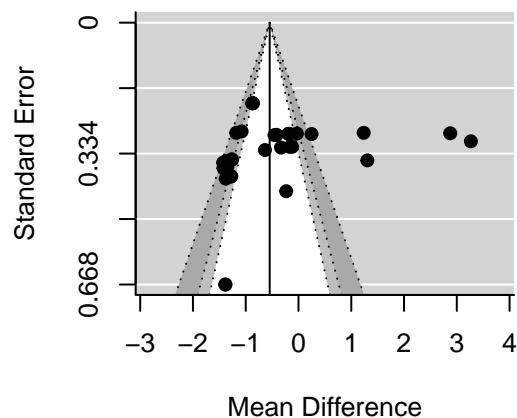
Heterogeneity: WM FA Left



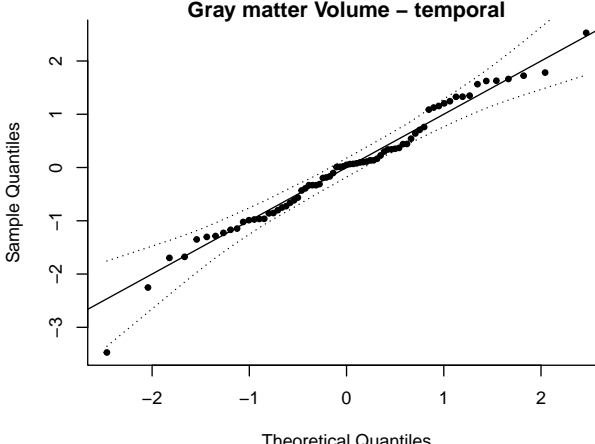
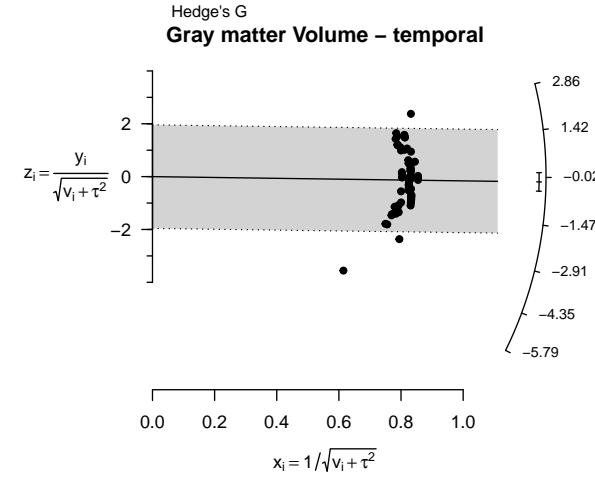
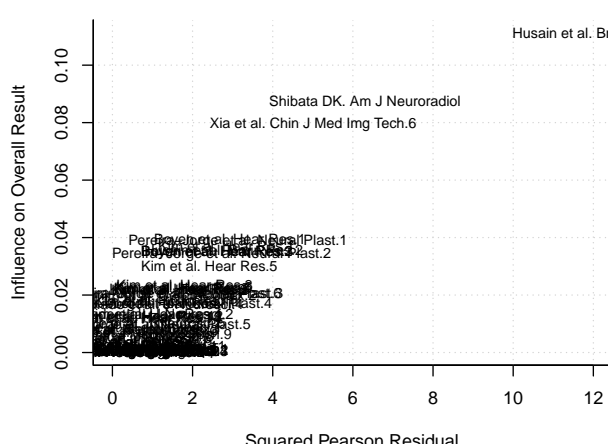
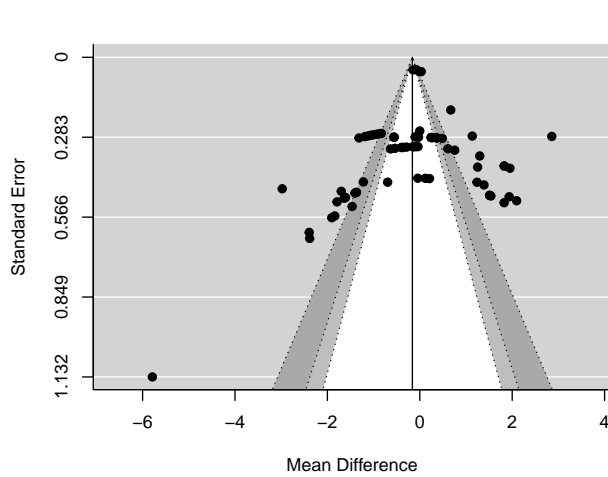
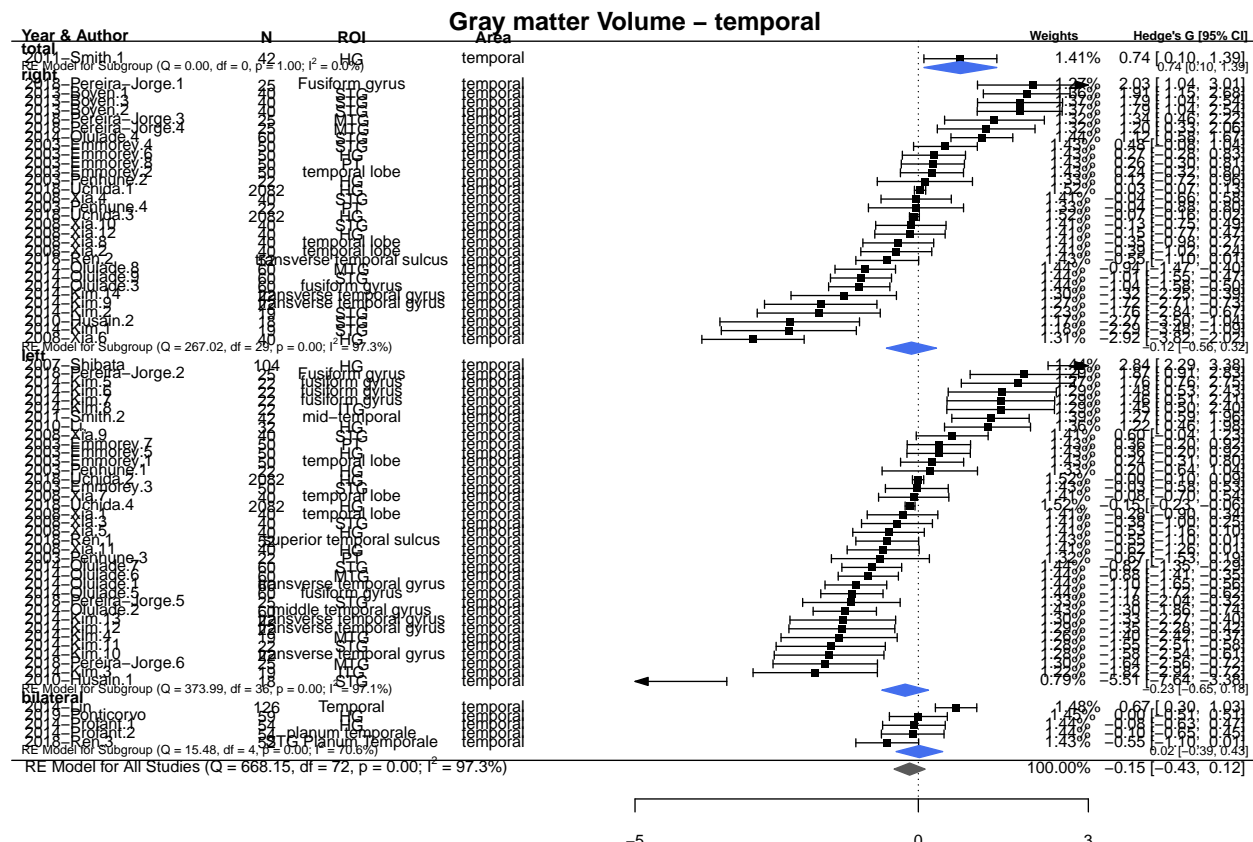
Heterogeneity: WM volume Right

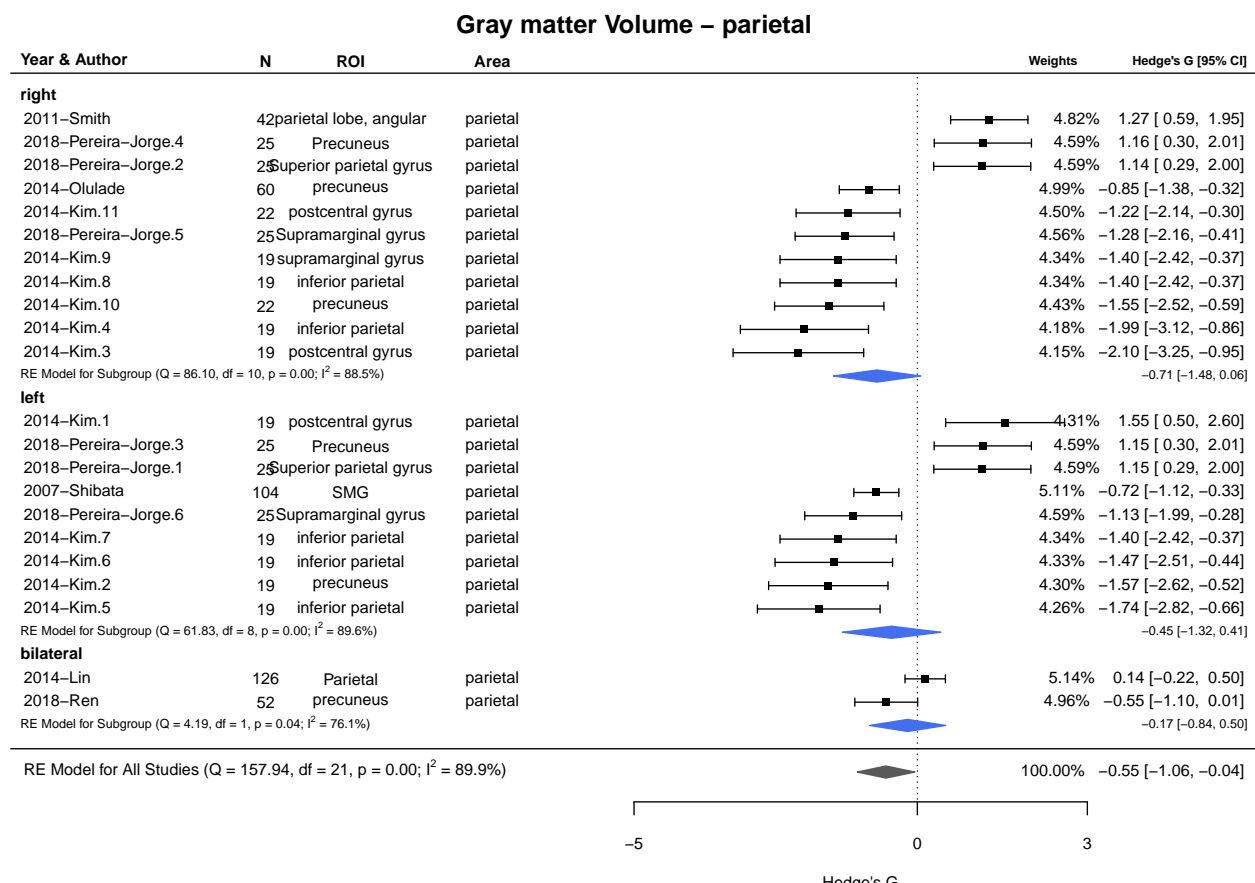
**WM volume Right**

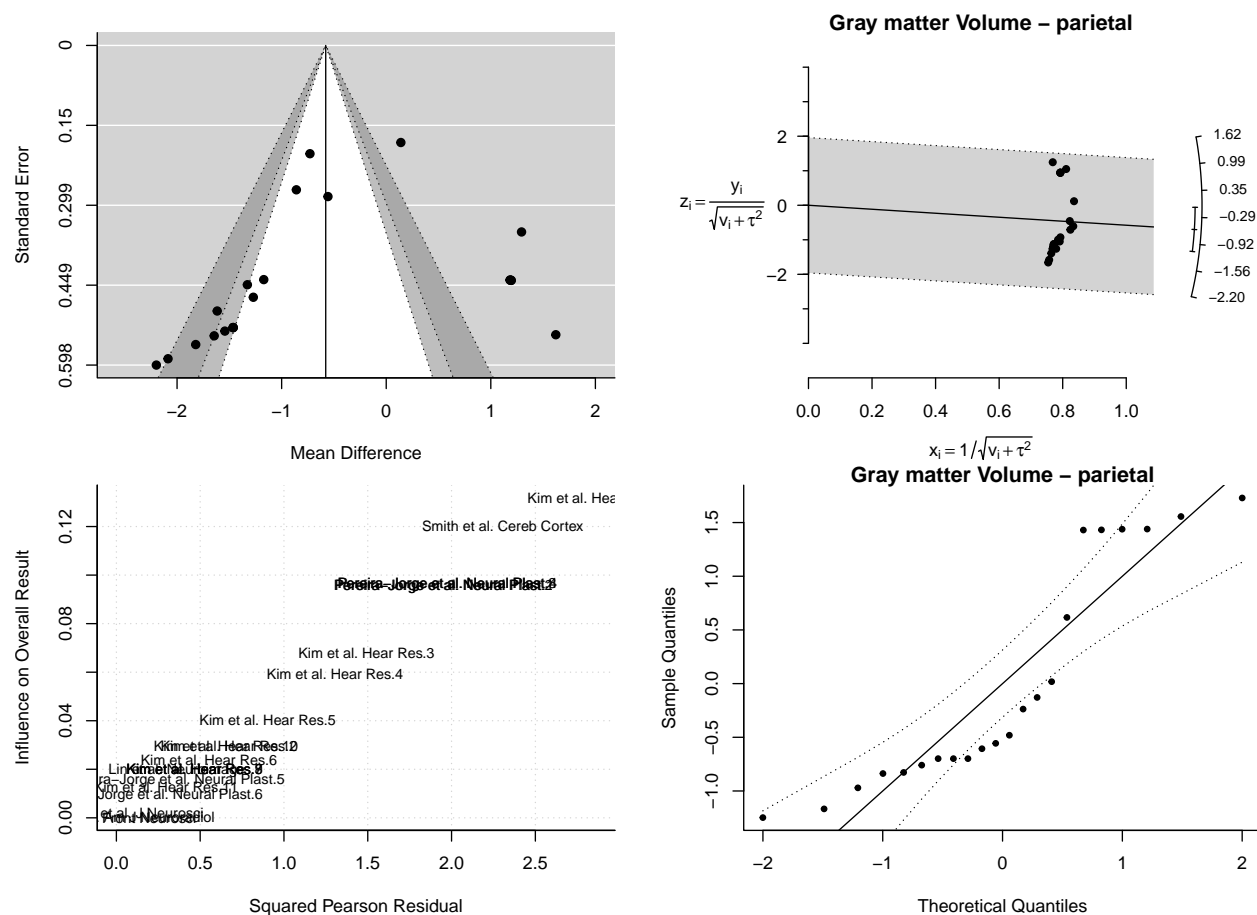
Heterogeneity: WM volume Left

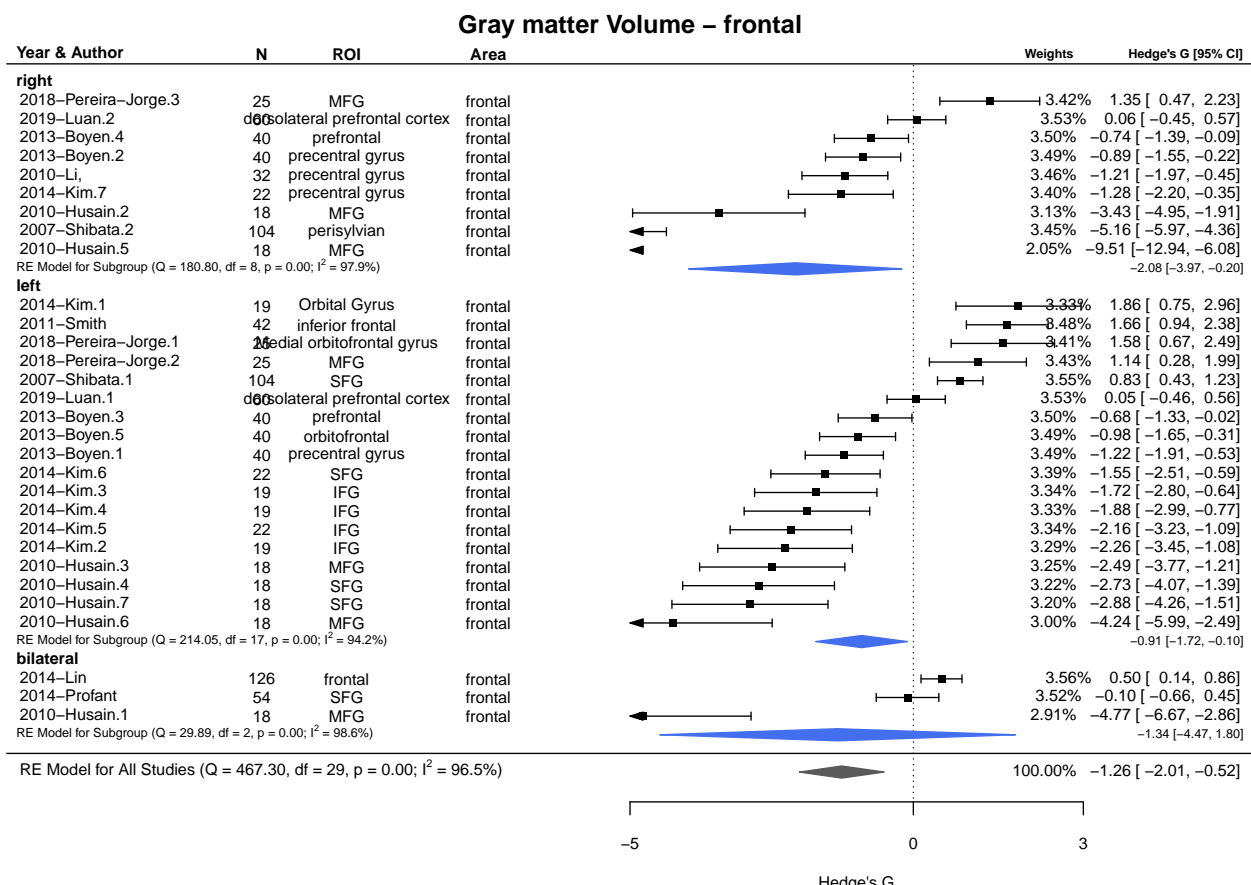


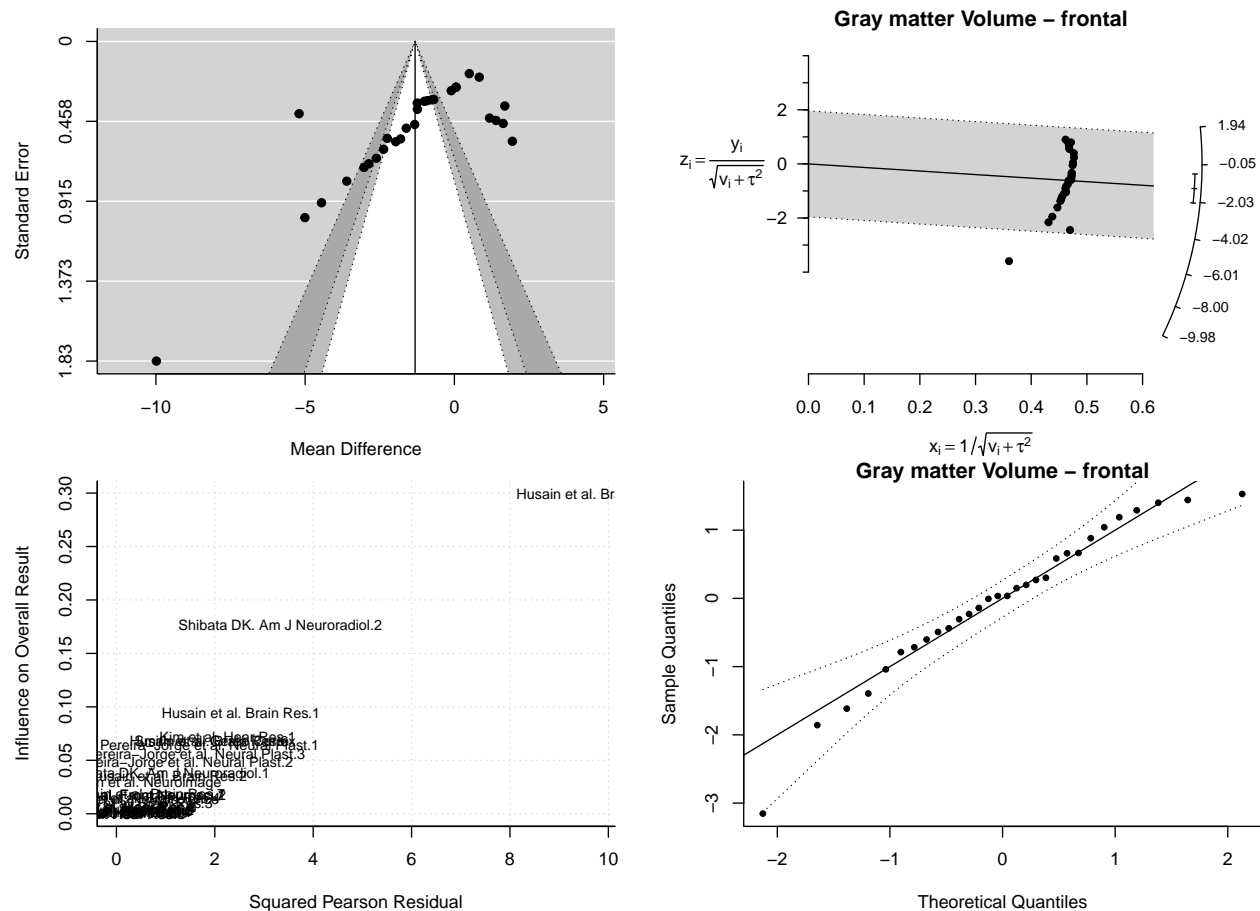
Meta-regressions of Gray Matter Volume & Brain Areas: Random effects model no intercept covariated by Side

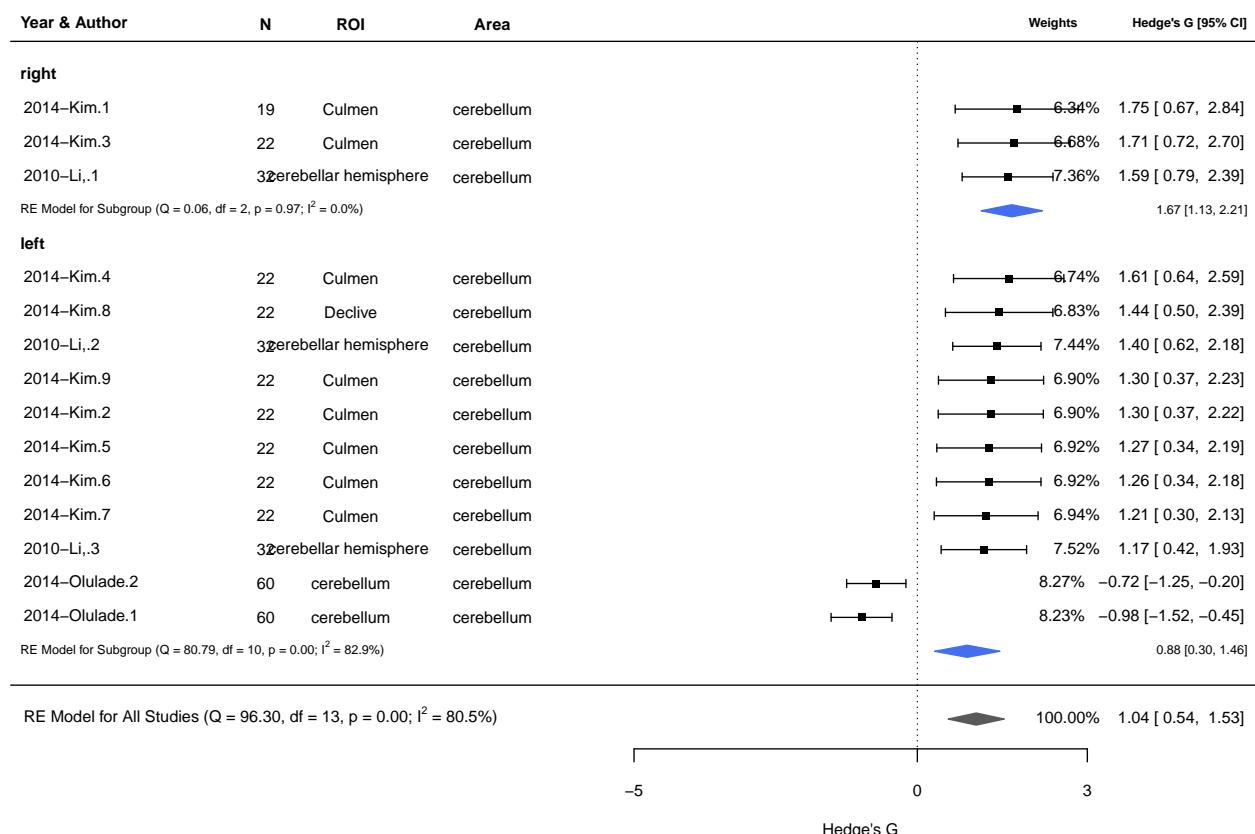


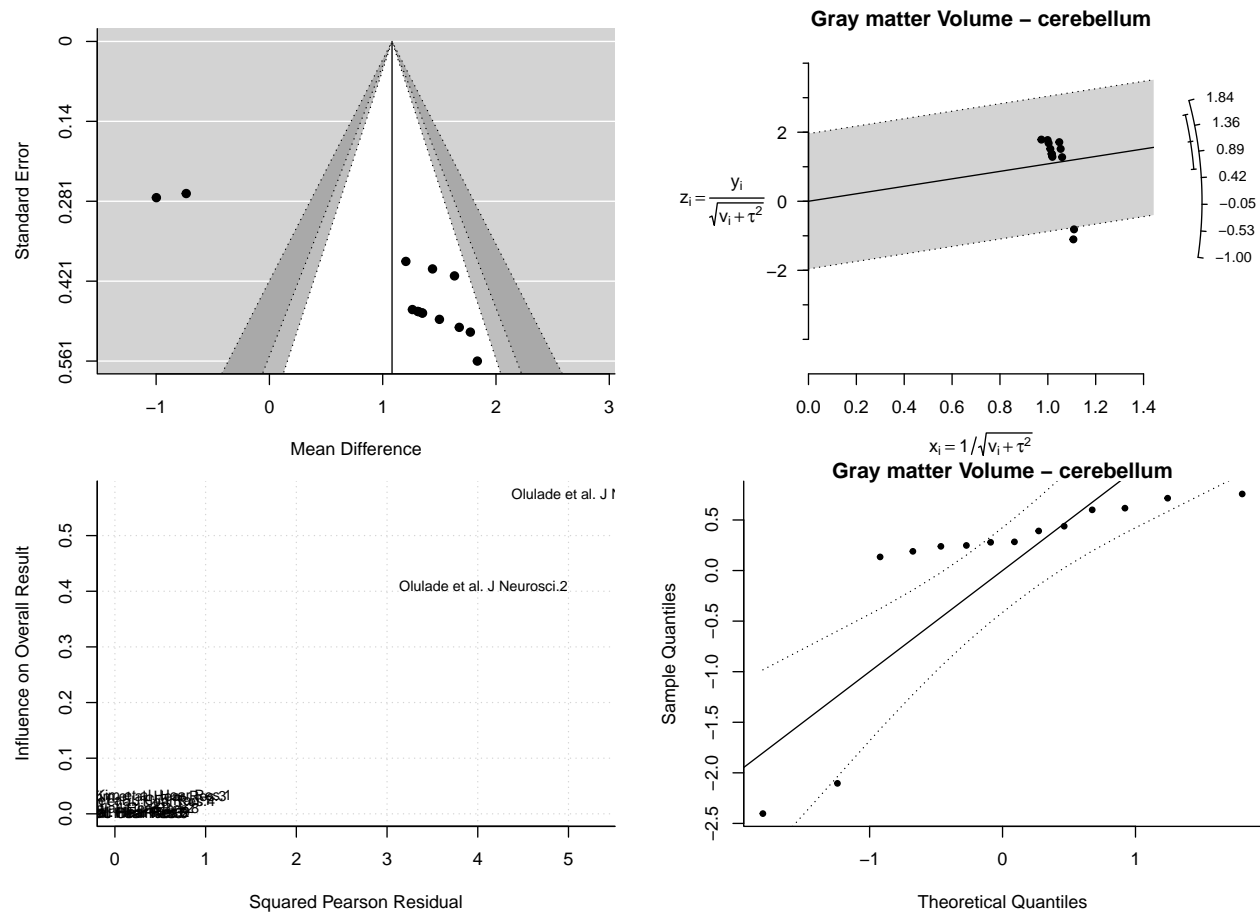


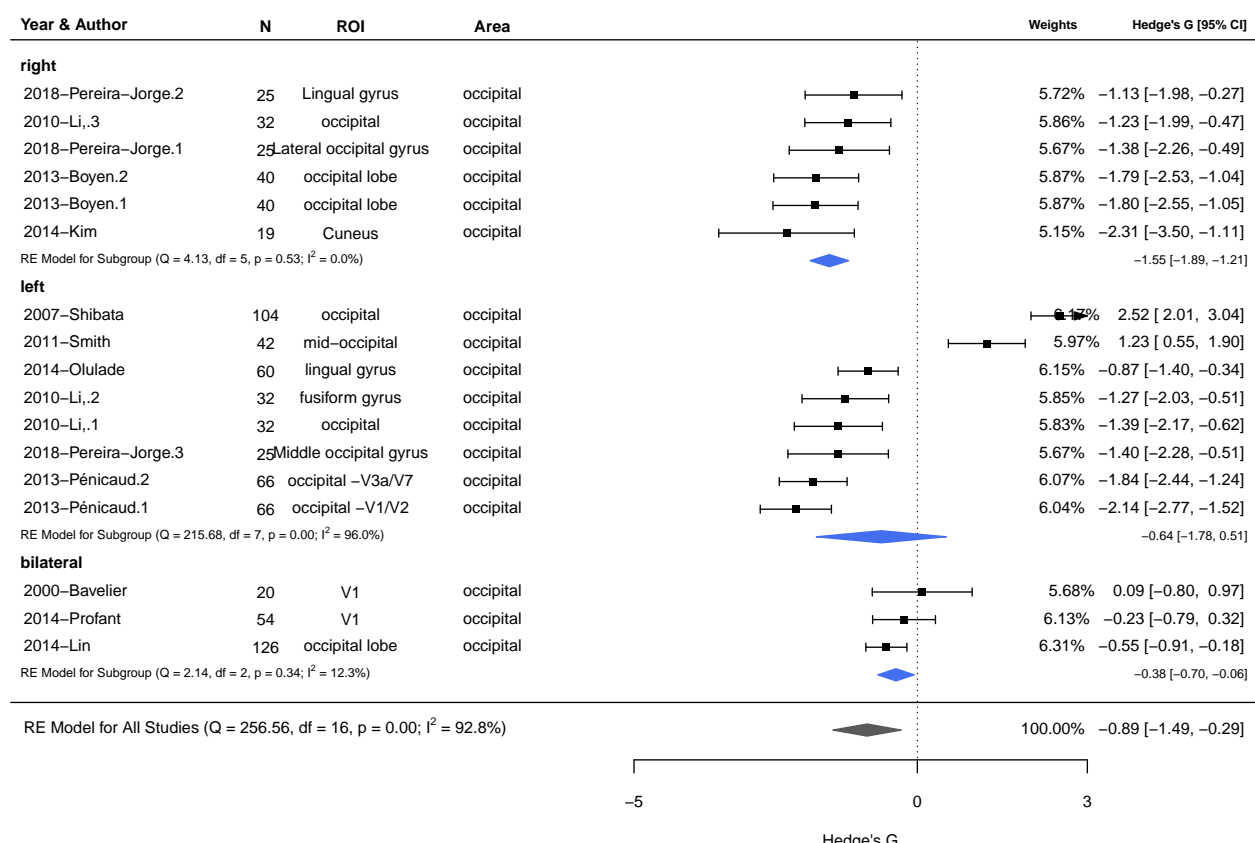


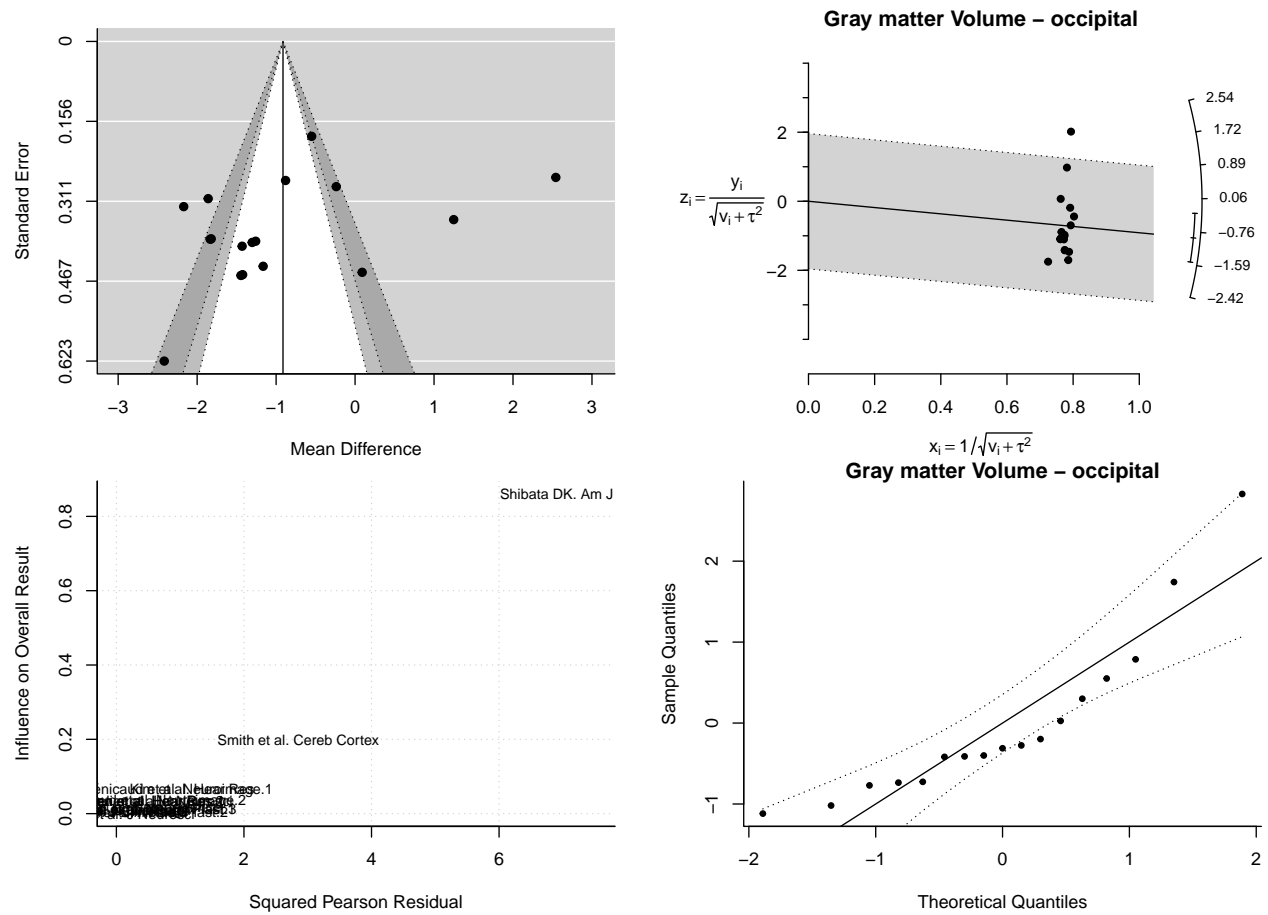


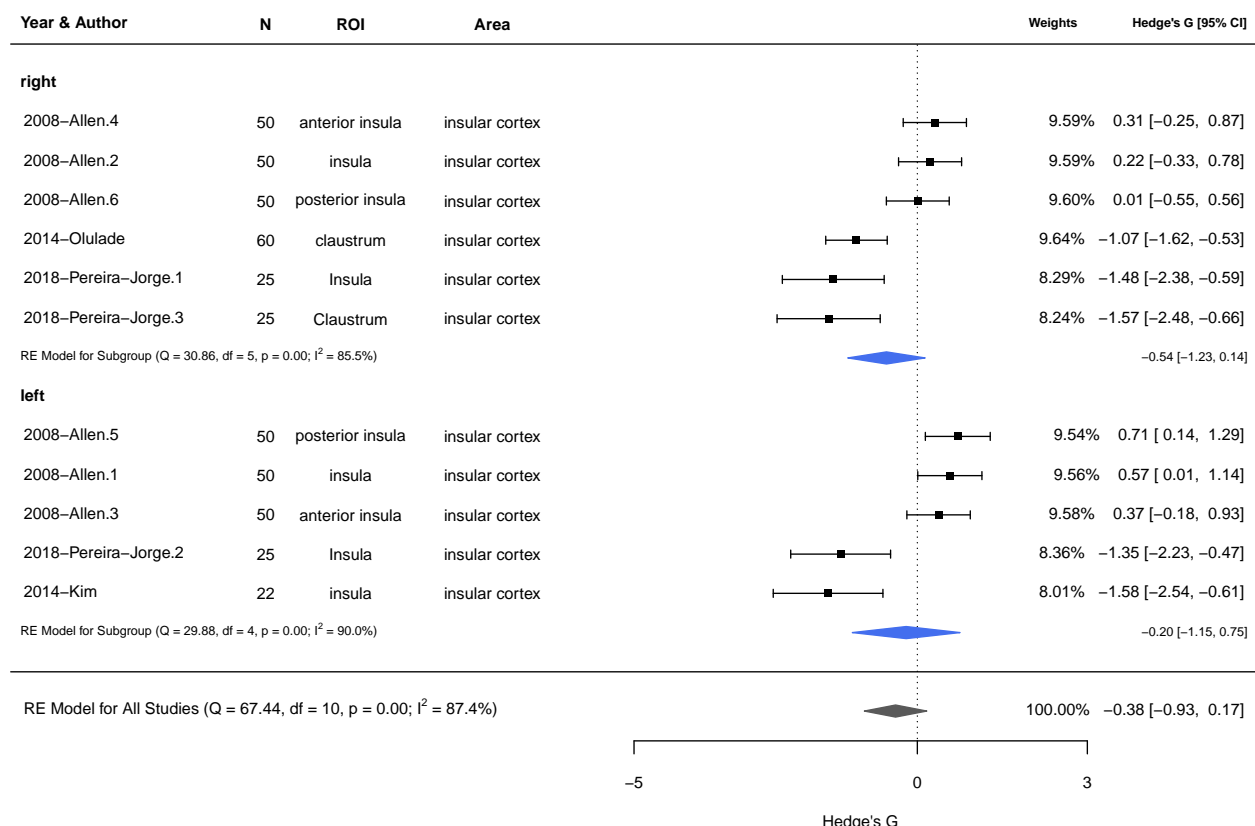


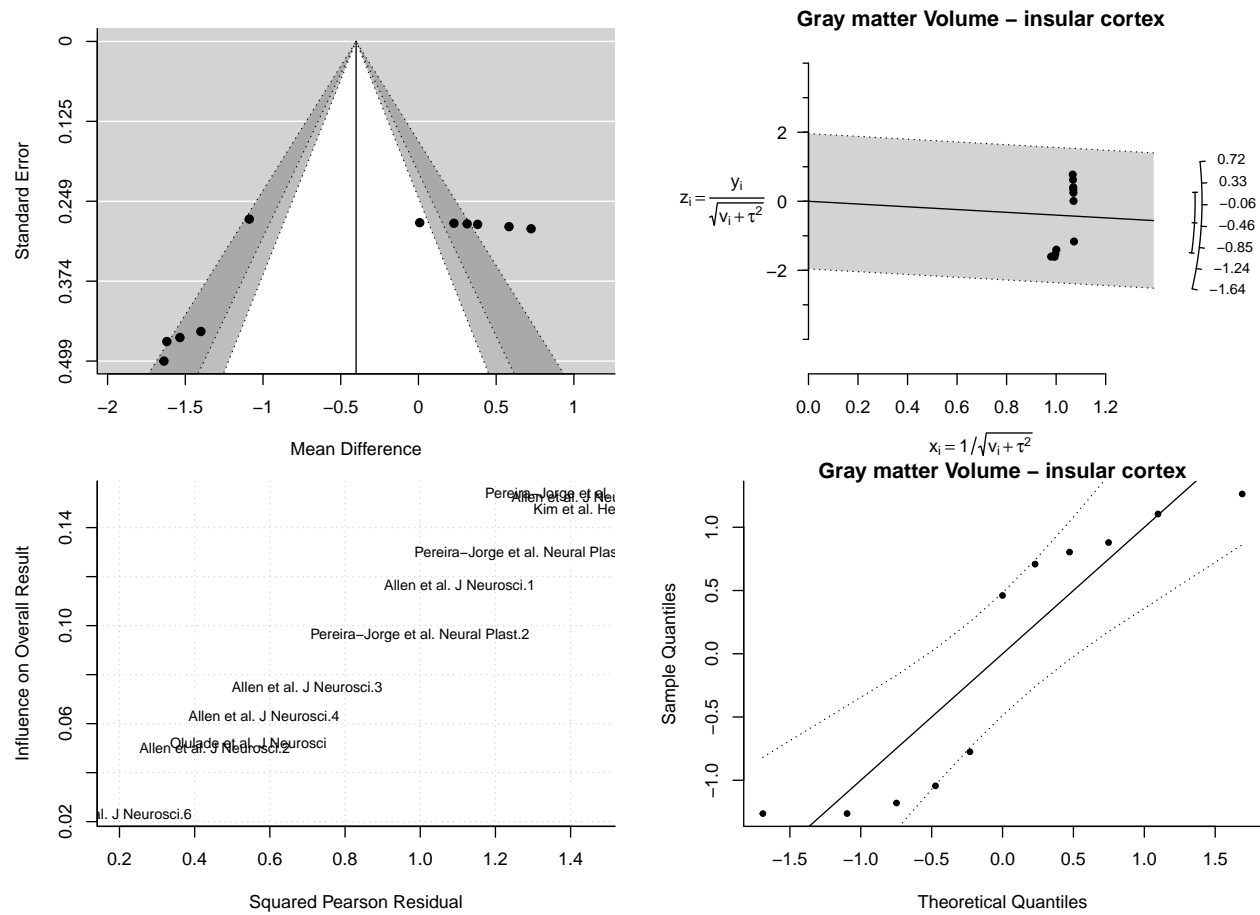
Gray matter Volume – cerebellum



Gray matter Volume – occipital

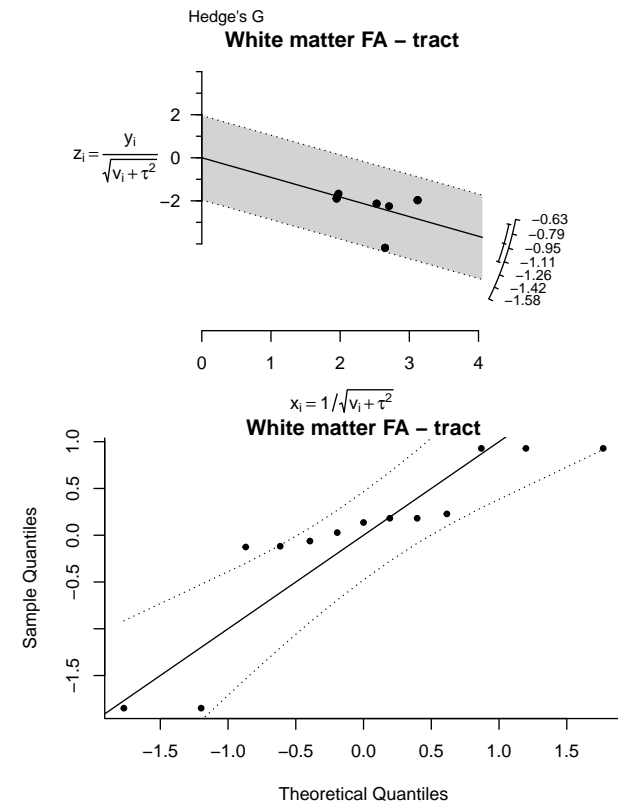
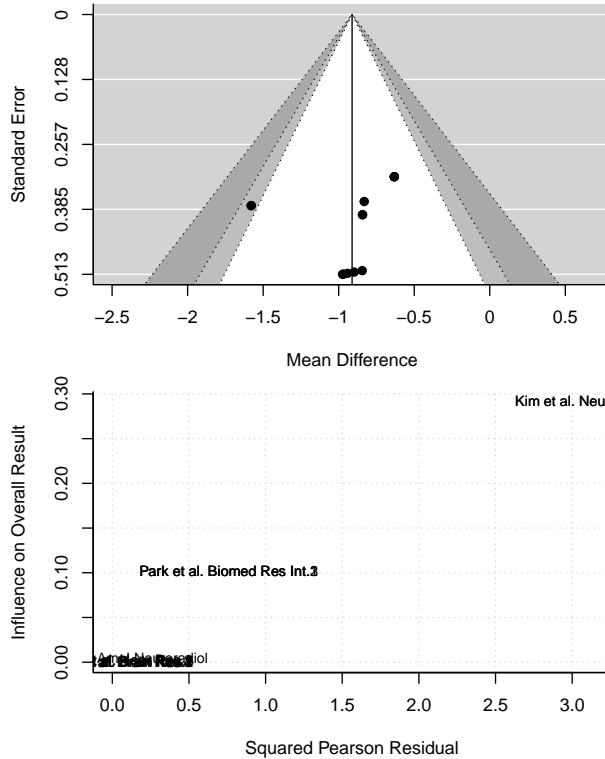
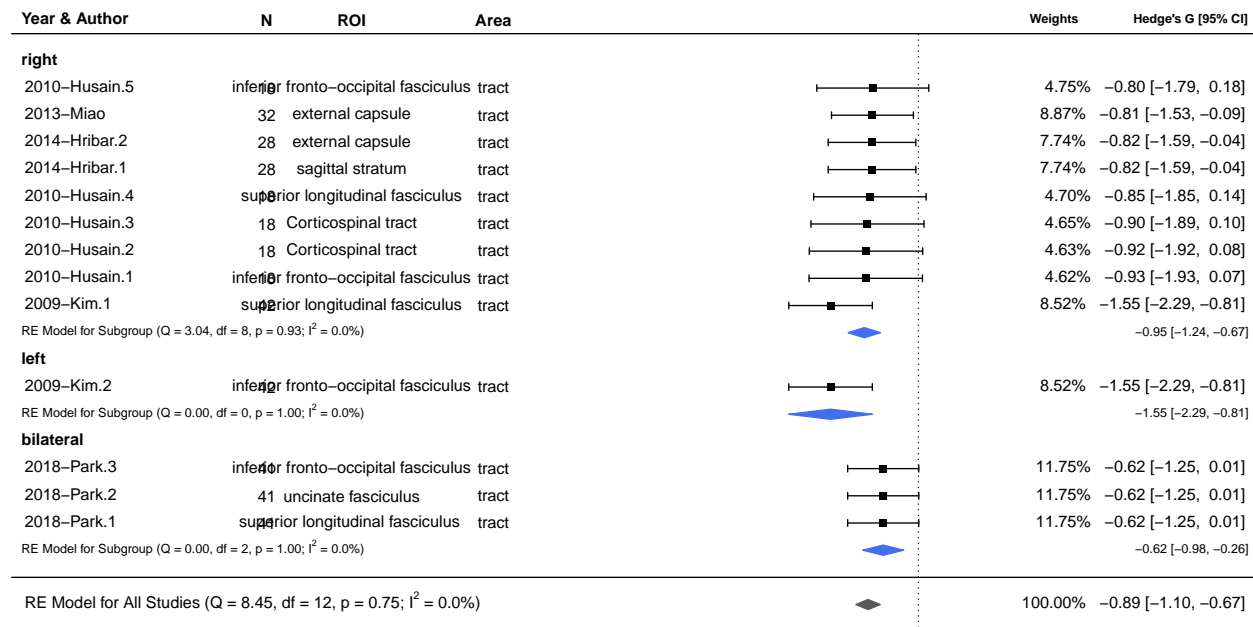


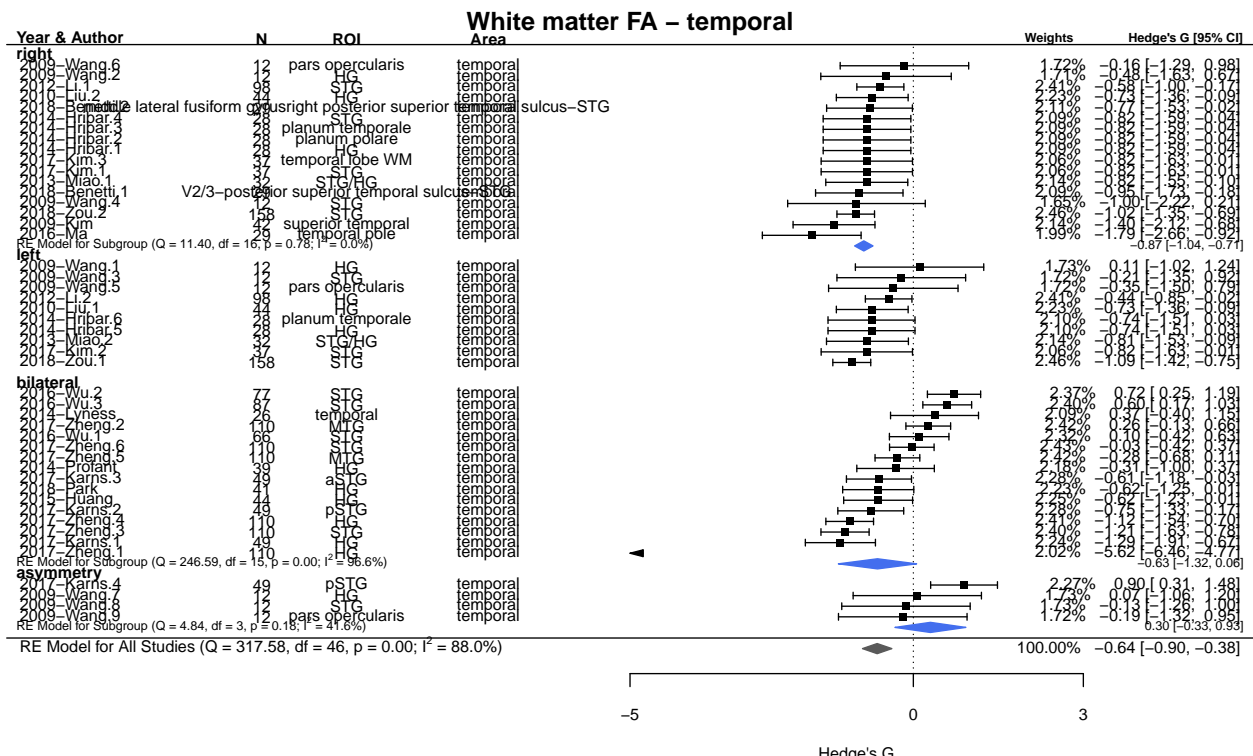
Gray matter Volume – insular cortex



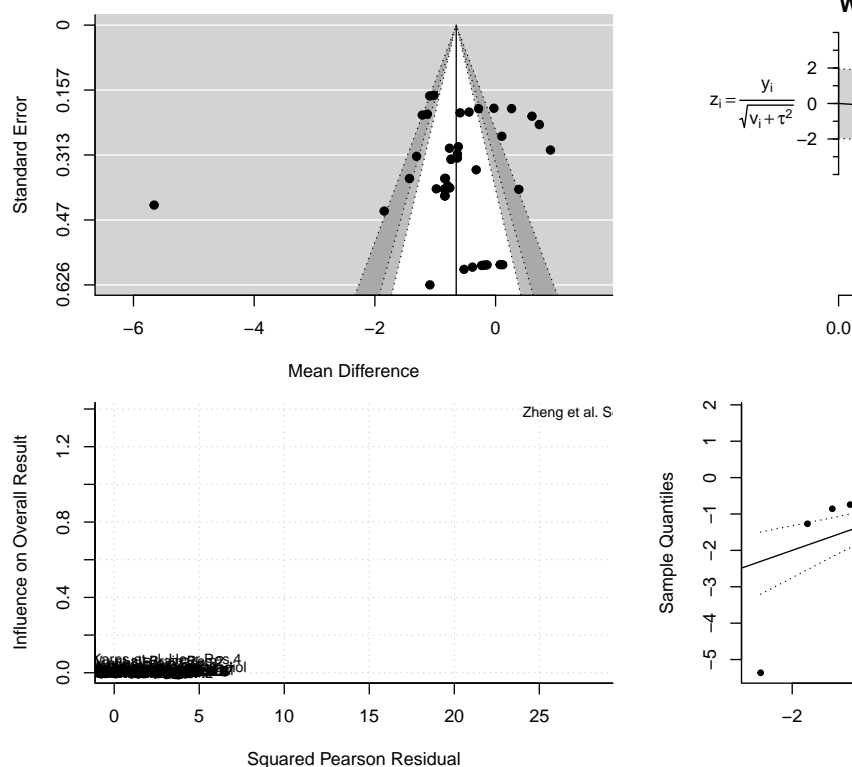
Meta-regressions of White Matter FA & Brain Areas: Random effects model no intercept covariated by Side

White matter FA – tract

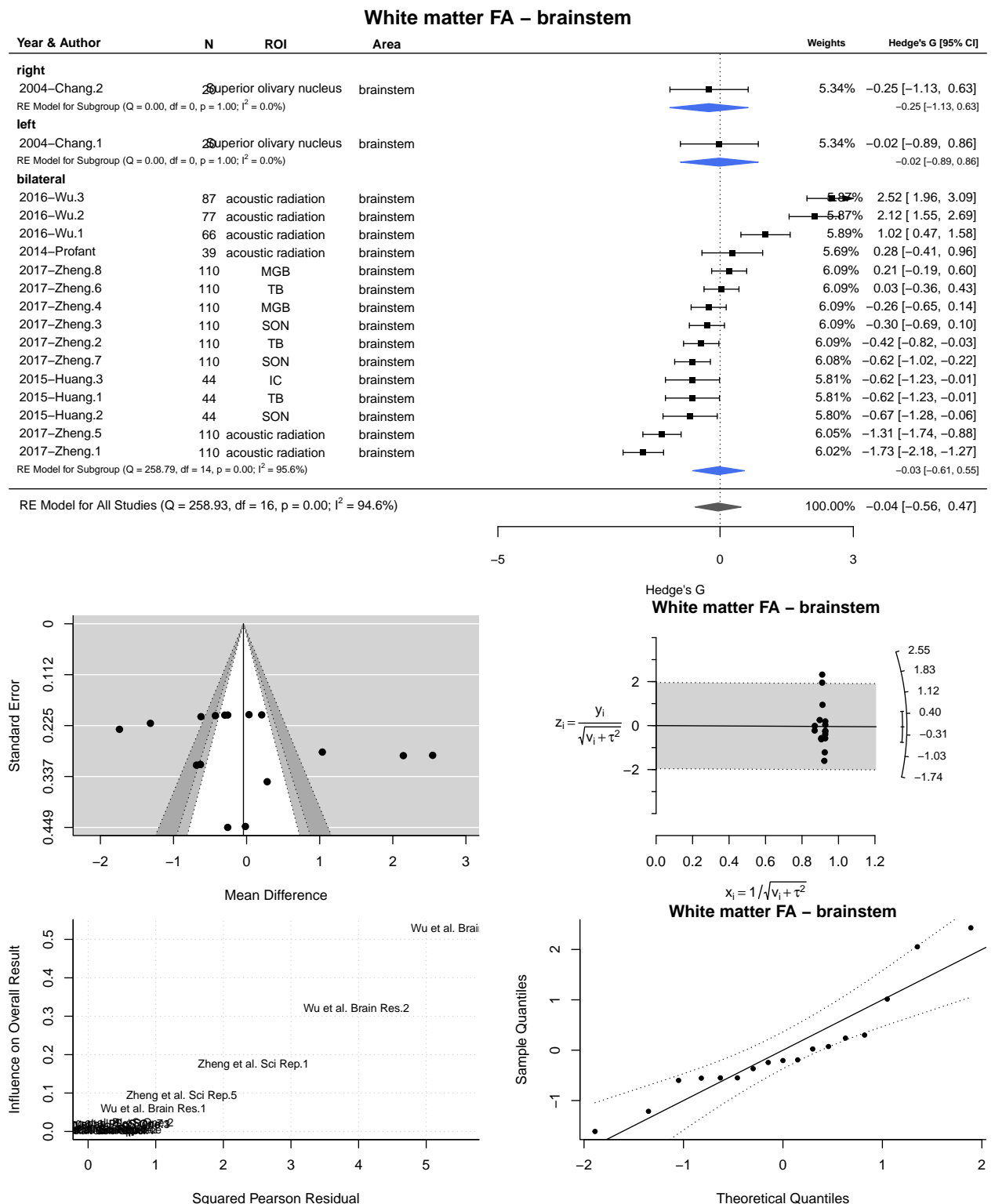


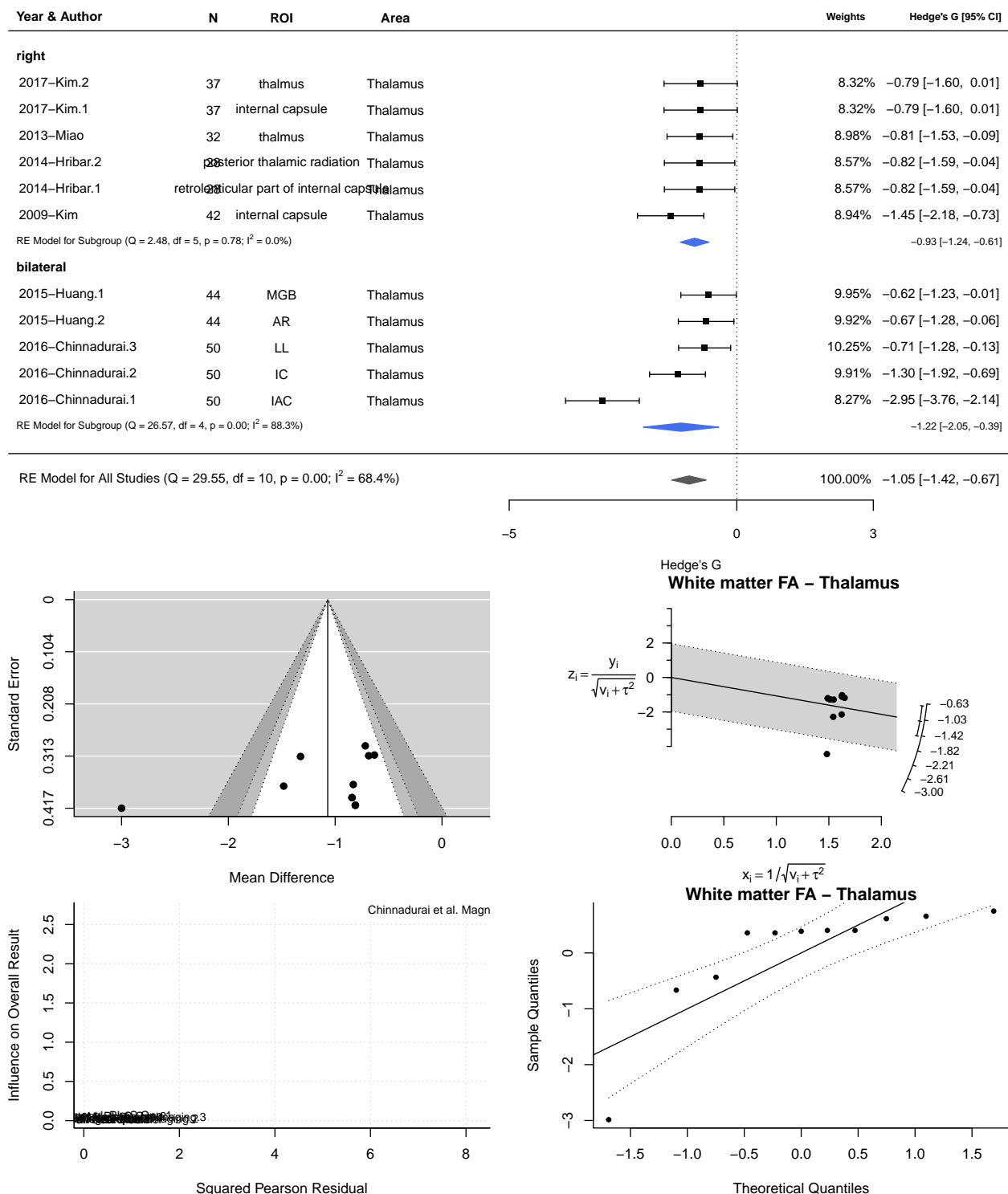


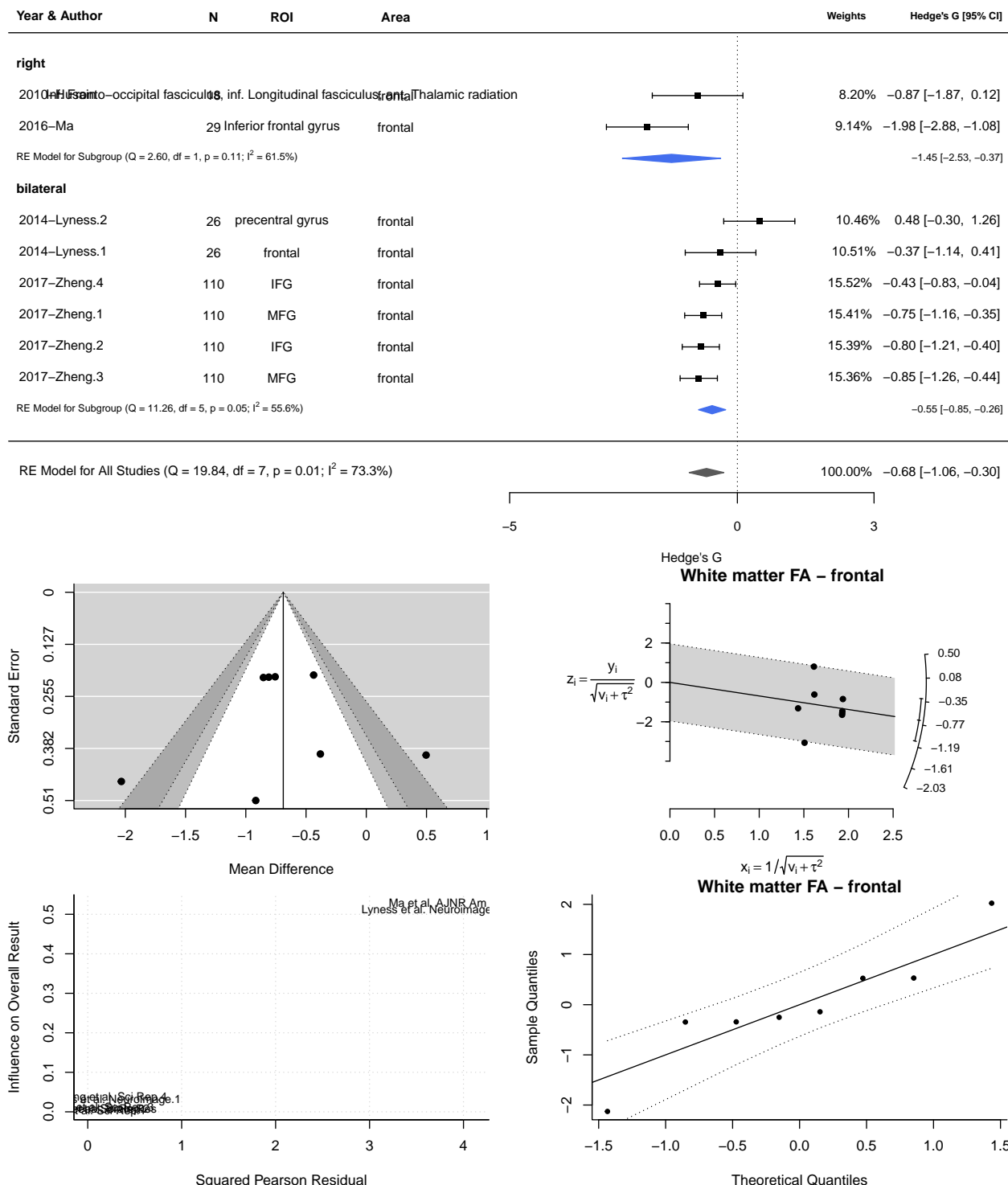
Error in rma(yi = hedgesG, vi = varG, data = meta.mod, measure = "MD", : Fisher scoring algorithm did



not converge. See 'help(rma)' for possible remedies.

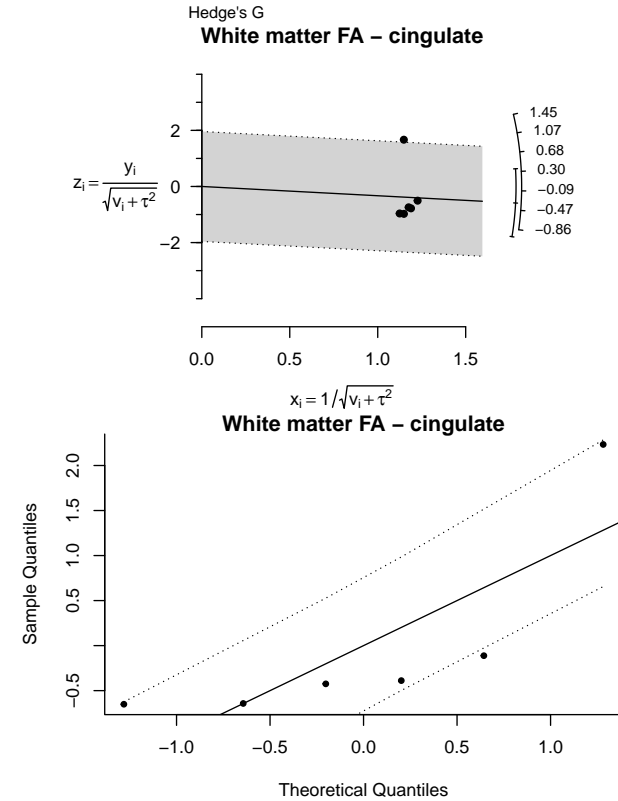
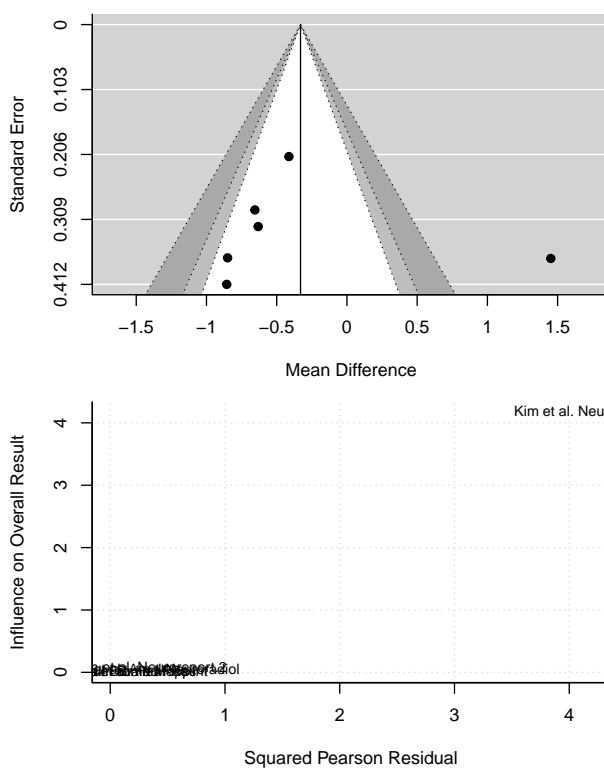


White matter FA – Thalamus

White matter FA – frontal

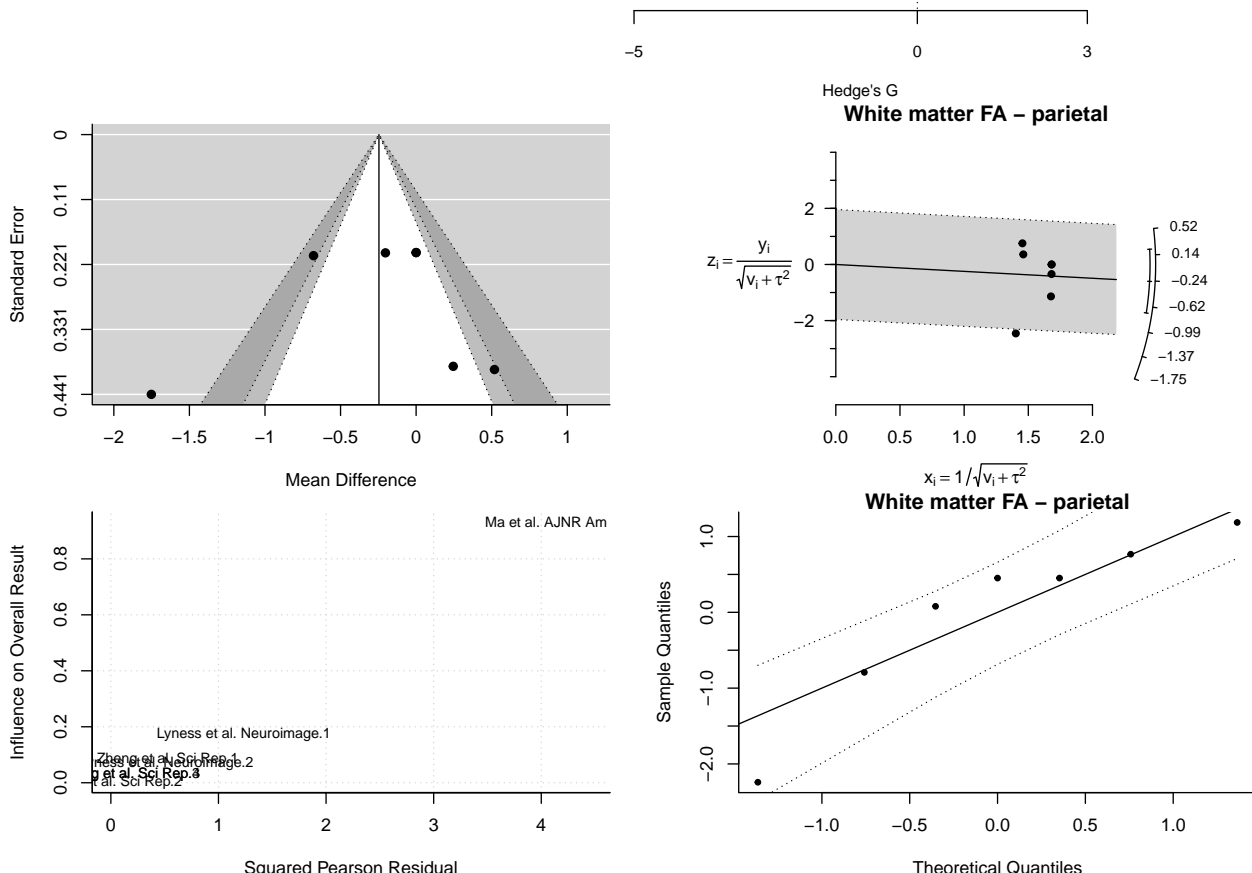
White matter FA – cingulate

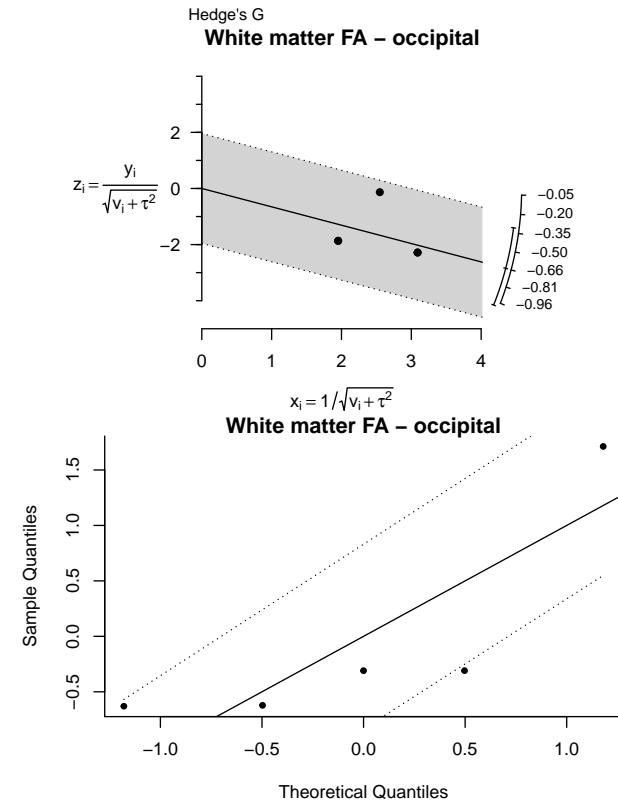
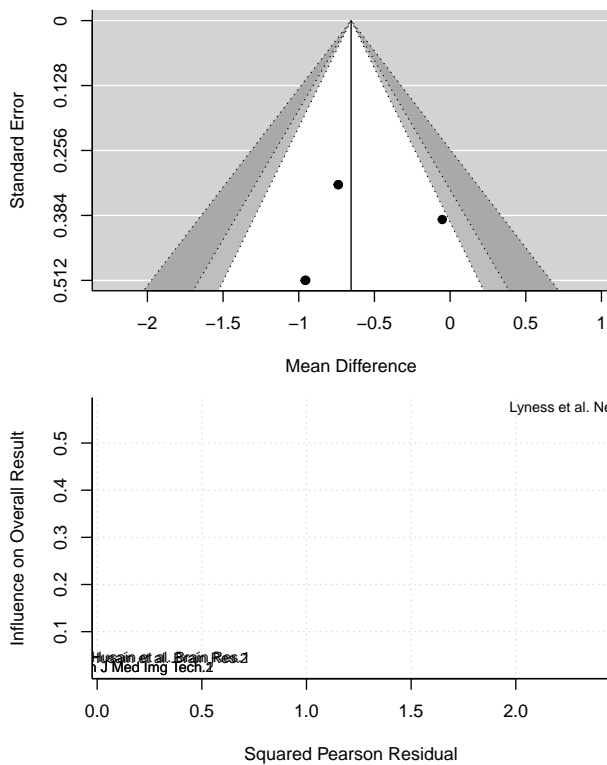
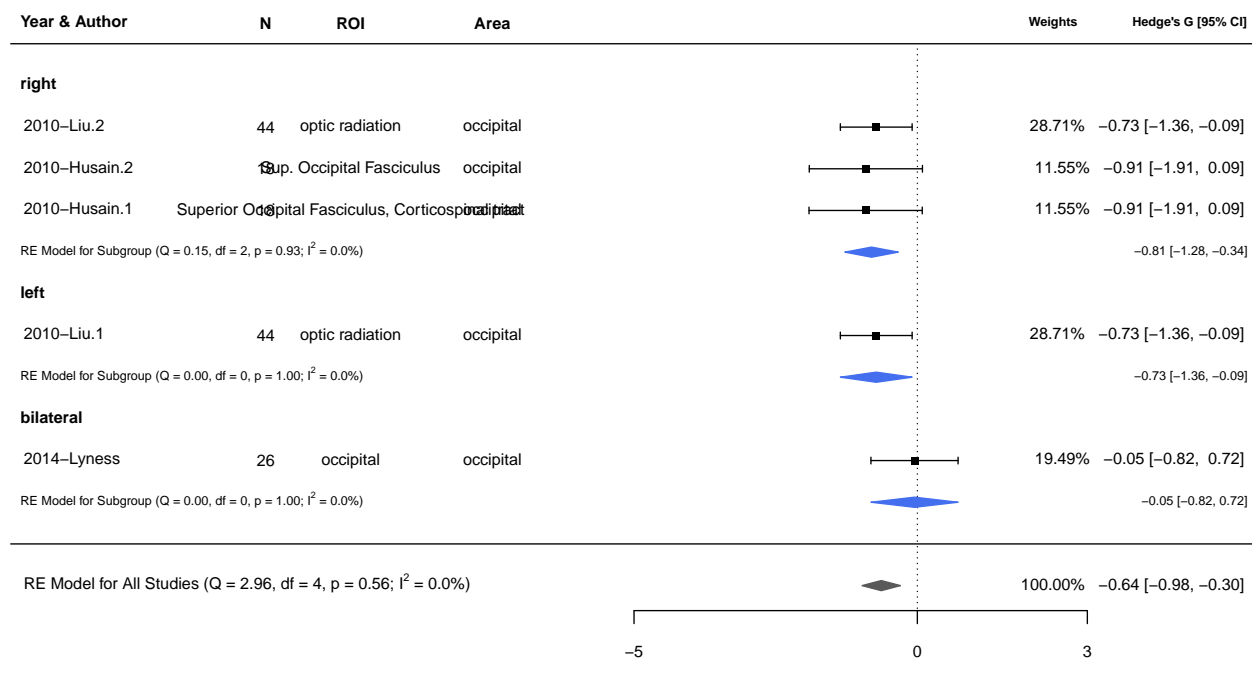
Year & Author	N	ROI	Area	Weights	Hedge's G [95% CI]
left					
2009-Kim	42	Bilateral forceps major	cingulate	16.06%	1.42 [0.70, 2.15]
2013-Miao	32	corpus callosum	cingulate	16.07%	-0.83 [-1.55, -0.10]
RE Model for Subgroup ($Q = 18.57$, $df = 1$, $p = 0.00$; $I^2 = 94.6\%$)					
bilateral					
2012-Li	41	splenium of corpus callosum	cingulate	18.41%	-0.41 [-0.82, 0.00]
2018-Park	41	forceps major	cingulate	16.85%	-0.62 [-1.25, 0.01]
2017-Karns	41	splenium of corpus callosum	cingulate	17.25%	-0.64 [-1.22, -0.07]
2017-Kim	41	splenium of corpus callosum	cingulate	15.37%	-0.84 [-1.64, -0.03]
RE Model for Subgroup ($Q = 1.09$, $df = 3$, $p = 0.78$; $I^2 = 0.0\%$)					
RE Model for All Studies ($Q = 27.88$, $df = 5$, $p = 0.00$; $I^2 = 85.8\%$)					



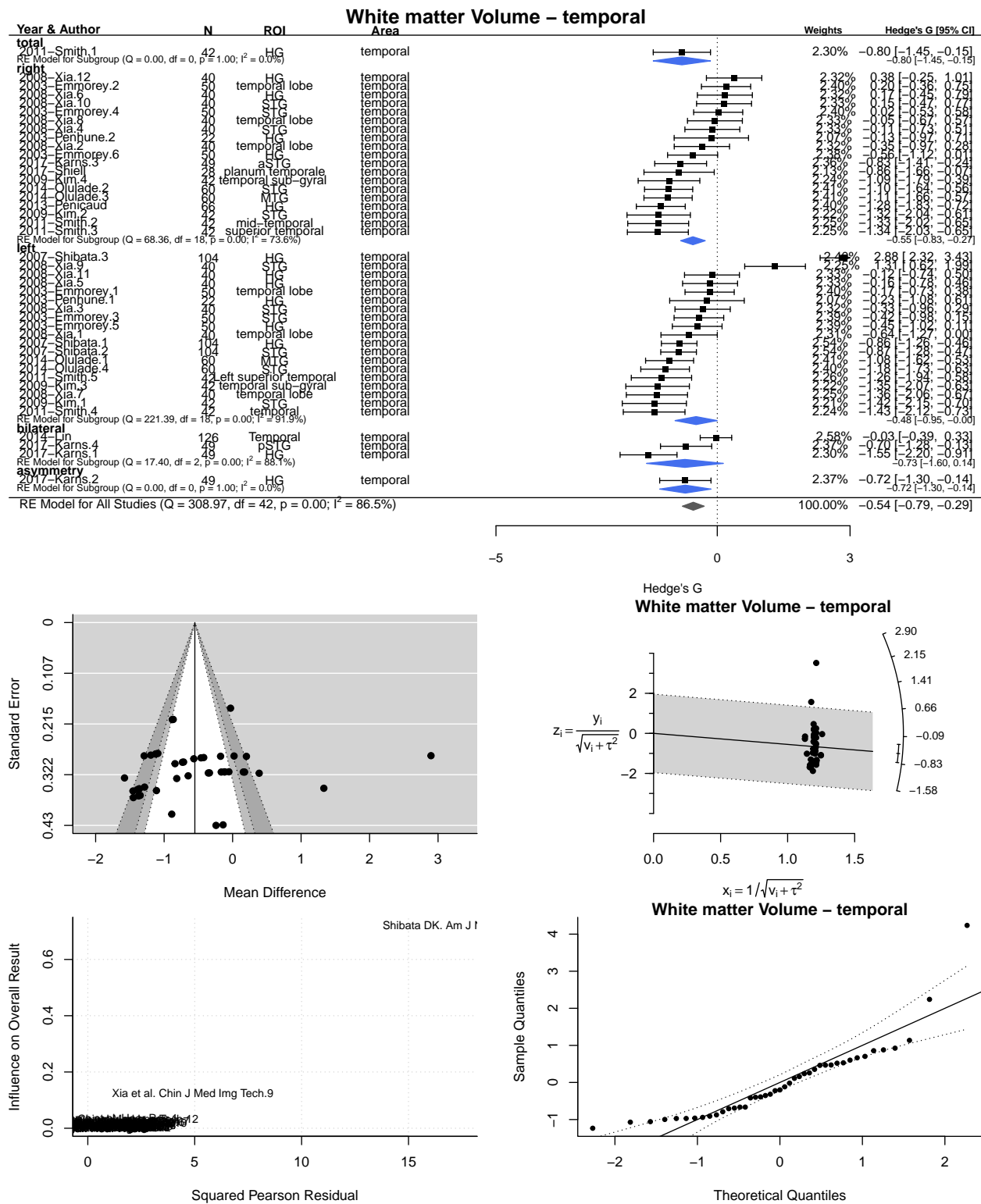
White matter FA – parietal

Year & Author	N	ROI	Area	Weights	Hedge's G [95% CI]
right					
2016-Ma	29	Angular gyrus	parietal	11.13%	-1.70 [-2.56, -0.84]
RE Model for Subgroup ($Q = 0.00$, $df = 0$, $p = 1.00$; $I^2 = 0.0\%$)					
bilateral					
2014-Lyness.1	26	postcentral gyrus	parietal	11.94%	0.50 [-0.28, 1.28]
2014-Lyness.2	26	parietal lobe	parietal	12.05%	0.24 [-0.53, 1.01]
2017-Zheng.4	110	supramarginal gyrus	parietal	16.25%	0.00 [-0.39, 0.39]
2017-Zheng.3	110	Angular gyrus	parietal	16.25%	0.00 [-0.39, 0.39]
2017-Zheng.2	110	supramarginal gyrus	parietal	16.24%	-0.20 [-0.60, 0.19]
2017-Zheng.1	110	Angular gyrus	parietal	16.15%	-0.67 [-1.08, -0.27]
RE Model for Subgroup ($Q = 11.32$, $df = 5$, $p = 0.05$; $I^2 = 56.5\%$)					
RE Model for All Studies ($Q = 23.38$, $df = 6$, $p = 0.00$; $I^2 = 82.0\%$)					



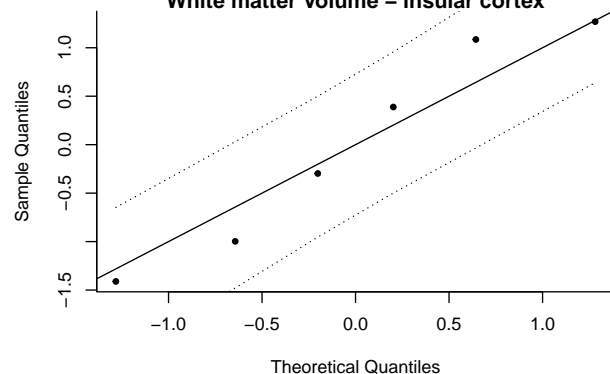
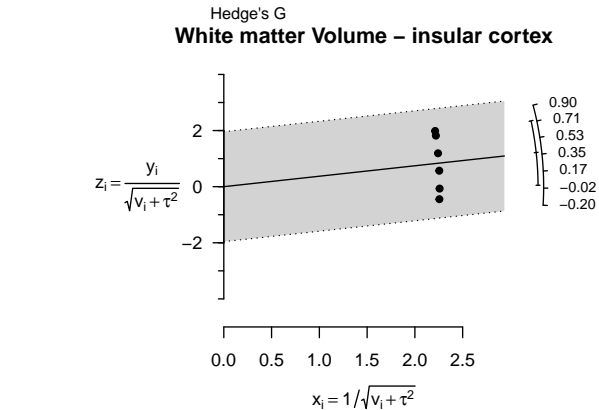
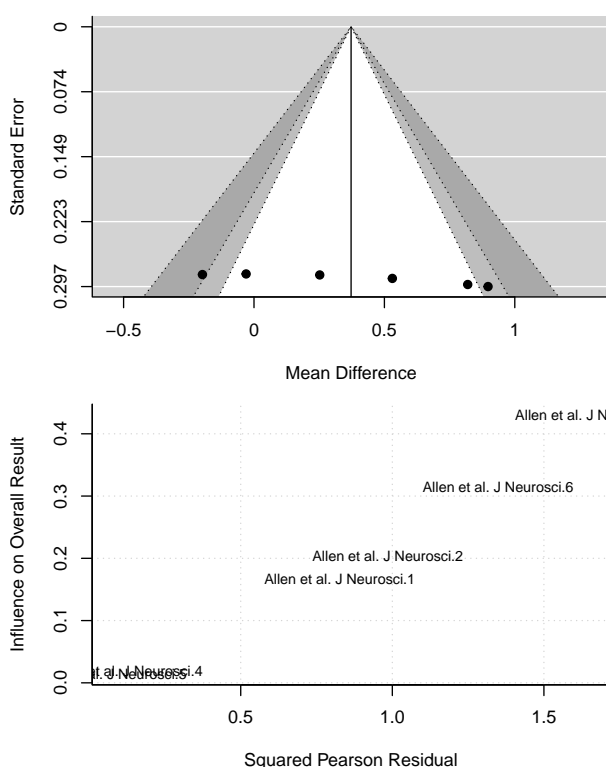
White matter FA – occipital

Meta-regressions of White Matter Volume & Brain Areas: Random effects model no intercept covariated by Side



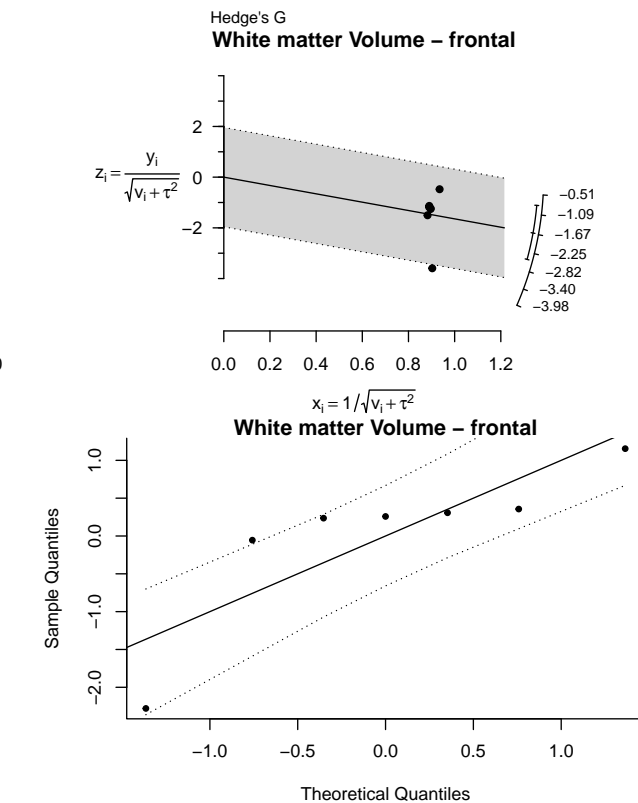
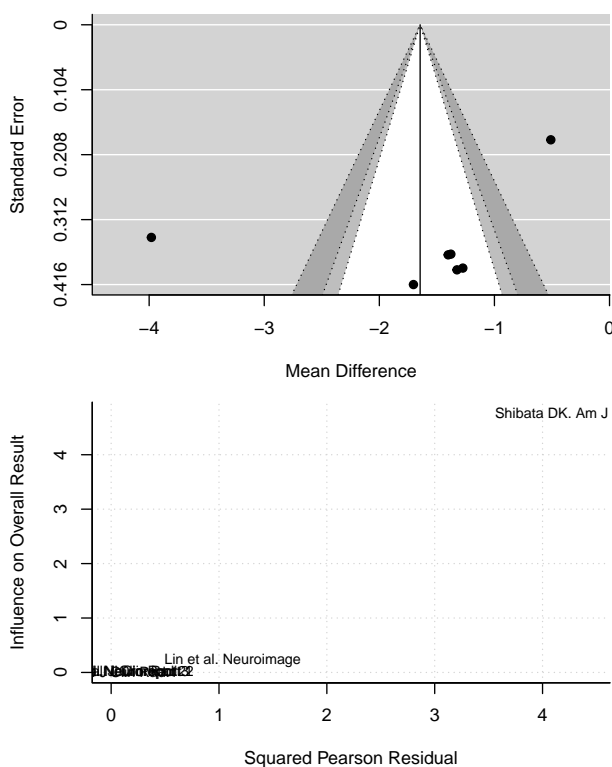
White matter Volume – insular cortex

Year & Author	N	ROI	Area	Weights	Hedge's G [95% CI]
right					
2008–Allen.6	50	posterior insula	insular cortex	16.24%	0.88 [0.30, 1.47]
2008–Allen.2	50	insula	insular cortex	16.35%	0.81 [0.23, 1.38]
2008–Allen.4	50	anterior insula	insular cortex	16.69%	0.52 [−0.04, 1.09]
RE Model for Subgroup (Q = 0.86, df = 2, p = 0.65; I ² = 0.0%)					0.73 [0.40, 1.06]
left					
2008–Allen.5	50	posterior insula	insular cortex	16.88%	0.25 [−0.31, 0.80]
2008–Allen.1	50	insula	insular cortex	16.94%	−0.03 [−0.58, 0.52]
2008–Allen.3	50	anterior insula	insular cortex	16.90%	−0.19 [−0.75, 0.36]
RE Model for Subgroup (Q = 1.24, df = 2, p = 0.54; I ² = 0.0%)					0.01 [−0.31, 0.33]
RE Model for All Studies (Q = 11.60, df = 5, p = 0.04; I ² = 57.0%)					
				100.00%	0.37 [0.01, 0.72]



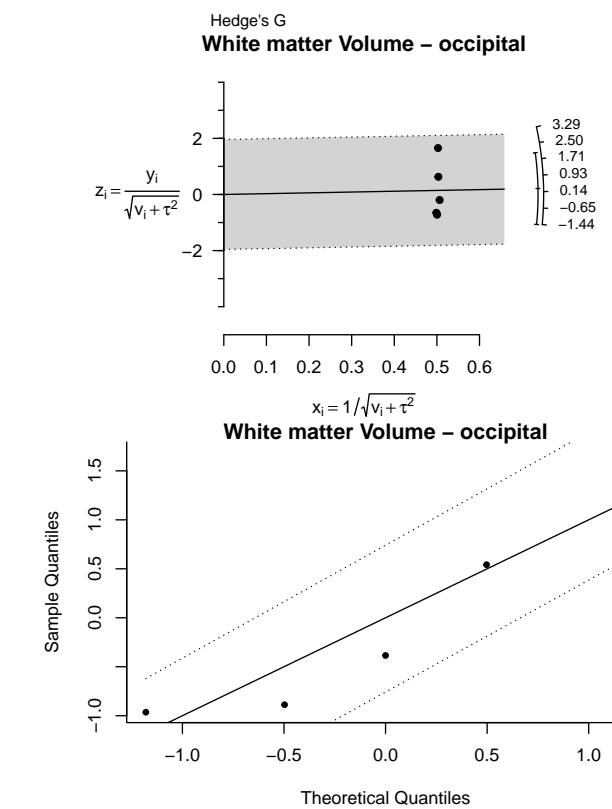
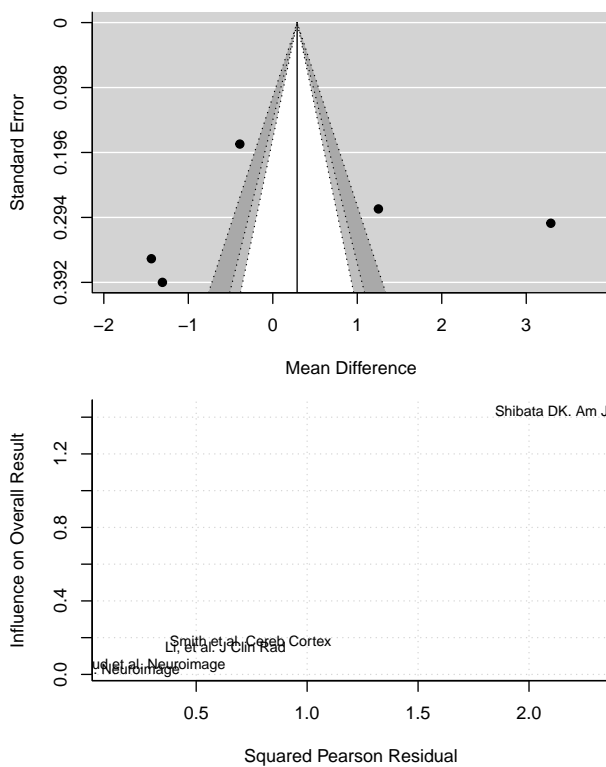
White matter Volume – frontal

Year & Author	N	ROI	Area	Weights	Hedge's G [95% CI]
right					
2010-Li,3	32	prefrontal cortex	frontal		
2010-Li,1	32	prefrontal cortex	frontal		
2007-Shibata	104	perisylvian	frontal		
RE Model for Subgroup (Q = 32.91, df = 2, p = 0.00; $I^2 = 93.3\%$)					-2.30 [-3.96, -0.63]
left					
2010-Li,2	32	prefrontal cortex	frontal		
2009-Kim,2	42	medial frontal	frontal		
2009-Kim,1	42	superior frontal	frontal		
RE Model for Subgroup (Q = 0.03, df = 2, p = 0.99; $I^2 = 0.0\%$)					-1.34 [-1.77, -0.92]
bilateral					
2014-Lin	126	frontal	frontal		
RE Model for Subgroup (Q = 0.00, df = 0, p = 1.00; $I^2 = 0.0\%$)					-0.51 [-0.87, -0.15]
RE Model for All Studies (Q = 80.40, df = 6, p = 0.00; $I^2 = 91.1\%$)					100.00% -1.62 [-2.44, -0.80]



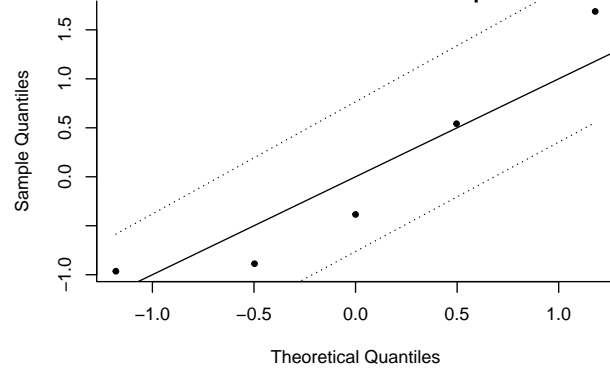
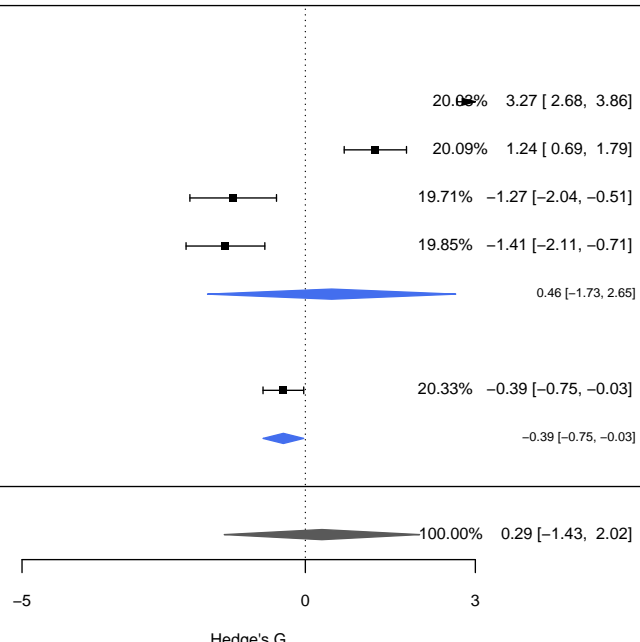
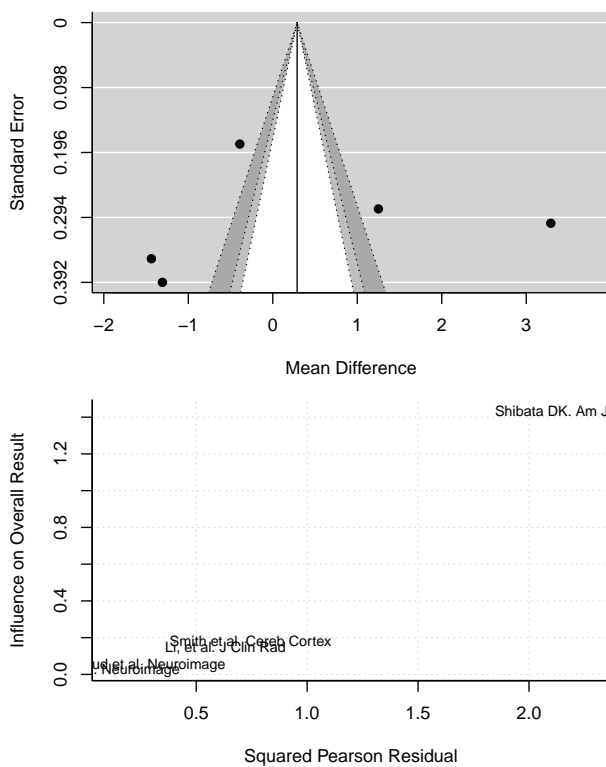
White matter Volume – occipital

Year & Author	N	ROI	Area	Weights	Hedge's G [95% CI]
left					
2007–Shibata	104	occipital	occipital	20.00%	3.27 [2.68, 3.86]
2013–Pénicaud	66	occipital –V3a/V7	occipital	20.09%	1.24 [0.69, 1.79]
2010–Li,	32	occipital cortex	occipital	19.71%	-1.27 [-2.04, -0.51]
2011–Smith	42	occipital	occipital	19.85%	-1.41 [-2.11, -0.71]
RE Model for Subgroup ($Q = 136.47$, $df = 3$, $p = 0.00$; $I^2 = 97.9\%$)					
bilateral					
2014–Lin	126	occipital lobe	occipital	20.33%	-0.39 [-0.75, -0.03]
RE Model for Subgroup ($Q = 0.00$, $df = 0$, $p = 1.00$; $I^2 = 0.0\%$)					
RE Model for All Studies ($Q = 161.69$, $df = 4$, $p = 0.00$; $I^2 = 97.9\%$)					



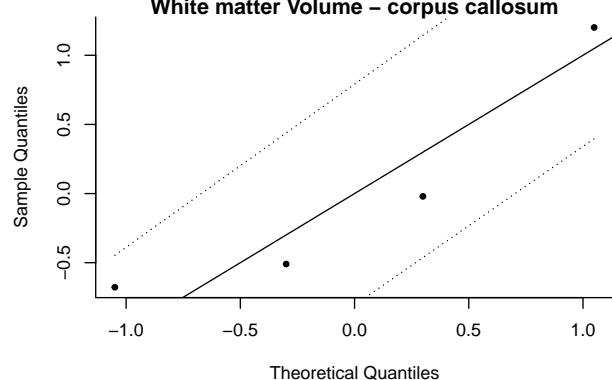
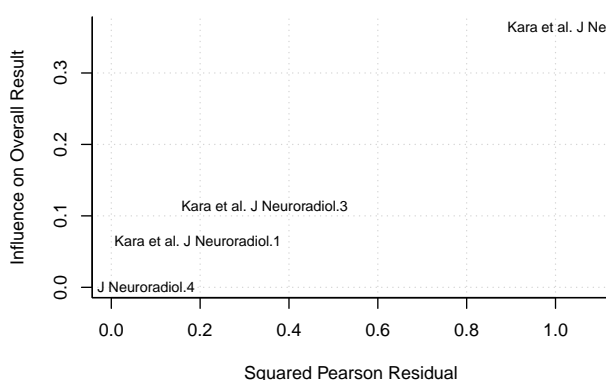
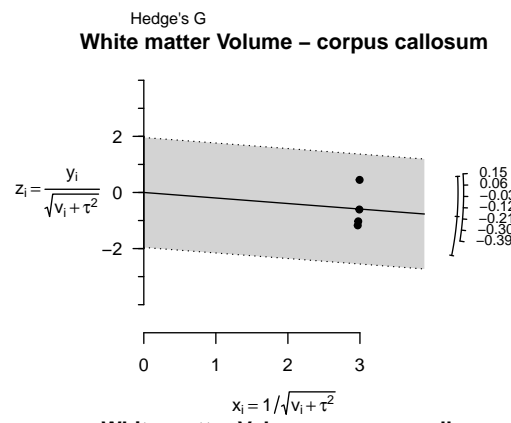
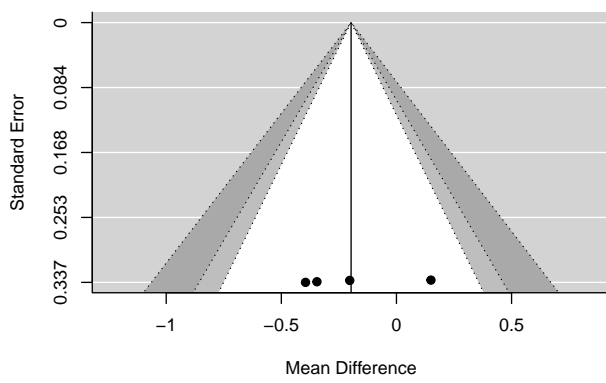
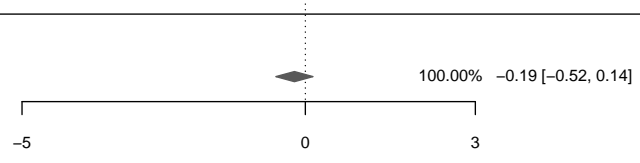
White matter Volume – occipital

Year & Author	N	ROI	Area	Weights	Hedge's G [95% CI]
left					
2007–Shibata	104	occipital	occipital	20.00%	3.27 [2.68, 3.86]
2013–Pénicaud	66	occipital –V3a/V7	occipital	20.09%	1.24 [0.69, 1.79]
2010–Li,	32	occipital cortex	occipital	19.71%	-1.27 [-2.04, -0.51]
2011–Smith	42	occipital	occipital	19.85%	-1.41 [-2.11, -0.71]
RE Model for Subgroup ($Q = 136.47$, $df = 3$, $p = 0.00$; $I^2 = 97.9\%$)					
bilateral					
2014–Lin	126	occipital lobe	occipital	20.33%	-0.39 [-0.75, -0.03]
RE Model for Subgroup ($Q = 0.00$, $df = 0$, $p = 1.00$; $I^2 = 0.0\%$)					
RE Model for All Studies ($Q = 161.69$, $df = 4$, $p = 0.00$; $I^2 = 97.9\%$)					



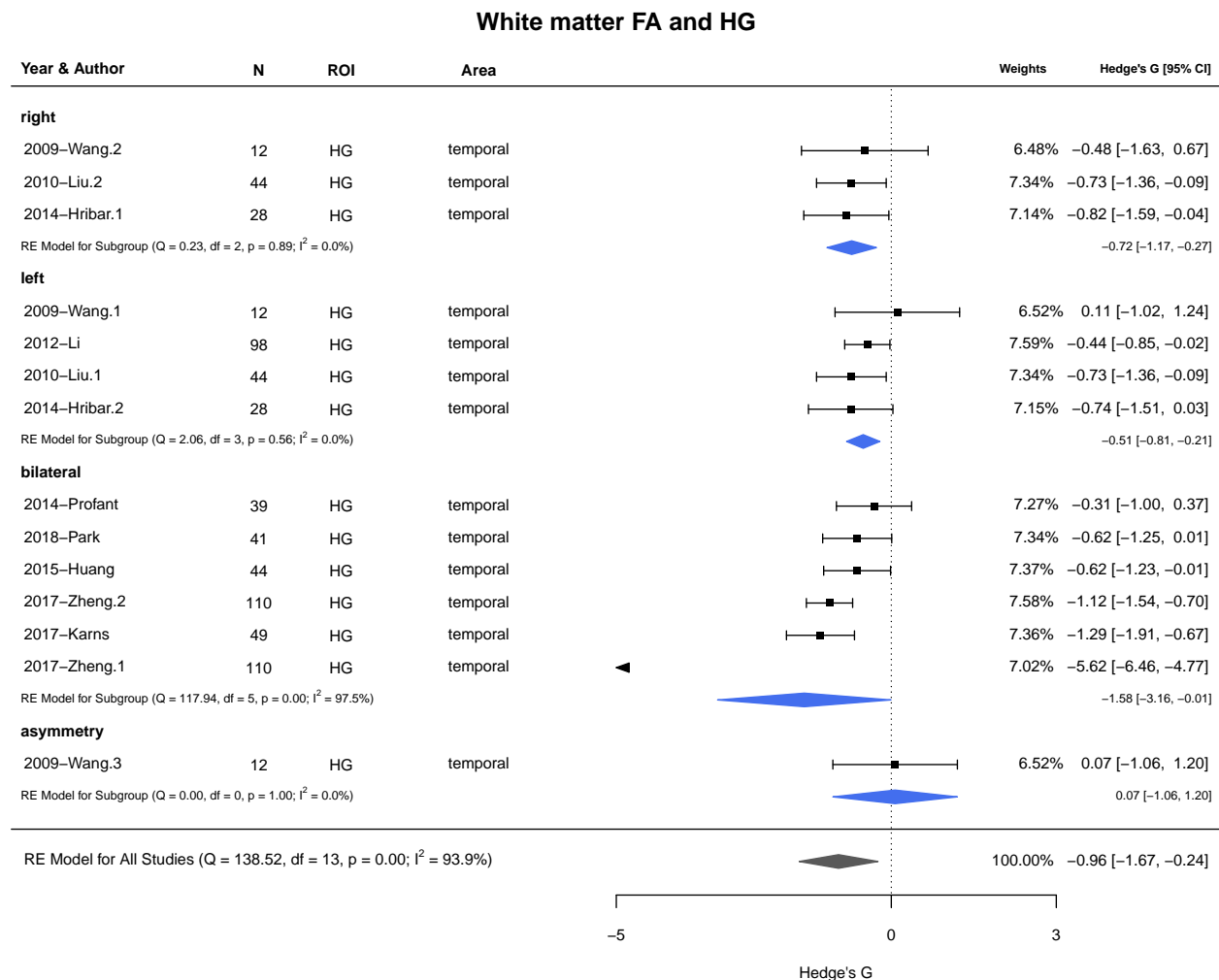
White matter Volume – corpus callosum

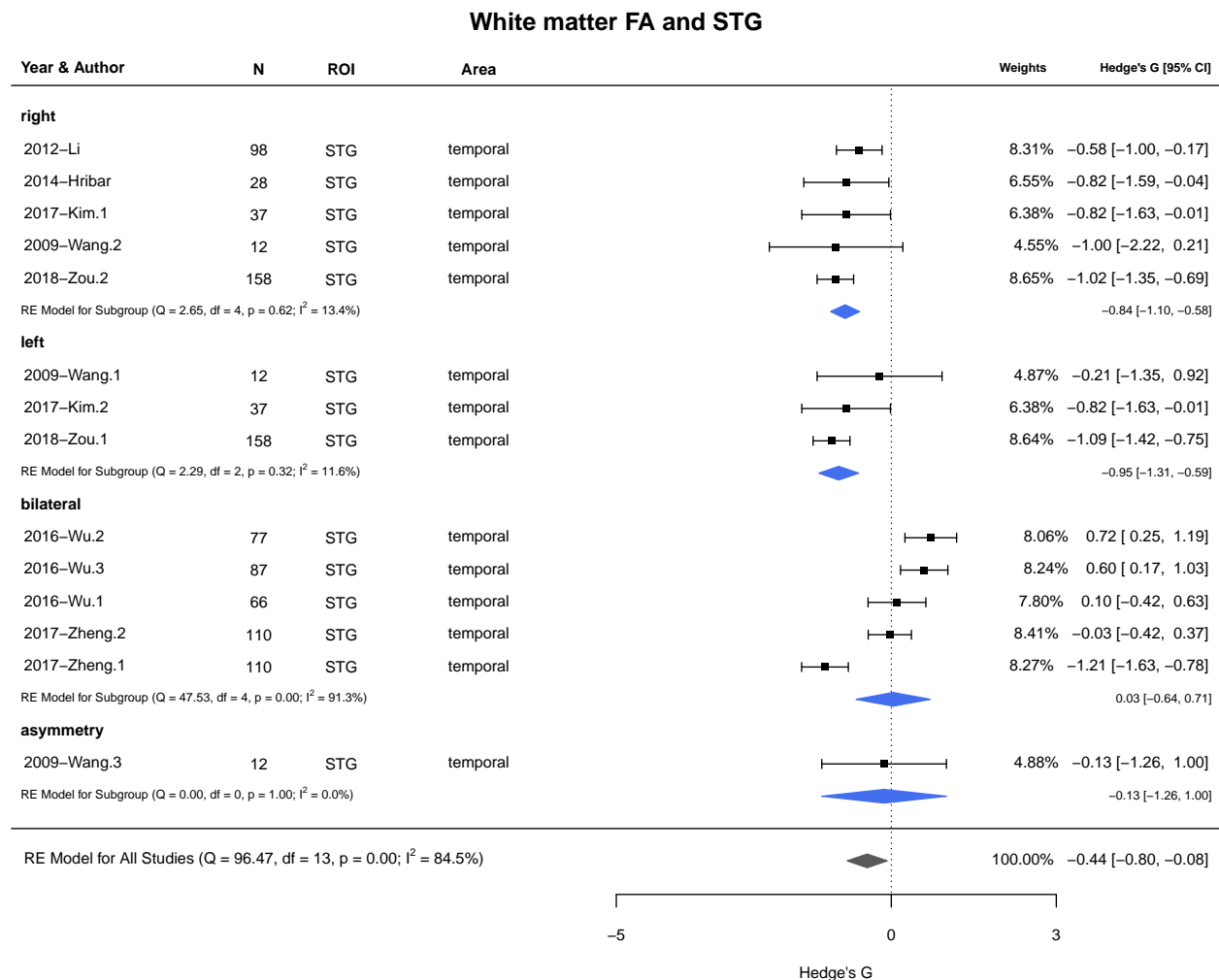
Year & Author	N	ROI	Area	Weights	Hedge's G [95% CI]
bilateral					
2006-Kara.2		corpus callosum (middle area)	corpus callosum	25.20%	0.15 [-0.51, 0.80]
2006-Kara.4		corpus callosum (total area)	corpus callosum	25.14%	-0.20 [-0.85, 0.46]
2006-Kara.1		corpus callosum (anterior area)	corpus callosum	24.89%	-0.34 [-1.00, 0.32]
2006-Kara.3		corpus callosum (posterior area)	corpus callosum	24.78%	-0.39 [-1.05, 0.27]
RE Model for Subgroup ($Q = 1.55$, $df = 3$, $p = 0.67$; $I^2 = 0.0\%$)					
RE Model for All Studies ($Q = 1.55$, $df = 3$, $p = 0.67$; $I^2 = 0.0\%$)					



Supplementary material: Forest-plots of other Measures

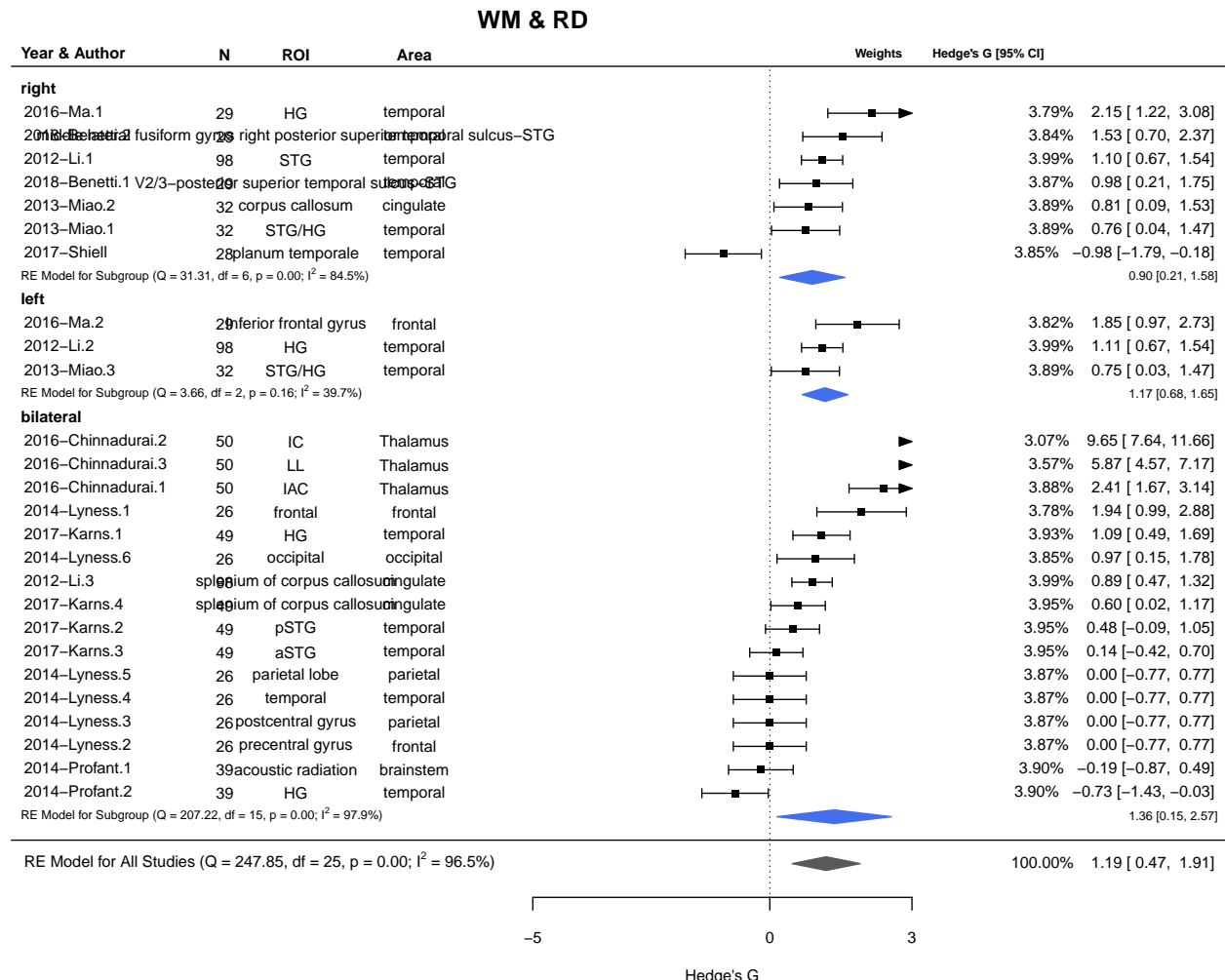
Hesch gyrus FA white matter



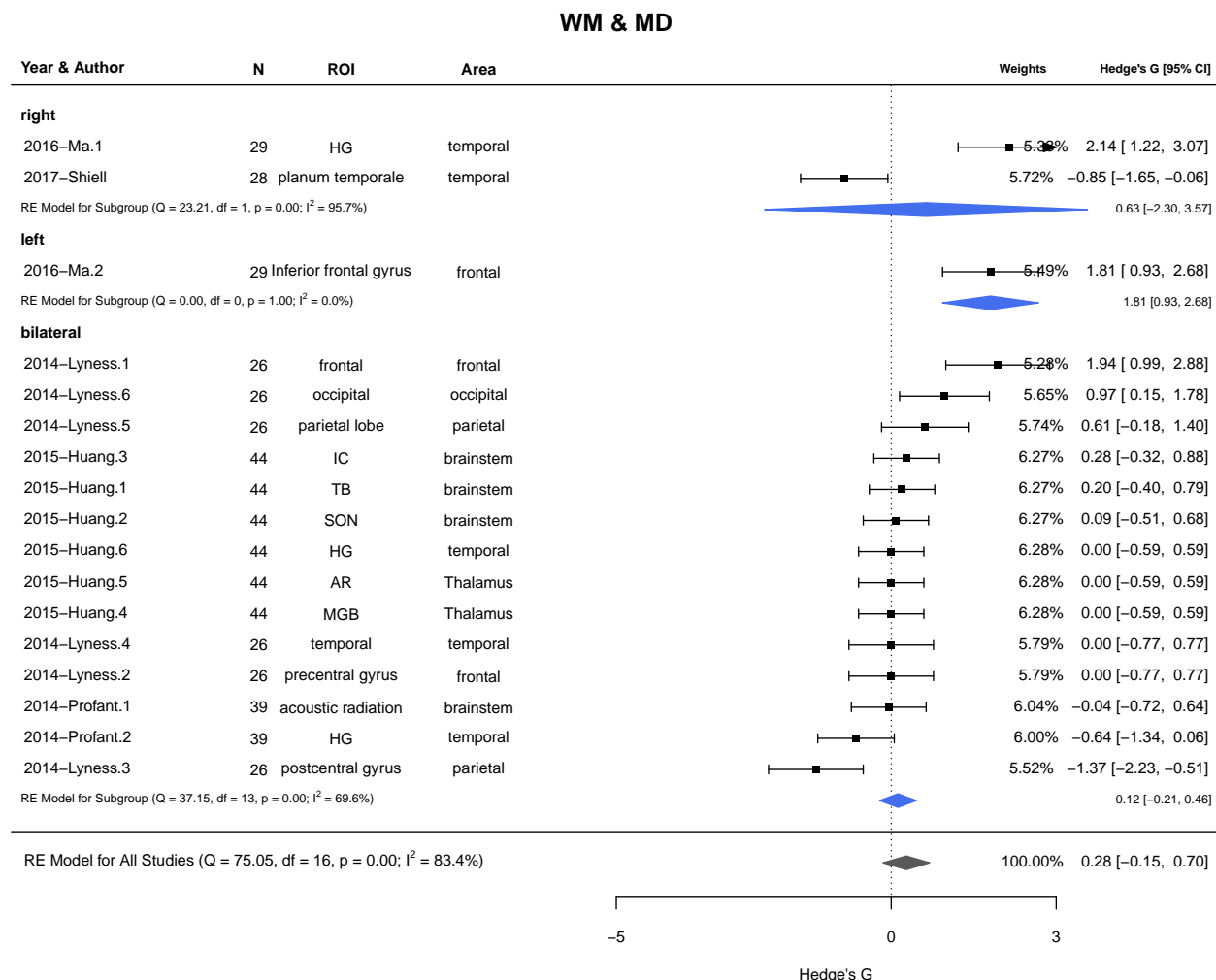
STG Volume White matter

Measures of White matter Integrity

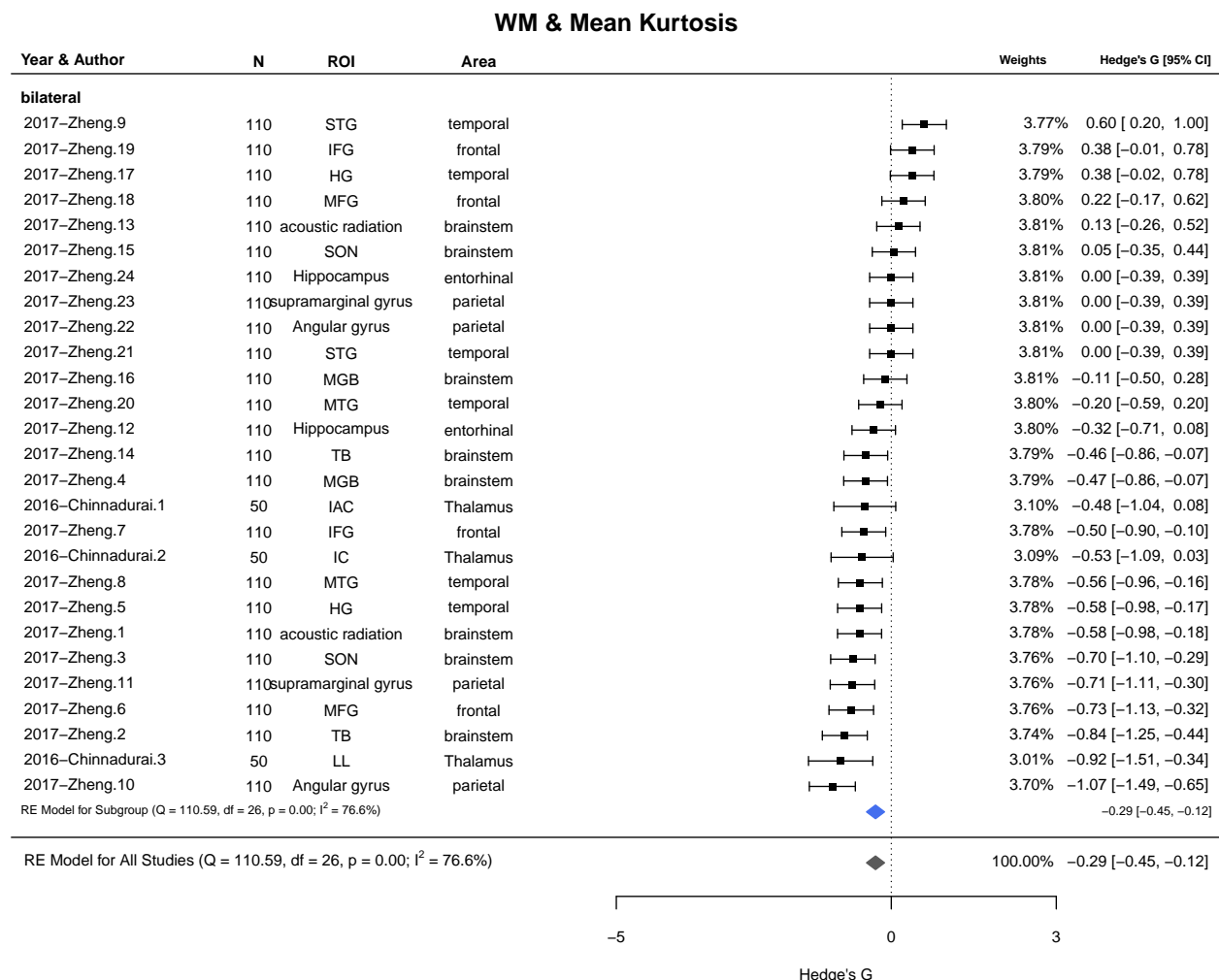
White matter: RD



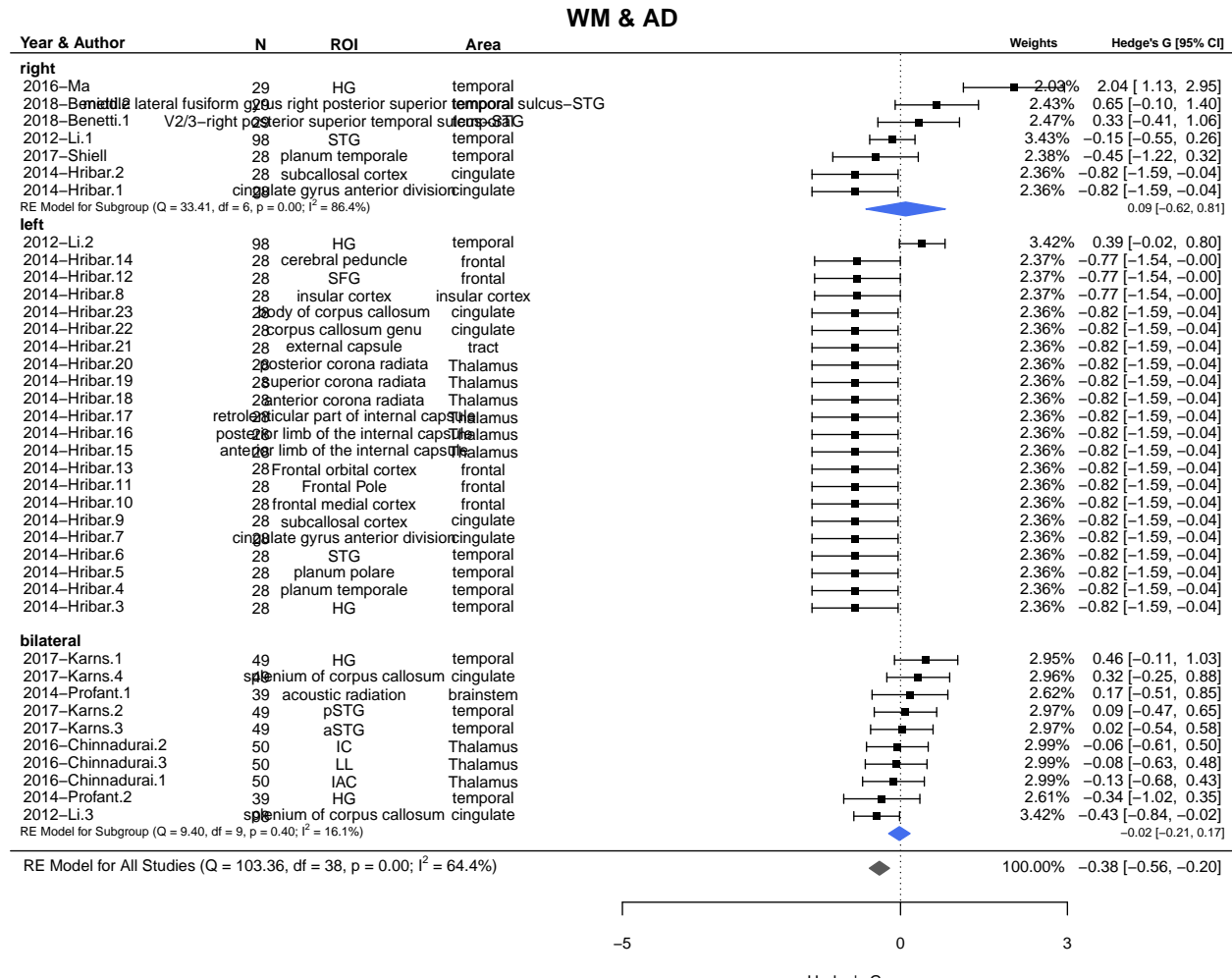
White matter: MD



White matter: Mean Kurtosis



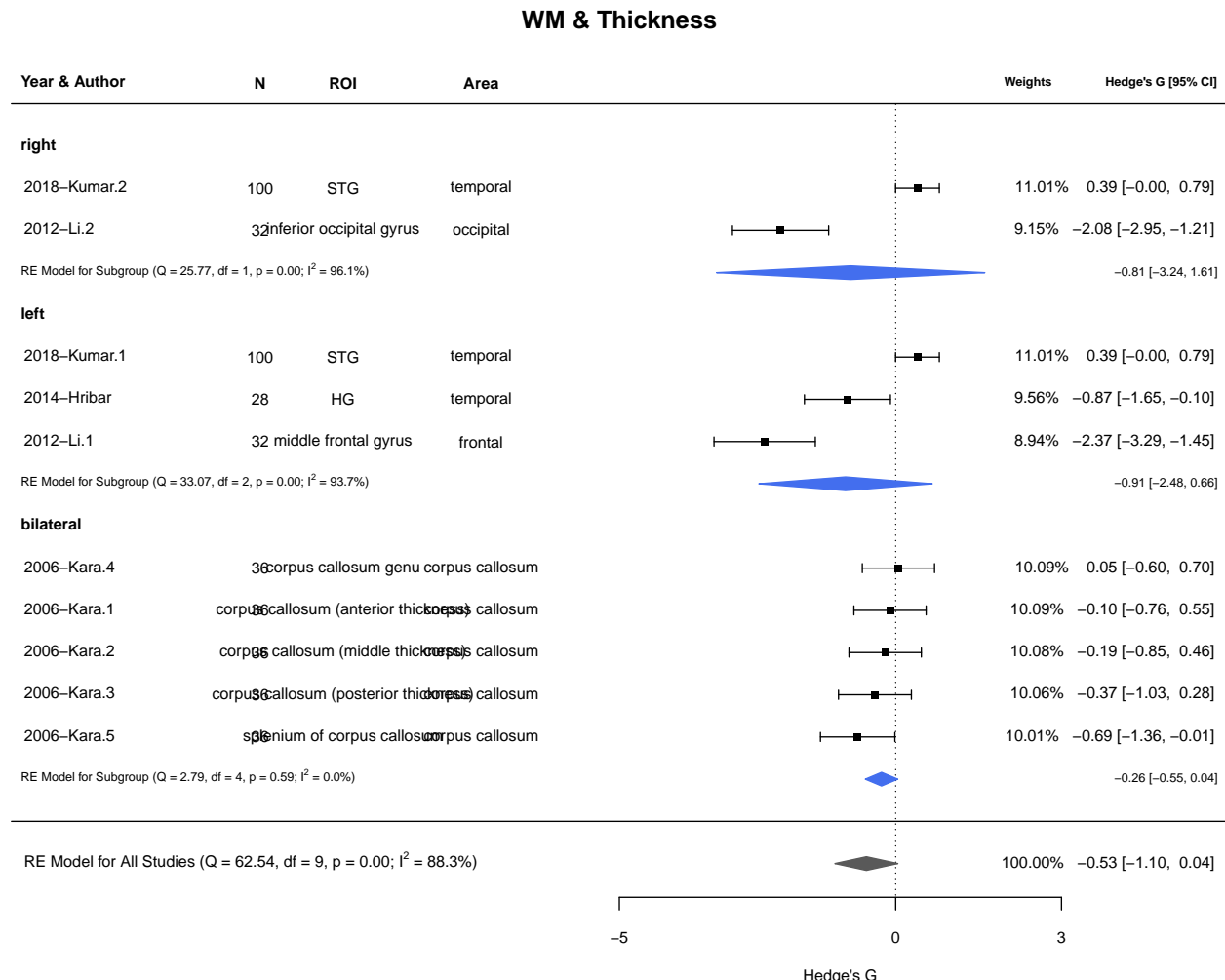
White matter: AD



Error in rma(yi = hedgesG, vi = varG, data = meta.mod, measure = "MD", : Fisher scoring algorithm did not converge. See 'help(rma)' for possible remedies.

Other Measures of White Matter

White matter: Thickness



White matter: VBM

